

# Pedaling Asymmetry During Lower Limb Pedaling After Stroke

Benjamin Rappaport  
*Marquette University*

---

## Recommended Citation

Rappaport, Benjamin, "Pedaling Asymmetry During Lower Limb Pedaling After Stroke" (2019). *Master's Theses (2009 -)*. 551.  
[https://epublications.marquette.edu/theses\\_open/551](https://epublications.marquette.edu/theses_open/551)

# PEDALING ASYMMETRY OF THE LOWER LIMBS AFTER STROKE

By

Benjamin Rappaport, B.S.

A Thesis submitted to the Faculty of the Graduate School, Marquette University, in  
Partial Fulfillment of the Requirements for the Degree of Master of Science

Milwaukee, Wisconsin

August 2019

ABSTRACT  
PEDALING ASYMMETRY DURING LOWER LIMB PEDALING AFTER STROKE

Benjamin Rappaport, B.S.

Marquette University, 2019

People with stroke pedal asymmetrically. There may be differences in their pedaling kinetics between their non-paretic and paretic lower limbs and compared to healthy age matched controls. Previous studies have measured pedaling related impairments and impairments with interlimb coordination using electromyography (EMG). These studies did not use torque as a measurement for pedaling related impairments and interlimb coordination impairments. Pedaling symmetry in the laboratory measuring the torque and work production will fill the gaps of the knowledge about motor compensation during lower limb pedaling. As well, pedaling symmetry has not been measured during fMRI because of the inability to measure torque during fMRI pedaling. The purpose of this study was to redesign a torque measurement device used for pedaling safely in an MR environment and measure impairments of the paretic limb during pedaling and impaired interlimb symmetry. To achieve this purpose, a torque measurement system was redesigned for accurate and precise torque measurements. Participants were asked to pedal on a novel pedaling device, at low loads (work < 40 J), outfitted with the torque measurement system in both the laboratory and an MRI. During either session, there were no differences in pedaling symmetry between groups. The stroke group showed significantly more negative work with greater minimum torque in their paretic limb during both sessions. Similar symmetry measurements between groups suggest that at low loads there is not enough resistance or too low of a work load to exacerbate the asymmetries in pedaling. However, the increased negative work and greater minimum work in the paretic limb suggest that the strategy the stroke group uses for their paretic limb is different than that of their non-paretic limb or controls. Stroke group positive work was correlated with the Fugl Meyer and the symmetry was correlated with Fugl Meyer. These data suggest that the Fugl Meyer may be a predictor of higher positive work and a symmetry index close to 0. Overall, this study describes the design of a torque measuring device that can be used in an MR environment and provides insight into the impaired interlimb symmetry and pedaling dynamics after stroke.

## ACKNOWLEDGMENTS

Benjamin Rappaport, B.S.

There are many people to thank for helping me along the way to complete this thesis. First, this would not have been possible without the guidance from Dr. Sheila Schindler-Ivens. I have learned so much from you through the process of designing experiments, collecting and processing data, and organizing my data and thoughts into papers. I will apply these lessons through the rest of my career as they transfer over into industry. Thank you very much for everything you have done for me.

I would like to thank my advisor, Dr. Brian Schmit and my other committee member Dr. Jay Goldberg for their feedback and support through this process. You have provided me helpful insights and perspectives on my work and helped me to improve my understanding of the work included in this thesis. I appreciate the time and effort that you willingly invested in me.

The current and past lab members of the lab I would like to thank. I would like to thank Brice Cleland for your time acclimating me to the pedaling device and showing me the basics of the lab. I would like to thank Kaleb Vinehout for working with me to complete all the fMRI procedures during my data collection. Finally, I would like to thank Tom Ruopp, Christine Smith, Gillian Scanlon, Amanda Waldera, and Ahn Nayun for all your help over the past couple years. Besides help with the work on my thesis, you all have been good friends. Thank you so much for the amount of time and effort you have spent helping me.

There are others I would like to thank who have helped me throughout my time. Thank you to Tim Thelaner for aiding me in the initial circuit diagramming and troubleshooting. Thank you to the MRI technicians at the Medical College of Wisconsin who ran the experiments. Thank you to all my professors who have taught me so much along the way and for all their support.

Lastly, I would like to thank all of my family and friends for their love and support during this time. Thank you to my mom, dad, stepmom, and sister for all of the support you have shown me. Most of all, thank you to my fiancé, Cassidy. You have been there for me through it all and I could not have done this without you. Thank you.

## TABLE OF CONTENTS

ACKNOWLEDGMENTS.....	i
TABLE OF CONTENTS.....	ii
LIST OF TABLES.....	iv
LIST OF FIGURES.....	v
CHAPTER 1: LITERATURE REVIEW .....	1
Pedaling asymmetry in stroke.....	3
Kinetics of Pedaling.....	3
Asymmetric kinetics, torque, and work in stroke survivors .....	5
Muscular causes of asymmetry .....	7
Neural causes of asymmetry.....	10
Pedaling and Torque Measurement Devices .....	13
Conclusion.....	16
CHAPTER 2: DESIGN OF TORQUE TRANSDUCER .....	18
Introduction .....	18
Torque Measurement System .....	19
Design Changes .....	22
User Experience .....	23
Data Accuracy and Precision.....	25
Calibration Methods .....	28
Procedure.....	28
Statistical Analysis.....	31
Results.....	33
Design Changes .....	33
Calibration 1: Left and Right .....	34
Unused Calibration Fits.....	39
Calibration 2: Left.....	41
Calibration 2: Right .....	45
Analysis of Torque Transducer.....	48
Discussion .....	50
Circuit Board Components and Layout.....	51
Transducer Calibration.....	53
Comparison to Similar Devices .....	56

Measure of Pedaling Asymmetry.....	58
When a New Calibration is Needed .....	59
Limitations .....	60
Conclusion.....	61
CHAPTER 3: ASYMMETRY IN PEDALING AFTER STROKE .....	62
Introduction .....	62
Methods.....	64
Participants .....	64
Clinical Measures .....	65
Equipment and Procedures .....	66
Data Analysis.....	69
Statistics .....	70
Results.....	71
MRI Pedaling Data.....	85
Familiarization versus fMRI pedaling.....	98
EMG activity .....	101
Relationships between mechanical work and clinical measures.....	104
Discussion .....	105
Pedaling in Laboratory Setting.....	105
Pedaling During fMRI .....	109
Differences Between Familiarization and fMRI Pedaling.....	110
Pedaling Symmetry .....	112
Limitations .....	113
Conclusion.....	114
CHAPTER 4: CONCLUSION AND FUTURE DIRECTIONS .....	116
Summary of Results .....	116
Future Studies .....	118
BIBLIOGRAPHY .....	119
APPENDIX A: SUPPLIMENT TO CHAPTER 3 .....	124

## LIST OF TABLES

Table 2.1: Measurement system error for beginning calibration

Table 2.2: Error measurements for unused calibration fits

Table 2.3: Measurement system error for end calibration

Table 2.4: Comparison of other devices to the designed device

Table 3.1: Participant demographics

Table 3.2: Individual torque and work data for all control participants

Table 3.3: Individual torque and work data for all stroke participants

Table 3.4: Multilinear regression model for control group

Table 3.5: Multilinear regression model for stroke group

Table 3.6 Group average control and stroke torque and work kinetics

Table 3.7: Degrees of positive work

Table 3.8: Individual torque and work values for control participants during fMRI pedaling

Table 3.9: Individual torque and work data for all stroke participants during fMRI pedaling

Table 3.10: Control and stroke pedaling kinetics for fMRI pedaling

Table 3.11: Multilinear regression for control group during fMRI

Table 3.12: Multilinear regression for stroke group during fMRI

Table 3.13: Comparison of familiarization and fMRI pedaling values

Table 3.14: Muscle activity for control and stroke group during familiarization session

## LIST OF FIGURES

- Figure 2.1: Novel pedaling device
- Figure 2.2: Simplified schematic representation
- Figure 2.3: Wheatstone bridge with strain gauges
- Figure 2.4: Transmitter circuit board schematic
- Figure 2.5: The receiver circuit board schematic
- Figure 2.6: Calibration setup
- Figure 2.7: Free body diagram of calibration
- Figure 2.8: Equation graphs
- Figure 2.7: Overview of calibration
- Figure 2.8: Frequency output of transmitter circuit
- Figure 2.9: Frequency spectrum
- Figure 2.10: Calibration for the left and right transmitters
- Figure 2.11: Conversion of the calibration
- Figure 2.12: Calibration curve of left torque sensor
- Figure 2.13: Calibration curve of right torque sensor
- Figure 2.14: Conversion of the left calibration
- Figure 2.15: Conversion of the right calibration
- Figure 2.16: Single linear fit for torque calibration curve
- Figure 2.17: Linear fit with intercept torque through zero
- Figure 2.18: Polynomial fit for calibration curve
- Figure 2.19: Left torque transducer calibration
- Figure 2.20: Overall left calibration
- Figure 2.21: 5 day calibration conversion: left

Figure 2.22: Total calibration conversion of the left torque transducer

Figure 2.23: Right torque transducer calibration

Figure 2.24: Overall right calibration

Figure 2.25: 5 day calibration conversion: right

Figure 2.26: Total calibration conversion of the right torque transducer

Figure 3.1: Novel Pedaling Device

Figure 3.2: Position, velocity, and torque over time

Figure 3.3: Symmetry of control participants

Figure 3.4: Magnitude of the left and right torque and work data for controls

Figure 3.5: Torque and work correlations for control participants

Figure 3.6: Symmetry of stroke participants

Figure 3.7: Magnitude of the paretic and non-paretic torque and work data for stroke participants

Figure 3.8: Torque and work correlations for stroke participants

Figure 3.9: Overlaid torque curves for control group

Figure 3.10: Overlaid torque curves for the stroke group

Figure 3.11: Symmetry of control participants during fMRI pedaling

Figure 3.12: Magnitude of the left and right limbs for torque and work values for controls during fMRI pedaling

Figure 3.13: Torque and work correlations for control participants during fMRI pedaling

Figure 3.14: Symmetry of stroke participants during fMRI pedaling

Figure 3.15: Magnitude of the paretic and non-paretic torque and work data for stroke participants during fMRI pedaling

Figure 3.16: Torque and work correlations for stroke participants during fMRI pedaling

Figure 3.17: Overlaid torque curves for control group during scanning

Figure 3.18: Overlaid torque curves for stroke group during scanning

Figure 3.19: Comparison of the familiarization and scanning pedaling for the control group

Figure 3.20: Comparison of the familiarization and scanning pedaling for the stroke group

Figure 3.21: EMG amplitude data averaged across cycle for control and stroke participants

Figure 3.22: EMG modulation index differences across muscles

## CHAPTER 1: LITERATURE REVIEW

The purpose of this thesis is to present the pedaling symmetry of chronic stroke survivors and compare the symmetry with healthy age matched controls. It is hypothesized that stroke survivors will pedal less symmetrically than those with a healthy nervous system because of functional deficits in their lesioned hemisphere and paretic lower limb. To measure the symmetry while pedaling, an MRI safe torque transducer was redesigned for measuring the torque and work production of each lower limb while pedaling. As well, this thesis aims to quantify any differences in pedaling performance between a laboratory and MRI setting. These topics need to be reviewed because there is limited literature regarding the symmetry of pedaling with stroke survivors and the use of torque measurement systems in pedaling research with stroke survivors is incomplete. This chapter aims to describe asymmetry in stroke in relation to pedaling, contrast pedaling in stroke with pedaling in healthy adults, and the different devices used for pedaling and measuring pedaling torques.

The motivation for this thesis is primarily based on previous work completed in our laboratory. Previous work completed described the supraspinal control of locomotion in stroke survivors and its relationship to locomotor impairment (Promjunyakul, Schmit and Schindler-Ivens 2015). Functional magnetic resonance imaging (fMRI) was used to record human brain activity while pedaling was used as a model of locomotion. This research provided evidence that there are differences in the hemodynamic responses recorded during fMRI between stroke survivors and healthy controls (Promjunyakul et al. 2015). Stroke survivors had reduced volume of activation in the sensorimotor cortex ad

cerebellum. The sensorimotor cortex activity was symmetrical in stroke survivors, but the cerebellar activity was asymmetrical and lateralized toward the lesioned hemisphere. It was concluded that neural adaptations for producing locomotor hemiparetic movements post stroke are completed by a compensatory role in the spinal cord and cerebellum. Promjunyakul compared the activation responses during pedaling with a locomotor task, but these comparisons could not be done directly (Promjunyakul et al. 2015). The comparisons were not direct comparisons because the tasks were completed separate of one another, so the comparisons were inferred. This motivates the work of this thesis because this thesis aims to provide the direct evidence of comparisons between pedaling torque, work, and asymmetry in the laboratory and the MRI scanner that was not previously known. This thesis support the work completed by Promjunyakul.

Asymmetric contributions to locomotor tasks in chronic stroke survivors affect the way stroke survivors are able to complete tasks. These asymmetries are from long-term motor dysfunction in the limbs (Kautz and Brown 1998). Asymmetries are common after a stroke. These asymmetries lead to compensation, which allows stroke survivors to complete functional movements, but the non-paretic limb does a majority of the work (Brown and Kautz 1998). Compensation may allow for stroke survivors to complete activities of daily living but causes repeated neglect to the paretic limb. As a result, stroke survivors can have trouble with walking, eating, performing detailed tasks, and other tasks of daily living. Symmetric movements are important factors for having an independent lifestyle among stroke survivors.

As such, stroke can cause a diminished ability to use the lower limbs in locomotor tasks. Pedaling on a cycling device is an intervention used to analyze the differences in

symmetry. Pedaling is used because it can measure speed, endurance and coordination in stroke survivors. Mechanical work, torques applied to the device, and phasing can all be measured from a pedaling device. These measurements can be used to determine impairments in people with stroke (Ambrosini et al. 2012). Stroke survivors may pedal differently than healthy, age matched, adults due to their learned asymmetric movement contributions.

### **Pedaling asymmetry in stroke**

Measuring pedaling asymmetry in stroke is important because it can be used to quantify the asymmetry of kinetics, muscle function, and cortical activation and volume of stroke survivors. The kinetics of pedaling incorporate the movement during pedaling along with the torque and work production during the task. Muscle function changes are a result of decreased activity, abnormal timing of the muscles, and decreased interlimb coordination. As well, there are changes in cortical activation and volume which may promote asymmetry.

### *Kinetics of Pedaling*

During bilateral pedaling, the mechanical work of the lower limbs increases during the beginning of the downstroke, reaches a maximum slightly after 90 degrees, decreases until near 180 degrees, and then repeats this pattern for the opposite leg at the downstroke. The resulting upstroke does not follow the same pattern. Pedaling has phasic work production and EMG activity. As the work increases during the downstroke of one limb, the other is completing the upstroke with the limb generating a different work

output. The phasing of EMG happens in the main muscles used for pedaling. The rectus femoris (RF), vastus medialis (VM), biceps femoris (BF), semimembranosus (SM), tibialis anterior (TA), gastrocnemius (GAS), and soleus (SOL) are the prime movers in pedaling regardless of forward or backward pedaling (Ting et al. 1999). During the extending phase, 0 to 180 degrees, the RF, VM, GAS, and SOL are most active to provide pedaling through this region. The flexor phase, 180 to 360 degrees, the BF, SM, and TA are most active to return to 0 degrees. The top transition requires the RF, VM, and TA to transition between the flexor and extensor phases, while the BF, SM, GAS, and SOL are needed for transferring from the extensor to flexor phase at the bottom of the cycle (Neptune and Herzog 1999). These muscles have been shown to perform all movements in pedaling and can represent the pedaling cycle. The muscles used for pedaling produce the torque needed for rotating the crank through the pedal cycle.

Torque generation on the crank is another way to view the kinetics of pedaling. Studies have tried to explain the differences in the work done during pedaling by comparing the idea of effective crank force generation. The perpendicular crank forces are the only forces that can rotate the crank for pedaling while ineffective forces do not aid in pedaling. Ineffective forces can be described as forces that are not radial to the crank. The radial forces should not be ignored because a significant amount of radial force results from contributions of gravity, Coriolis, and centripetal forces (Kautz and Neptune 2002). It was described that the radial forces are likely to play a role in the crank forces. There is a limited ability to control the orientation of the force and, as a result, the radial component of the crank force will be produced. Eliminating the radial force would require the recruitment of additional muscles for offsetting the force but is not possible by

paretic limb. The negative crank power component during the upstroke of the pedal cycle has shown to add mechanical costs but has been refuted as well. More muscular work would be required to eliminate the resistive work (Kautz and Neptune 2002). The resistive work may simply be described as a transfer of energy from the downstroke limb to upstroke limb, which is normal in pedaling. This is normal because the resistive work comes from a deactivation of the muscles from the downstroke portion of the cycle. The resistive work is mainly the dissipation of energy by negative muscle work caused by the muscle deactivation resulting in the leg being pushed upward (Kautz and Neptune 2002). It may be inefficient and become poor performance if there is a significant amount of resistive work completed.

#### *Asymmetric kinetics, torque, and work in stroke survivors*

Lower limb movement is asymmetrical post stroke but symmetrical in healthy controls (Kautz and Brown 1998). Stroke related asymmetry can be seen in the differences in kinematics and the torque and work output during pedaling. During gait, stroke survivors use their non-paretic limb for 60% of forward locomotion and in pedaling, stroke survivors use their non-paretic limb for 59% of the positive work and 36% of the negative work (Bowden et al. 2006, Cleland 2018). This reveals asymmetries in both gait and pedaling. The non-paretic limb is completing more of the work it takes to move while walking or to rotate the cranks in pedaling. Asymmetries are not seen in healthy controls because of the lack of impairments. However, healthy adults may have differences in their symmetry with age (Sacchetti et al. 2010, Patterson and Moreno 1990, Hagberg et al. 1981, Liu and J. 2010, Dorel et al. 2010). This is important to know because stroke survivors tend to be older and age matched controls are accordingly older

too. Younger adults pedal at higher rotations per minute than older adults. The older adults' efficiency decreases as pedaling rates increase. Kinematic quantification of the range of motion (ROM) of older adults have shown that knee ROM, ankle ROM, maximum knee extension, and maximum ankle dorsiflexion are all decreased compared to their younger counterparts (Seo et al. 2016). This suggests that age may play a role in pedaling asymmetry in stroke survivors because healthy adults' symmetry becomes more asymmetric with age.

Bilateral asymmetry of pedaling in stroke survivors is related to the impairments in the paretic limb. Pedaling asymmetry can be measured by the difference in the amount of net mechanical work completed or power generated by each limb. It has been shown that the paretic lower limb is unable to produce the same amount of power as the non-paretic limb and is unable to coordinate the power as well as the non-paretic limb (Kautz and Brown 1998, De Marchis et al. 2015). The net mechanical work done by the paretic limb in stroke survivors is greatly reduced. There is a great variability of work done by the paretic limb. The paretic limb's variability comes from both the positive work and the resistive work. The paretic limb can provide a net resistance to crank progression which results in a net work done on the crank being resistive (Kautz and Brown 1998). Similarly, another study found that the paretic limb does not move similarly to a normal leg pedaling. The dissimilarities cause improper muscle work because the work can no longer be decreased by doing unnecessary work (Kautz and Neptune 2002). Unnecessary work is when there is a difference in pedaling form between the two limbs at unloaded pedaling with the paretic limb not completing external work.

The active forces produced by stroke survivors differ between their paretic and non-paretic lower limbs. The paretic limb produces a smaller amplitude during the downstroke and typically has a second smaller peak in the upstroke phase (De Marchis et al. 2015). The upstroke's increase in force would be resulting from the pulling action with the hamstrings. The reduction in the second smaller peak causes asymmetry in the force production. This corresponds well to level of motor impairment (De Marchis et al. 2015). Analyzing the force production of the pedaling cycle for stroke survivors helps to provide an understanding of how they pedal.

#### *Muscular causes of asymmetry*

Asymmetry is caused by decreased muscle activity, abnormal timing of the muscles, decreased interlimb coordination and changes to the interlimb reflexes. Each of these mechanisms contribute to asymmetry in stroke survivors.

Decreased muscle activity may cause asymmetry because reduced activity in a single limb may cause differences in force output. A difference in force output of the two limbs leads to asymmetry. This is caused by multiple factors. A decrease in motor units, change in fiber type, and decrease in motor unit firing rate can all cause the lowered muscle activity. McComas et al were among the first to document the loss of the motor units and other studies have reported similar findings of loss of motor units post stroke (McComas et al. 1973). They found dysfunctions in that neurons failed to respond to the presence of denervation by axonal sprouting and collateral fiber innervation, as would be expected in normal neurons. Atrophy of the muscles leads to decreased muscle activity because of the decrease in fast-twitch fibers and conversely, hypertrophy of the slow

contracting fibers. Such changes could alter the force producing capabilities of the muscles (Arene and Hidler 2009). The decrease in motor unit firing rate leads to decreased muscle activity because of the trouble with maintaining a constant level of force. When stroke survivors try to maintain a constant level of force, EMG recordings often show irregularities not observed in normal participants (Arene and Hidler 2009). These factors which lead to decreased muscle activity are related to impaired motor performance. Altered motor control in hemiparesis has been described by decreased muscle activation. With the decreased activation, there is no increased strength reflex response, instead, there is reduced activation of two or more groups of muscles. This response occurs in both the shortening and lengthening of the muscles (Arene and Hidler 2009).

Impaired motor performance is also caused by the abnormal timing of muscles. The abnormal timing of muscles may cause asymmetry because of inappropriate muscle contractions between the agonist and antagonist muscles. Typical examples of abnormal motor activation are the early onset of contraction by the calf muscles. When the calf muscles contract early, energy in the lower limb is transferred to the knee causing the calf muscles to not push (Arene and Hidler 2009). This allows for compensation where the other limb does more work to continue the task. There are also increases to muscle latencies in the muscle response (Sharafi et al. 2016). These muscle latencies significantly delay stroke survivors' control of their lower limbs. This increased latency is irrespective of the paretic and non-paretic limb as found in a study by Sharafi et al. They observed that the onset latencies of responses in the control group were below reported thresholds for voluntary reactions suggesting the automatic nature of the

response. They proposed that the difference in magnitudes between the two may reflect on the involvement of the supraspinal pathways (Sharafi et al. 2016). Similarly, stroke survivors had a significantly less prominent inhibitory response compared to healthy controls (Stubbs et al. 2012). The responses were significantly modulated by stimulus. This showed that a short-latency interlimb reflex is impaired differently in chronic stroke patients and is abnormal compared to controls (Stubbs et al. 2012). The poor coordination may show an inability to maneuver around unexpected obstacles.

Decreased interlimb coordination may cause asymmetry because each of the lower limbs influences the other causing the paretic limb to negatively impact and bias the non-paretic limb. The motor output of the paretic leg during bilateral movement may be facilitated by interlimb pathways that couple pattern generators of the two limbs (Kautz and Patten 2005). Muscle activation patterns from neurologically healthy humans show neuronal interlimb coupling affecting muscle activation and coordination patterns (Kautz and Patten 2005). It is suggested that interlimb pathways may be responsible for a portion of the paretic leg locomotor output. Dysfunctional paretic muscle coordination patterns can adapt to somatosensory inputs with the sensorimotor state of the non-paretic limb influencing the paretic limb (Alibiglou and Brown 2011a). It is well established that the sensorimotor state of one limb can influence another limb and, therefore, bilateral somatosensory inputs make an important contribution to interlimb coordination post stroke (Alibiglou and Brown 2011a). The paretic or non-paretic limbs must adjust and adapt to a new phasing to maintain an interlimb coordination strategy to perform locomotor movements (Kautz and Patten 2005).

Interlimb reflexes are controlled and organized bilaterally (Kautz and Patten 2005). Interlimb reflexes must have substantial flexibility for task use in healthy controls. The interlimb reflexes may change after stroke. Increases to the length and velocity feedback of targeted muscles can induce gait impairments often in hemiparetic gait (Jansen et al. 2014). Similarly, a change in reflex modulation patterns were found in the soleus, vastus lateralis, vastus medialis, and rectus femoris (Jonkers, Delp and Patten 2009). Altered reflex patterns to these muscles causes excessive plantar flexion of the toes and hyperextension of the knee and hip. These patterns can cause hindered movement of the lower limb.

#### *Neural causes of asymmetry*

Functional magnetic resonance imaging (fMRI) has been used to investigate cortical contributions to upper limb movement in persons with post-stroke hemiparesis. The current body of literature has contributed to the development of several models explaining how the brain adapts to injury, but this has only been done with upper limb studies. Few studies have used fMRI to examine brain activation during lower limb movement of the paretic limb. Mainly, existing studies have used single joint movements of the ankle and knee (Luft et al. 2005, Jang et al. 2005, Enzinger et al. 2008, Enzinger et al. 2009). These studies provide some insight to the control of the lower limbs of stroke survivors. These studies lack depth in the functional movements which are bilateral, reciprocal, and multi-joint movements inherently.

Pedaling as a paradigm used during fMRI has shown that there is a reduction in activation volume of the brain in stroke survivors compared to age matched controls

(Promjunyakul et al. 2015). Decreased brain activation and volume can cause asymmetry in stroke because of impaired processing of afferent signals. This may contribute to abnormal muscle activation and movement patterns. Changes in activation and movement patterns represents a shift from well-functioning group II afferents to a less effective group I system (Arene and Hidler 2009). Inhibition of group II signals at the spinal cord level along with a failure to block the group I afferent signals causes abnormalities in movement. For stroke participants with asymmetrical movements, it may be difficult to perform reciprocal movements in the lower limbs such as walking or pedaling.

Reduced volume could not be completely explained by differences in pedaling rate or head motion because it may be due to anatomic or physiologic changes post stroke (Promjunyakul et al. 2015). It was associated with the work production of the paretic leg during pedaling. The reduced volume was statistically significant in all regions except the M1 and S1 (Promjunyakul et al. 2015). There was shown to be a tendency for a decreased volume in the M1 and S1 which may have reached significance in a larger sample. It can be concluded that there is generally reduced volume in the brain in stroke survivors compared to healthy age matched adults (Promjunyakul et al. 2015, Jang et al. 2005). It is possible that the reduced pedaling related brain activation volume post stroke is due to a reliance on spinal and or brainstem structures for lower limb movement. This is supported by seeing asymmetries in the corticospinal tract (CST) which were strongly related to interlimb differences (Madhavan et al. 2011). As well, findings from Jang's group showed that the lesioned hemisphere lacked the pathway from the sensory motor 1 (SM1) of the lesioned hemisphere to the CST while there was a pathway in the unaffected hemisphere. The effects of the damaged CST are shown to increase

asymmetry (Jang et al. 2005). The change in the physiology and structure of the CST suggests that the function of the affected motor cortex shifted to the unaffected motor cortex via reorganization of the motor pathway. Evidence from stroke survivors suggest that locomotor interlimb coordination is strongly influenced by cerebral inputs (Kautz and Patten 2005). Conversely, Alibiglou and Brown found that there were no significant differences between the paretic and non-paretic tibialis anterior, which indirectly indicates that the cortical areas are not a primary factor in controlling interlimb coordination (Alibiglou and Brown 2011a).

However, the detractor from viewing the asymmetry work in relation to cortical activity and volume is how passive pedaling during fMRI shows cortical activation in areas that are associated with pedaling even though there is no active pedaling (Cleland 2018). The change in pedaling symmetry and decreased volume may be correlated but not causal. This needs to be examined by measuring the cortical activity during fMRI while measuring the symmetry during pedaling.

Damage to the descending neural pathways causes alterations in stretch reflexes (Teixeira-Salmela et al. 1999). Reductions in the reflex excitability may be attributed to the atrophy of the muscle. Similarly, the stretch reflex activation adds to the normal antagonist coactivation, which effects the restraint in concentric movements becoming abnormally high (Engardt et al. 1995). Stretch reflexes may act in synergy with voluntary commands leading to high tension in the muscles, which is unfavorable for movement because it may cause a change in muscle output during gait. If the stretch reflexes are activated, they are activated in the agonist that is lengthening, so the reflexes can act in synergy with the voluntary effort, which is different than previously stated. The reflex

acting with the voluntary effort may be used to help gait because it could increase the output of the muscle. The differences may be the reason that eccentric movements had better effects on voluntary strength (Engardt et al. 1995). The differences between the concentric and eccentric movements is attributed to the importance of motor functions of daily life.

### **Pedaling and Torque Measurement Devices**

Several torque measurement devices, specific to pedaling, have been designed by labs for lower limb usage (Brown and Kautz 1998, van Duinen 2007, Turkseven and Ueda 2013, Cheng et al. 2003, Gusso et al. 2012). There have been few of these devices capable to be used in an MR safe environment. One device in particular was designed for torque measurement in an MRI for index finger actuation strength. This device was the basis for the original torque transducer design for a novel pedaling device prior to this study (Arand 2013). This device was designed with a strain gauge Wheatstone bridge to measure torque and uses a fiber optic cable to connect to the controller room to reduce risk of radio frequency (RF) destroying the signals. Strain gauges are often used for torque transducers because they are very precise in measuring small and fast forces and they are mechanically simple to use (van Duinen 2007). This device was adapted to work as a torque measurement pedaling device for use in an MR environment for the study in the proceeding chapters.

Pedaling devices have been used in many studies of the lower limbs. Studies have looked at the force production of the lower limbs on the pedals and muscle responses during pedaling. Brown and Kautz have designed a standard ergometer with a frictionally

loaded flywheel. The device measures reaction forces oriented normally and fore-aft to the pedal surface using an instrumented pedal (Brown, Kautz and Dairaghi 1998). There were no reports of the accuracy or specificity of the system. Similarly, Chinworth and Zimmermann designed a force sensing pedaling device using strain gauges (Chinworth and Zimmermann). The gauges were mounted such that only perpendicular forces could be measured from the pedaling device. They described difficulty with reducing noise in the system and troubles with breaking components. They reported an average deviation of 4.0 percent. Conversely, Hull and Davis designed an instrumentation system that measured 6-axis pedal loading using 32 strain gauges that were mounted within a modified pedal body (Davis and Hull 1981). These gauges were connected to eight Wheatstone bridge circuits in different locations for measurement of force. Similarly, Gregor's group designed left and right side pedals using strain gauges to build a force cube to measure forces on the pedals (Broker and Gregor 1994). These two pedaling devices were designed primarily for use with a road bike but showed high accuracy and quick response times to the forces applied.

A few devices have been designed for pedaling capability for use during MRI scanning procedures to measure pedaling activity during MRI. Of the devices, one was designed for use in an open magnet MRI scanner viewing muscular ischemia. This device was designed for MR compatibility, a crank tower that pivots about the flywheel allowing for different angles, a power transmission system with a timing belt, a freewheel mechanism for pedaling, load generation and measurement, and workload acquisition. This device calculates torque by calculating the angular velocity from counting revolutions and torque by computing deflection of the pendulum (Cheng et al. 2003). The

device required patients to sit upright for pedaling, so it would be impossible to be used in a standard MRI scanner. Few devices have been designed for a standard 3T MRI scanner, but they all have similar designs. They are designed for supine pedaling. There are only a few with velocity and force measurements. Each of the devices uses a different tactic to measure force (Pedersen et al. 1999, Gusso et al. 2012). Gusso's group uses MRI-compatible load cells with both tension and compression measurements. The device measures both the extension and retraction forces applied by each foot. The device does not measure off axis forces that relate to forces that do not aid in pedaling. It was calibrated using a mechanical testing system (Instron 5800 series). It has a high degree of linearity ( $R^2=0.999$ ) with a sensitivity of  $14 \mu\text{V/N}$  (Gusso et al. 2012). Separately, another group uses a MR ergometer (MRI cardiac ergometer, Lode BV, Groningen, The Netherlands) for pedaling (Roest et al. 2001, Pedersen et al. 1999). This device is very large, not easily transportable and cannot be used outside the MRI scanner. It has a large workload band with computer adjustable workload control. The device is limited to 80 rotations per minute (rpm) for a constant load. The device has a 3% accuracy rating above 100W and a 3W accuracy below 100W. Both groups collected cardiac related data in the MRI, not brain related images and there have not been studies using this device for fMRI imaging of the brain.

A few groups have designed their own ergometers for use in the MRI. An ergometer was designed for specific use in a 3.0 T, 640mm diameter superconducting magnet (IMRIS, Winnipeg, MB, Canada) (Raymer et al. 2006). It was designed for a head only scanner because of the dimension restrictions of the ergometer. This device was designed to measure force of the ankle joint using a potentiometer and measuring

angular displacement. The device's accuracy was not given, but the potentiometer accuracy was less than 0.5 dB (Raymer et al. 2006). Another group designed an MR-compatible bicycle ergometer that was used for cardiac and musculoskeletal data collection. This bicycle ergometer was designed with adjustable resistance using aluminum weights (Jeneson et al. 2010). There were no pedaling measurements that were collected from this system.

There have been a number of devices designed for use in pedaling studies, but of those designed, few were usable in an MR environment. The devices created tend to be reported to have high accuracy, yet few values are reported. For the most part, the devices are used strictly for pedaling and allow for continuous motion. There has been little reporting of results from the design and calibrations of the different devices.

## **Conclusion**

The purpose of this chapter was to describe the pedaling symmetry of stroke survivors and the use of force measurement systems in pedaling research. It aimed to describe asymmetry in stroke, compare pedaling in stroke with healthy adults, and describe different devices used for pedaling and measuring pedaling forces. Stroke survivors pedal differently than healthy age matched controls and are more asymmetric. The differences come from changes in pedaling kinetics, muscle function, and cortical activation and timing. These abnormalities cause a change in the torque production while pedaling, which shows a decreased positive work and increased negative work. Timing abnormalities are not as prevalent in all the lower limb muscles. The most affected muscles are the RF, VM, BF, and SM. The muscles are the power production muscles, so

they affect the amount of work is done from pedaling. The asymmetric contributions to pedaling come from long term motor dysfunction in the lower limbs. The asymmetries lead to the compensation seen in stroke survivors.

Measuring these abnormalities are essential for characterizing the work completed during pedaling. It has been shown that there are several devices that have been used for measuring pedaling kinetics. A majority of the devices are capable of measuring torque. Fewer devices are capable of being used in an MRI scanner. There is an importance to being able to measure torque in the scanner because it allows for a direct correlation of the work completed and the resulting cortical activity. This study fills those holes where symmetry is not fully understood in an MRI scanner and aims to show the relationship between pedaling in a laboratory and scanning setting.

## CHAPTER 2: DESIGN OF TORQUE TRANSDUCER

### Introduction

Within our lab, a novel pedaling device was created with a split crank shaft which allows for bilateral coupled, unilateral, and bilateral uncoupled pedaling. The different types of pedaling are accomplished using a crankshaft coupler. The coupler pairs the two halves together when in place and allows for separate movement of the sides when removed. The device has an assistance system to simulate the presence of the non-contributing limb while pedaling unilaterally or bilaterally uncoupled. The device was designed with integrated position and velocity sensors to measure the position and velocity of the crank shaft. The pedaling device was created in such a way to make it safe within or near an MRI machine. The device was made from polymeric materials and wood. The bulk of the design making up the base, uprights, and pulley system were plastics and wood. These plastics and wood were chosen to be strong enough to withstand long term use of the bike. This device was used for a study of bilateral vs. unilateral locomotor control during fMRI (Arand 2013). The pedaling device was meant for more studies thereafter. After the study from Arand, the device was outfitted with a torque strain gauge system. This system was important for measuring the amount the left and right lower limbs contributed to pedaling. The torque measurement system became a major target for the use of the device, but it did not work properly. Therefore, a redesign of the torque measuring device was necessary to improve device design, user experience, data accuracy, and precision. The purpose of this chapter is to explain the redesign of the torque measurement system and the calibration of the new design.

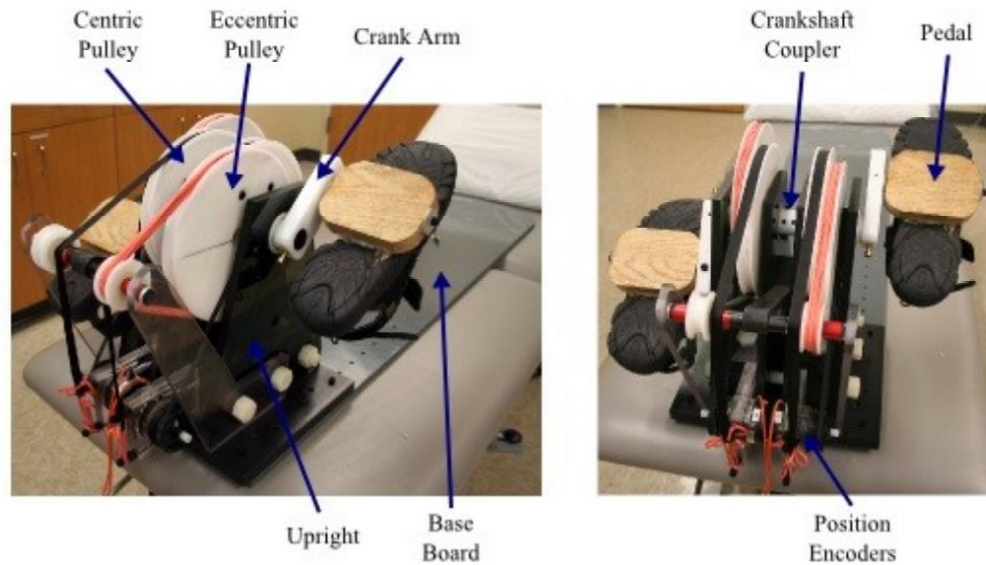


**Figure 2.1: Novel pedaling device.** The crankshaft and crank arm pictured are the primary focus for this chapter. The crankshaft runs from the crankshaft coupler to the crank arm and the crank arm connects the shaft to the pedal.

### Torque Measurement System

The design of the original torque measuring device was based on a finger flexor device designed by Duinen (Duinen 2007). Duinen's device was quick to respond to changes in force measuring 5 ms to reach maximum amplitude during a hammer strike. Being able to measure quick responses to changes in torque is important during pedaling because the measurement of fast torque changes is necessary to accurately depict what is happening with the device during pedaling. The device was designed to measure the torques placed on the pedal to rotate the crank shaft during pedaling.

The torque measuring device consists of a transducer and two circuits: a transmitter and receiver circuit (Figure 2.2). The design starts with the transducer. The transducer is two strain gauges, one placed on the top and bottom sides of the crank arm. The strain gauges are connected to the transmitter and part of a Wheatstone bridge for

measuring the changes in the gauges during use (Figure 2.3). The Wheatstone bridge is connected to an amplifier which amplifies the signal from the bridge. The signal is then converted from a voltage to a frequency signal by a voltage to frequency converter. The voltage to frequency converter used an integrated oscillator to control the frequency output. The oscillator was set to 7 kHz. The frequency signal is transmitted out of the receiver through an optical transmitter to the receiver circuit using a fiberglass cable. The transmitter circuit is powered by a 12 V Lithium Polymer battery and stepped down to nine volts by a voltage regulator.

The receiver circuit receives the frequency signal with an optical receiver. The signal is converted from a frequency to voltage with a frequency to voltage converter. Then, the signal is low-pass filtered at 200 Hz and amplified. The amplifier feedback potentiometer was set to  $15\text{k}\Omega$  to provide a gain of three. The output of the receiver is transmitted to an analog to digital converter (CED Micro1401 mkII, Cambridge Electronic Design, Cambridge, UK) and sent to a computer. The data is collected using the Spike2 (Cambridge Electronic Design, Cambridge, UK) program. The receiver circuit was powered by a wall outlet and stepped down to  $\pm 12\text{ V}$  and 5 V by an external power supply.

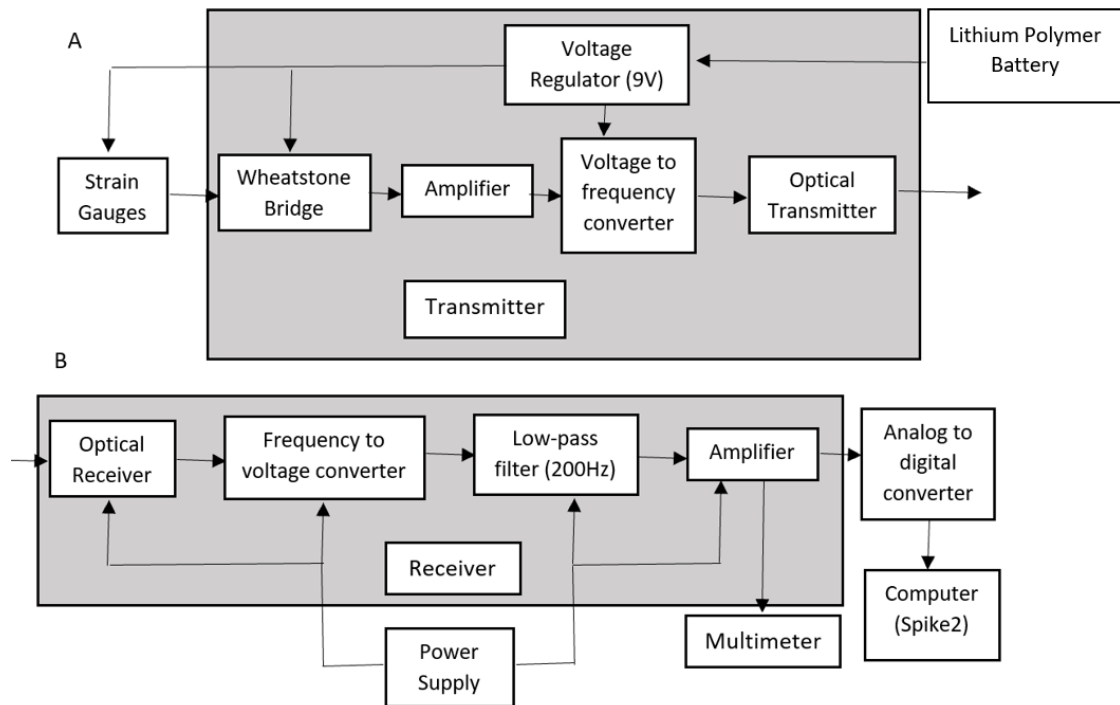


**Figure 2.2: Simplified schematic representation.** A) transmitter and B) the receiver (Duinen 2007). The transmitter circuit has the externally connected strain gauge and battery with both being the same make as the old model. The Spike program that gathers the data from the receiver circuit is the same program used with the old model.

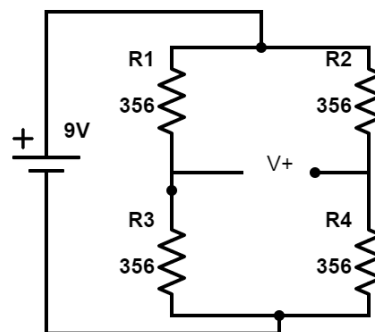


**Figure 2.3: Wheatstone bridge with strain gauges.** Representation of the Wheatstone bridge where R<sub>1</sub> and R<sub>3</sub> are the strain gauges and R<sub>2</sub> and R<sub>4</sub> are resistors. V+ goes to the amplifier and the circuit is supplied by a 9 V source.

### *Design Changes*

The overall design of the circuits needed to be addressed and changed to improve the device use. The transmitter circuit was designed on a printed circuit board (PCB) with both surface mount and through hole components. Using many through hole components may pose problems during use of the device because through hole components do not hold up as well as surface mount during mechanical movements. To remedy the circuit, a new transmitter circuit was designed with all available surface mount components. The original power supply for the receiver was exposed, which could cause problems during use.

Besides changing the transmitter components to surface mount, the layout of the circuit was changed. The original layout of the transmitter had poor placement of components such that important passive components were not near the connected integrated circuit components. As well, the battery and strain gauge wires laid across the entire circuit from the inside of the crank shaft to the outside. The redesign of the transmitter moved the passive components closer to the connecting integrated circuit components decreasing the trace length between components. The battery and strain gauge wires were moved to the end of the PCB near the outside of the crank shaft, so they did not lay across the entire circuit board.

The receiver circuit was originally designed on a protoboard with all through hole components. Many of the wires to connect the components crossed one another. The receiver circuit had a housing unit that could easily be opened, so the use of through hole components with crossing wires posed a problem. The crossing wires may have caused interference on the circuit adding to the issues that were seen with the signal output from

the receiver. The redesign of the receiver was designed on a PCB with all available surface mount components. Using the PCB and surface mount components allowed for components to be placed close together and for there to be no crossing traces. As well, the housing of the receiver was changed to be fully enclosed without easy opening. The housing unit would not need to be opened.

The crank shaft was made of a Delrin tube with an inside liner of a thin copper tube while the crank arm was made of acrylic. Delrin and copper are both sturdy materials, but both being cut to a thin tube decreased the durability of both and acrylic acted as a strong plastic but would not hold up for repetitive use on the pedaling device. The crank shaft was changed to a stainless steel 303 and the crank arm was changed to Delrin. The new Delrin crank arm was also made thicker by 0.5 inches.

The original power supply for the receiver was open with wires attached to the supply channels. These wires, if exposed could pose problems to the power supply or to the user. A new power supply was chosen that was fully enclosed and did not require small wires to attach and supply power externally. This improved the safety of the power supply.

### *User Experience*

Improvements to the user experience are necessary for having a properly working device. The original design had a difficult setup. The previous setup required users to adjust small potentiometers with a small screwdriver while holding a multimeter to different components to set the resistance or voltage on the device. This is a problem because the user had to maintain contact with the probes and test points on the receiver

circuit and had to be careful not to touch other components causing a short circuit. A short circuit would damage the components. These adjustments were completed inside the housing unit of the receiver directly to the receiver circuit.

The original design used single turn potentiometers for adjusting the setpoints of the receiver. As well, the design did not have test points for easy access for adjusting the setpoints. It was difficult to set the resistance and voltages precisely using a single turn potentiometer and placing probes on small wires inside the receiver. There were three adjustments that needed to be made. First, with the power to the receiver off, the adjustment of the first potentiometer was completed while holding a multimeter to pins 2 and 6 of the amplifier for adjusting the feedback resistance to 15 k $\Omega$ . This adjustment set the gain on the amplifier to three for amplifying the signal three times at the output. The second adjust, with the power on, with the second potentiometer had the multimeter probes place don the ground and opposite side ground resistor. The potentiometer was adjusted until the multimeter read 3 V. This adjustment was done to balance the offset of the amplifier. The third adjustment, with the power on, was completed using the third potentiometer and the multimeter probes on the output and ground wires. The potentiometer was adjusted until the multimeter read 0 V to set the output offset to 0 V. For simplifying these adjustments, 10-turn rotary potentiometers were used and attached to the external housing of the new housing unit for the receiver. Banana plugs were added to the external housing unit as well for each access to test points. The potentiometers and test points connected externally allowed for the housing unit to stay enclosed and not be opened during adjustments. The new design allowed for all adjustments to be easily made on the outside of the housing unit using the experimenter's hands to turn the

potentiometer and the multimeter for with easy access to all test points. The higher turn potentiometers enabled the user to more accurately tune the device to the necessary setpoints because of the higher resolution with more turns on the potentiometer.

### *Data Accuracy and Precision*

With the original design, during tests while using the device, issues were seen in the optical connection between the transmitter and fiberglass cable. As well, there were problems with the data accuracy and precision of the device. Accuracy is the relative closeness of the actual data to its expected value while precision is how close similar data points are to one another. Problems with accuracy and precision cause data to be less reliable meaning the data is more difficult trust as correct.

A strong optical connection between the optical transmitter and fiberglass cable is important because it allows for optimal data transfer. In the original design, the fiberglass cable was not secured in place with the optical transmitter, so it moved around. As well, the optical transmitter was not secured tightly to the transmitter circuit board, so the optical transmitter would move as well. Both components moving causes less optical data to be transferred between components, which affects the accuracy of the data. If all of data cannot be collected, there will be issues with the accuracy of the collected data. The new design tightened the connection between the optical transmitter and fiberglass cable by keeping the connector pins on the optical transmitter. As well, the optical transmitter was connected directly to the transmitter circuit board by extending the edges of the circuit, so the optical transmitter could slide onto the board. This connection kept the transmitter from moving out of place.

The baseline of the voltage signal would drift during a single trial while using the device. The baseline drift of the signal could range from -0.18 V to 0.34 V during a single trial. When the full scale output in one direction was 1.9 V, the signal to noise ratio was 3.65. This is a low signal to noise ratio. The drift of the voltage signal may have been related to the low tolerance of the transmitter components and the single turn potentiometer used for tuning the frequency oscillator. Drift in the signal made it difficult to process the data because of the less reliable torque data and the change in the torque under no load.

The original design used low tolerance components and single turn potentiometers. The component tolerances were  $\pm 5\%$ . Lower tolerance components mean less accuracy in the system. If the error from each component compound, problems will arise in the system. To improve upon the accuracy, components were upgraded to  $\pm 1\%$  tolerance. Improving tolerance will improve the accuracy in the system. Single turn potentiometers do not allow for great precision because the potentiometers are more difficult to set at a specific value. The potentiometers were upgraded to 10-turn potentiometers in the redesign because having a 10-turn potentiometer improves the precision of the component.

With the issues that plagued the original design of the torque transducer, a redesign was necessary to improve upon the circuits for better design, user experience, and increase accuracy and precision. The improvements of the redesign of the device for the setup, signal drift, and connection were all described and improved upon.

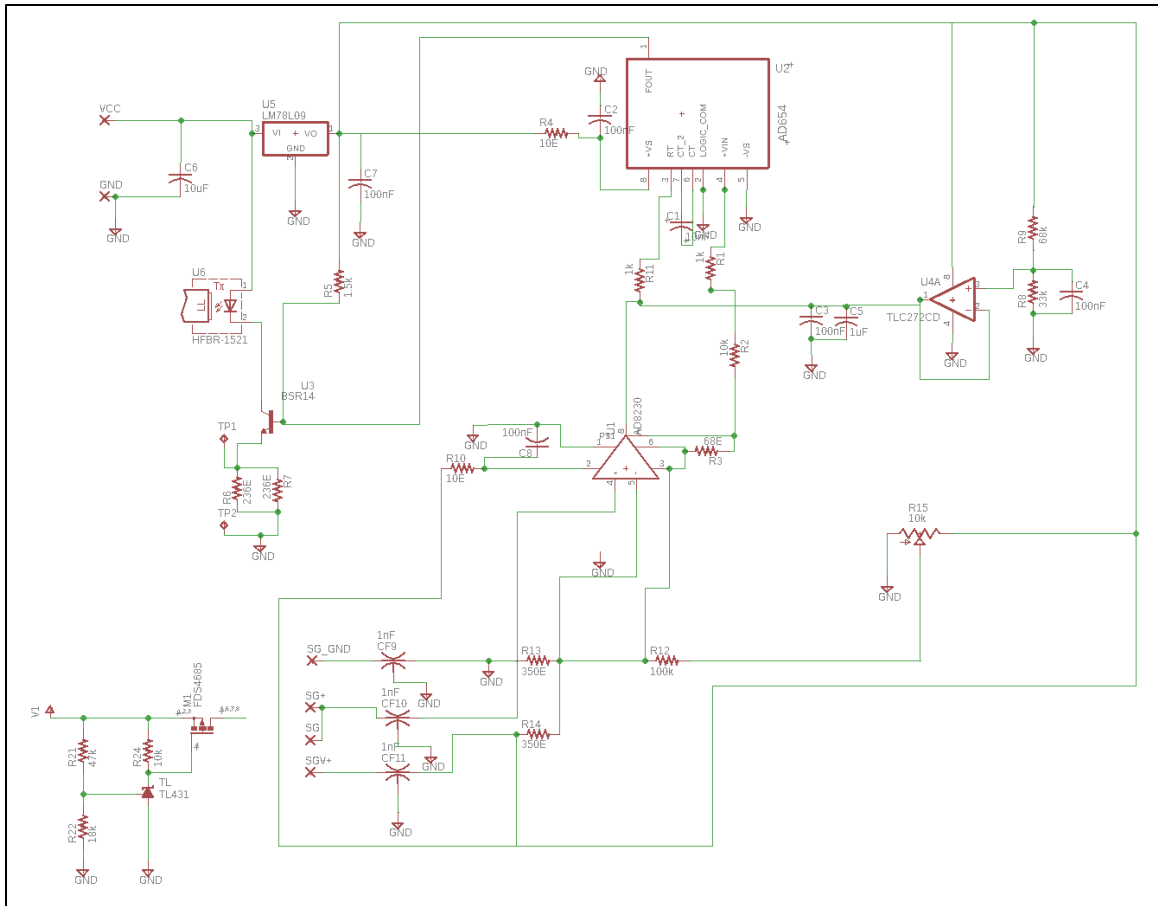


**Figure 2.4: Transmitter circuit board schematic.** Schematic shows both the main redesigned circuit and voltage breakdown circuit. The voltage breakdown circuit is designed to cut off the voltage to the circuit when the supply battery voltage drops below nine volts. This was unchanged from the previous design of the transmitter circuit.

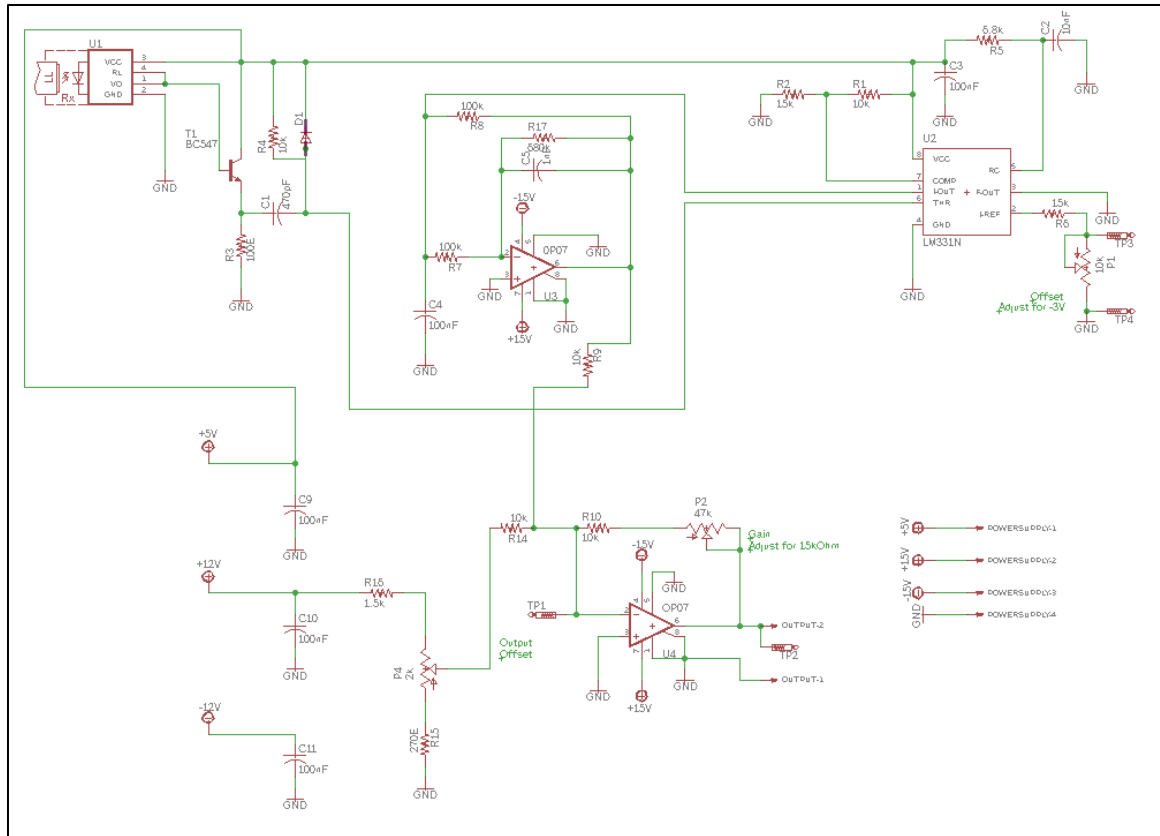


**Figure 2.5: The receiver circuit board schematic.** Schematic shows the redesign. Component values of the receiver were minorly changed from the previous version, but the materials of some of the components and the potentiometers were changed from the previous design.

## Calibration Methods

### Procedure

The calibration of the new torque measurement device was designed to measure the voltage output from a known and calibrated mass. The calibration of the device would provide the calibration curve for converting the voltage from the system's output to torque. Torque is the force applied to the crank arm multiplied by the distance from where the mass was hung to where the crank arm was stabilized. The distance was 0.06875 m. The calibration set up began with mounting the crank arm to a table vice. The

crank arm and the transmitter circuit were secured to a Delrin tube with a copper lining and fastened to a table vice. The crank arm was held off the table with the vice fastened to the table. The crank arm was hung horizontal and measured using a level for accuracy of the placement. A power supply (E3630A Agilent Triple Output DC power supply) was connected to the battery leads. The power supply was used instead of the battery because of the longer testing time than pedaling during a study. As well, the power supply would not decrease in voltage over time the way a battery would. A fiberglass cable was connected from the transmitter circuit to the receiver circuit allowing for data transmission. The receiver was connected to the analog to digital converter using a BNC cable. The receiver was powered from a separate power supply connected to a wall outlet. The power supply for the receiver is the same one used during experimental use. The analog to digital converter (ADC) inputted into the computer to be collected by the Spike2 program. All data were recorded from Spike2.

The calibration began with hanging no mass from the crank arm (Figure 2.6 and 2.7). Hanging the crank arm with no mass provides the baseline zero value. The receiver feedback resistance was set to 15 k $\Omega$  and the receiver output was set to a voltage of zero because there was no mass hanging from the crank arm. Masses were hung from the crank arm at the point where the pedal spindle is inserted into the crank arm. Masses were hung from this point because it is in line with the direction of the strain gauges and the direction of pedaling. As well, this point is in line with the torque generation point of the foot while pedaling on the device. Masses were hung from no mass to 7 kg by 0.5 kg increments. Mass were hung for one minute before increasing the total mass. The masses were stepped from no mass to 7 kg and back to no mass. The calibration was sampled at

2000 Hz. Stepping up and down the scale was completed three times. A second calibration was completed after six months. The first calibration took place on May 11, 2018 and the second calibration took place between January 28 and February 1, 2019. The second calibration was designed the same way as the first and was repeated for five consecutive days. The second calibration had the same setup as the first except for increasing masses to 10 kg, the use of a stainless steel tube for holding the crank arm instead of the Delrin tube with copper lining and a few component changes. The calibrated masses increased to 10 kg because of larger calibrated masses being found between calibrations. Due to damage to the device during the six months between calibrations, a new optical transmitter and transistor were exchanged, and the strain gauge wires were disconnected and reconnected during this process because the wires needed to be removed to replace the damaged parts. The transistor replaced was located between the voltage to frequency converter and the optical transmitter.

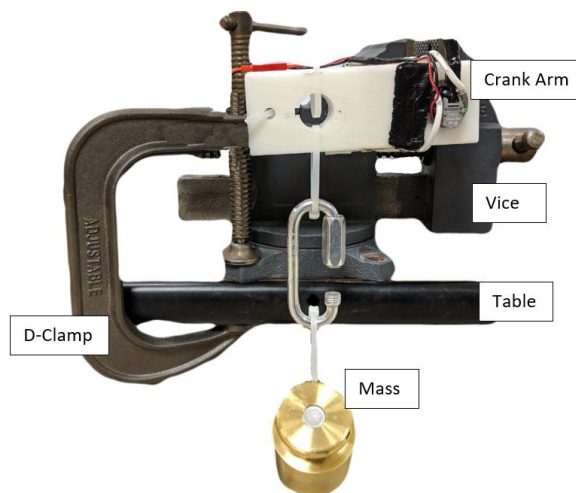


**Figure 2.6: Calibration setup.** Set up of the mass placement and hanging technique, as well as the securing of the table vice to the table. The crank arm is connected to the vice by a Delrin or stainless steel tube.

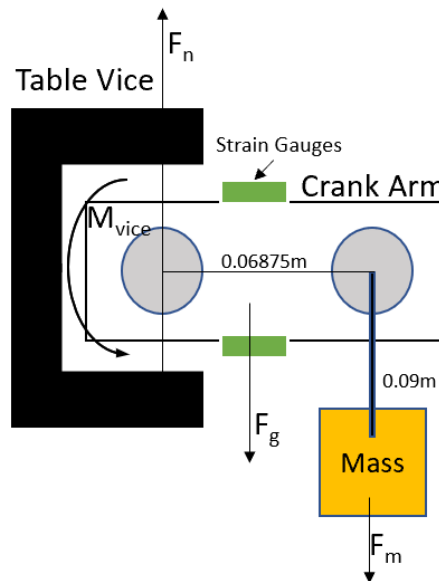


**Figure 2.7: Free body diagram of calibration.** This figure represents the forces and torques applied on the calibration.  $F_n$  is the normal force from the vice,  $M_{vice}$  is the moment opposing the rotation of the crank arm,  $F_g$  is the force of gravity, and  $F_m$  is the force of the mass. The mass times gravity produces the force of torque.

### *Statistical Analysis*

The calibration data collected were analyzed for statistical measures of non-linearity error, repeatability error, hysteresis error, maximum deviation from the mean, and total accuracy (Figure 2.8). Non-linearity error, hysteresis error, and total accuracy all determine the accuracy of the device while repeatability error and maximum deviation from the mean dictate the precision of the device. The voltage data during each one minute trial of mass hung from the crank arm was averaged separately and analyzed to compute standard deviation (std dev) for each trial. A trial consisted of one set of increasing and decreasing masses. The averaged values for each of the same masses were then averaged together to get an average for each mass of all trials. The overall average

masses were used for the conversion from voltage to torque. The linearity of the system was calculated from a line of best fit. Linearity provided the coefficient of determination ( $R^2$ ) and variation (R). Repeatability was calculated by finding the standard deviation of the mean at each mass. Hysteresis was computed by comparing the overall minimum ( $y_{min}$ ) and maximum ( $y_{max}$ ) values of torque with the minimum and maximum values at the midpoint ( $y_{nm}, y_{np}$ ). The maximum deviation is the maximum difference from the center point of the averaged data. Total accuracy was found from the total error of the system comparing the actual values ( $y_a$ ) with the expected values ( $y_o$ ) from the linear fit and divided by the total number of points (n).

$$Non - Linearity Error (\%) = \frac{\left(\frac{(y_{max} - y_{min})}{2} + y_{min}\right) - y_{np}}{\left(\frac{(y_{max} - y_{min})}{2} + y_{min}\right)} * 100$$

$$Repeatability Error = \frac{std\ dev}{\sqrt{n}}$$

$$Hysteresis Error (\%) = \frac{y_{nm} - y_{np}}{y_{max} - y_{min}} * 100$$

$$Total Accuracy (\%) = \frac{1}{n} \sum_{m=0}^n \frac{y_a - y_o}{y_a} * 100$$

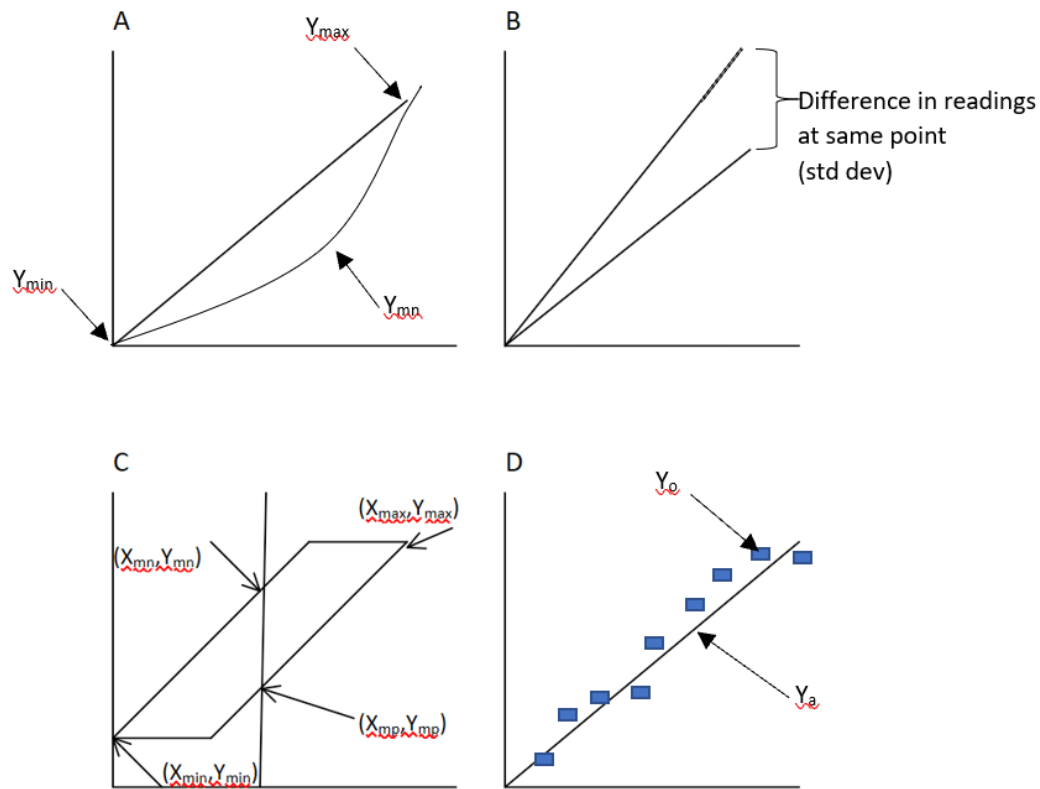


**Figure 2.8: Equation graphs.** This figure represents the different equations and the corresponding graphs for visual representation. A) Graph for non-linearity error. B) Graph for repeatability error. C) Graph for Hysteresis Error. D) Graph for total accuracy.

## Results

### *Design Changes*

The transmitter and receiver circuits were upgraded with resistors and capacitors with one percent tolerance compared to the five percent tolerance of the through hole resistors previously used. All integrated circuit components were made surface mount if available. Components were placed in closer proximity to one another because of the smaller component size. The shorter lead lengths provided low noise in the circuit. The frequency spectrum for measuring the frequencies that effect the calibration signals can be seen in Figure 2.9. The frequency spectrum shows that higher frequencies have more

power at no load than with load. The increased magnitude at higher frequencies affects the variability at no load. The magnitude of the frequencies do not level off on the low end until greater than 200 Hz at no load while with load reaches the same magnitude closer to 50 Hz.

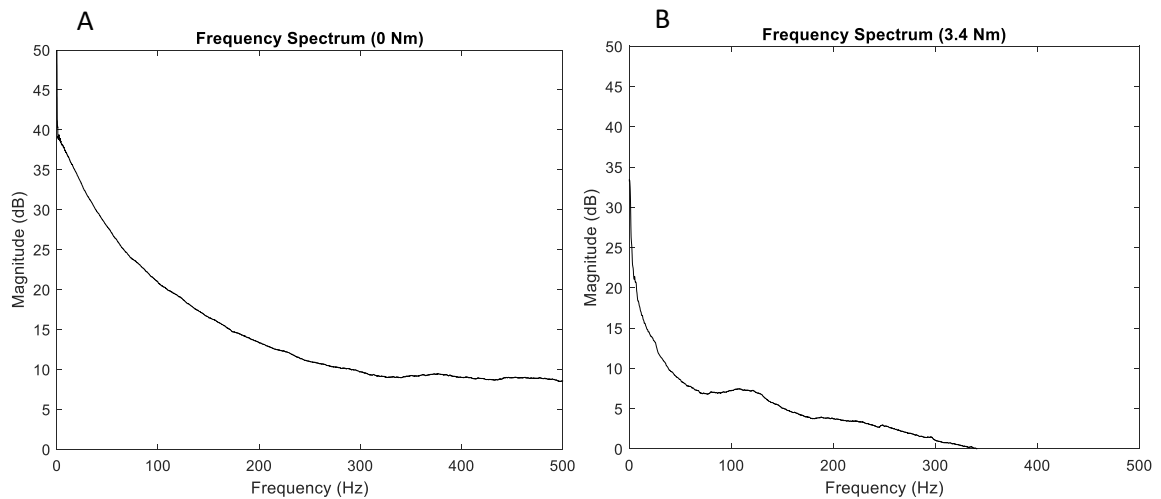


**Figure 2.9: Frequency spectrum.** The frequency spectrum shown from A) no torque and B) 3.4 Nm. The frequency spectrum represents the power of different frequencies that affect the signal.

### *Calibration 1: Left and Right*

The voltage calibration for the three loops for the left and right along with the loop average can be seen in Figures 2.10 and the inverse of the calibration showing the conversion to torque can be seen in Figure 2.11. The calibration is based on known torques, which can be seen in Figures 2.12 and 2.13. The conversion from voltage to torque provided by the first calibration can be seen in Figures 2.14 and 2.15 and results in 1 V being equal to 8.15 Nm and 4.27 Nm for the left and right transmitters, respectively for the positive torques. Negative torque provided a conversion of 9.33 Nm and 2.67 Nm

per volt for the left and right. The conversion is needed to find the amount of torque and work that is done during pedaling by a subject. These measurements are important for defining aspects of the pedaling characteristics.

The statistical analysis (Table 2.1) of the left and right calibration produced a high total accuracy at 98.9% and 98.1%. Error in the system came from repeatability, hysteresis, and linearity. The left calibration error was below 10% with hysteresis and linearity error being below 3%. The right calibration error was 5% and below for all measurements (Table 2.1). There was a low overall error in the device, and it is shown that the transducer error does not play a role in affected measurement outcomes.

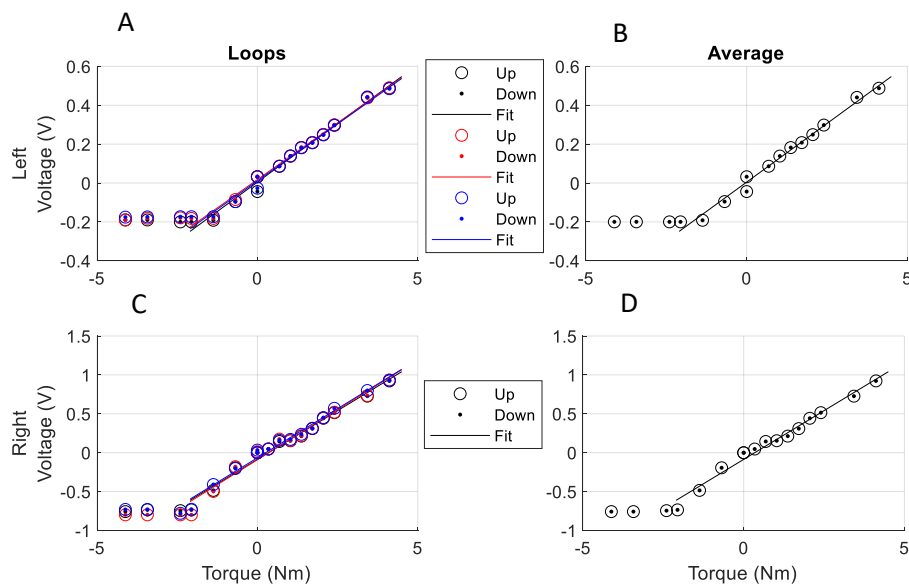


**Figure 2.10: Calibration for the left and right transmitters.** The A) left loops, B) left average, C) right loops, and D) right average transmitter and crank arm are shown. The above shows each loop completed during the beginning calibration of the conversion of torque to voltage. Torque is known by multiplying the mass, gravity and distance. The loops represent one cycle of adding and removing mass.

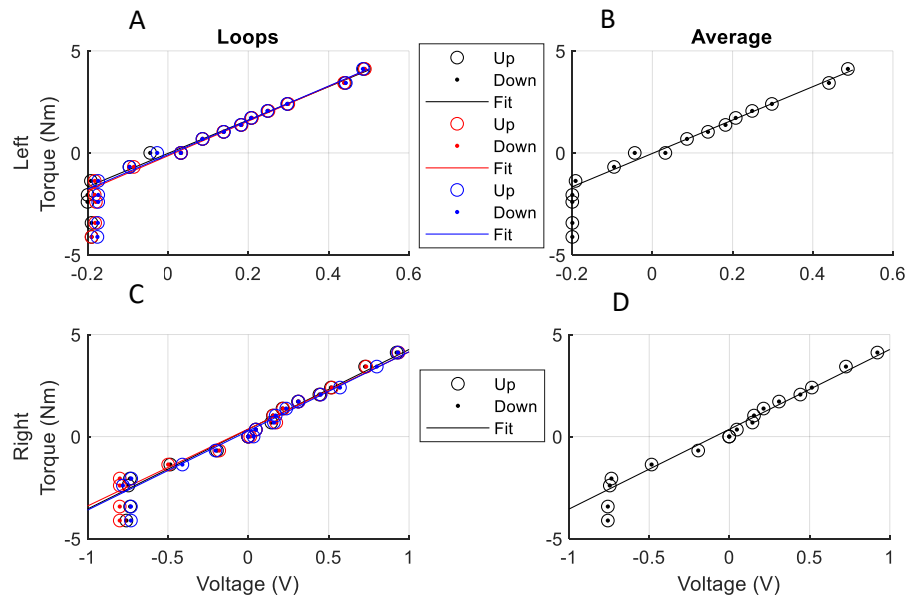


**Figure 2.11: Conversion of the calibration.** The left (top) and right (bottom) transmitter and crank arm. The above shows each loop completed during the beginning calibration of the conversion of voltage to torque. Torque is the dependent value calculated based on the voltage collected. The loops represent one cycle of adding and removing mass.

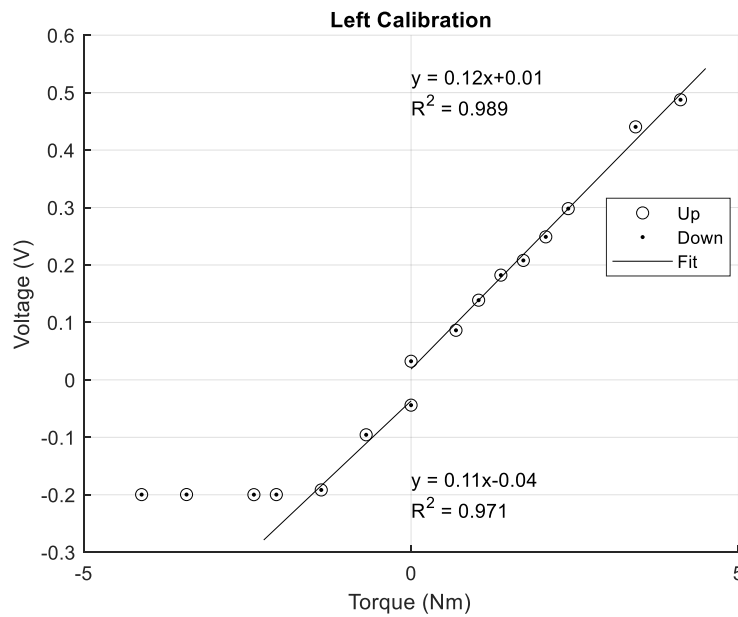


**Figure 2.12 Calibration curve of left torque sensor.** Positive and negative torques represent the different sides of the device. The positive torques apply to the top side of the device with negative torque applying to the bottom side of the device.

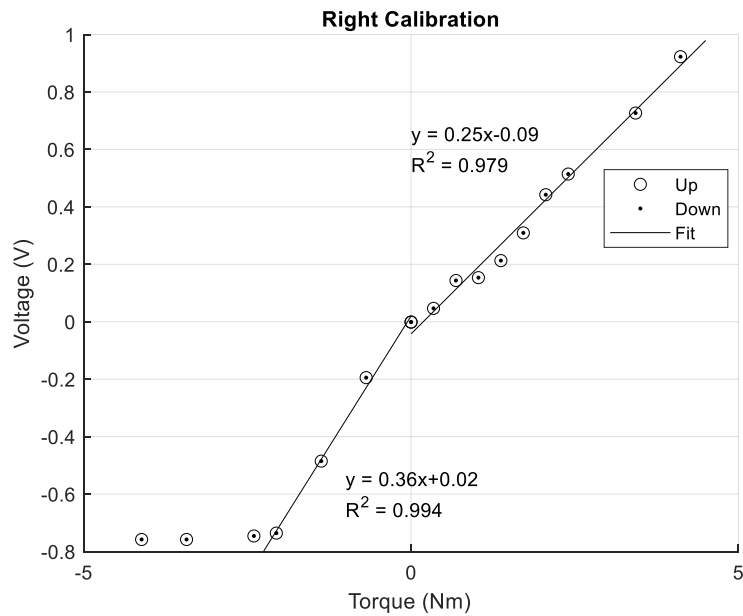


**Figure 2.13: Calibration curve of right torque sensor.** Positive and negative torques represent the different sides of the device. The positive torques apply to the top side of the device with negative torque applying to the bottom side of the device.

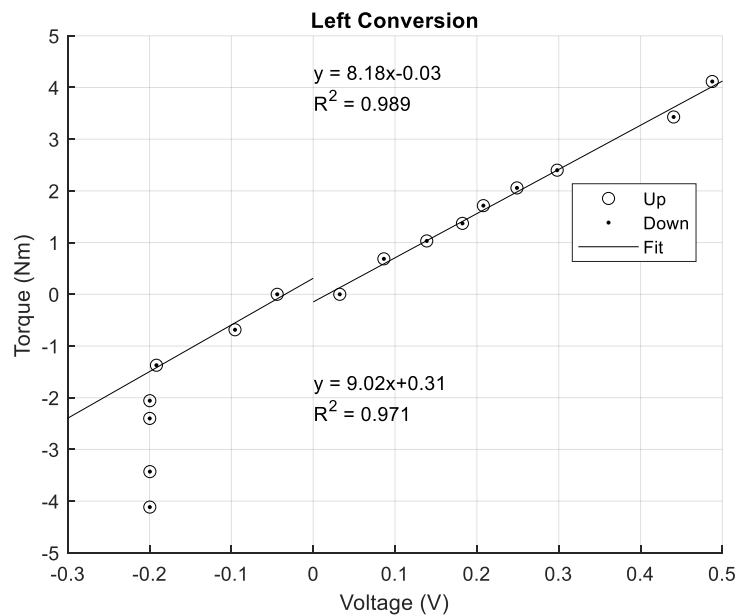


**Figure 2.14: Conversion of the left calibration.** The conversion provides voltage as the independent variable. Voltage as the independent variable is needed for data collection because voltage is the signal collected.

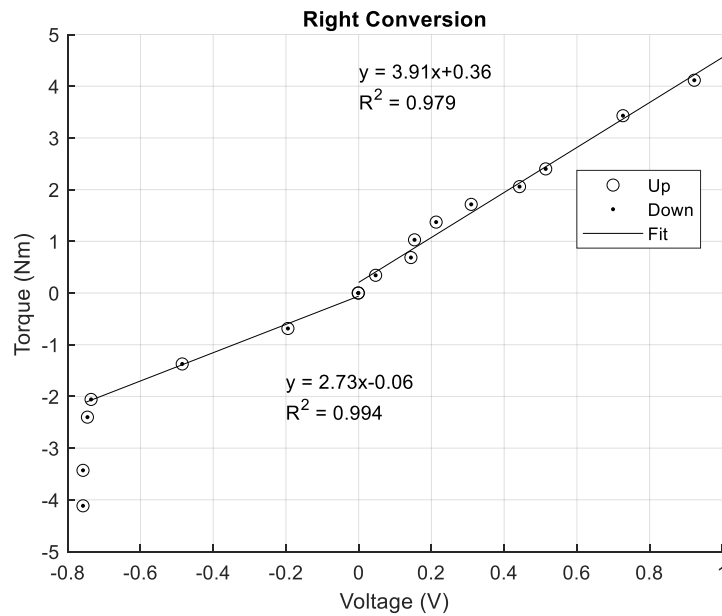


**Figure 2.15: Conversion of the right calibration.** Conversion to provide voltage as the independent variable. Voltage as the independent variable is needed for data collection because voltage is the signal collected.

Measurement	Left Calibration	Right Calibration
Conversion from voltage to torque	+1V = 8.15 Nm -1V = 9.33 Nm	+1V = 4.27 Nm -1V = 2.67 Nm
Total Accuracy	98.9%	98.1%
Coefficient of Determination ( $R^2$ )	+Nm 0.989 -Nm 0.971	+Nm 0.979 -Nm 0.994
Repeatability Error	2.5%	1.8%
Hysteresis Error (%)	2.22%	5.89%
Non-Linearity Error (%)	8.33%	5%
Maximum Deviation	0.0473V	0.0155V

**Table 2.1: Measurement system error for beginning calibration.** The error measurements provide the conversion from voltage to torque, total accuracy,  $R^2$ , repeatability, hysteresis, non-linearity, and maximum deviation errors.

### Unused Calibration Fits

There are three other fits for the calibration data that were used for comparison: a linear fit (Figure 2.16), piece-wise linear fit with zero intercept (Figure 2.17), and polynomial fit (Figure 2.18). These fits were unused because the piece-wise linear fit was the best fit for the calibration. The linear fit is a single linear line fitted to the whole calibration. The linear fit has an  $R^2$  of 0.987 for the left and 0.979 for the right calibration. The second fit is a piece-wise linear fit with a forced intercept through the origin. This fit produced an  $R^2$  of 0.989 and 0.979 for the positive values and 0.828 and 0.992 for the negative values for the left and right calibration. The last fit used was a piece-wise polynomial fit. The polynomial fit resulted in an  $R^2$  of 0.994 and 0.992 for the positive values and 0.999 and 0.997 for the negative values for the left and right calibration, respectively. The three unused fits had greater error due to linearity and hysteresis and had a lower total accuracy (Table 2.2). The polynomial fit could not be used because it was a non-linear fit.

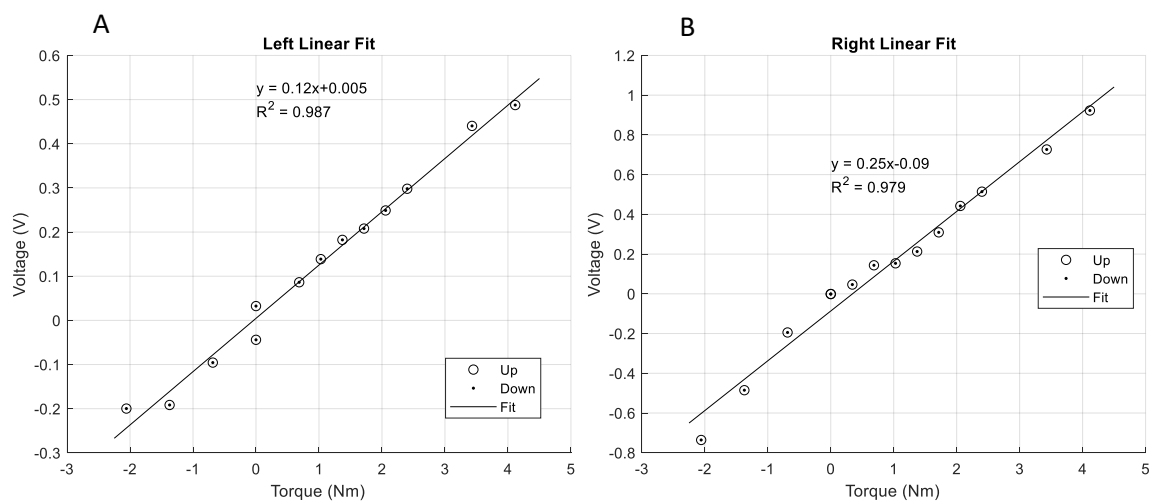


**Figure 2.16: Single linear fit for torque calibration curve.** Linear fit was placed as a single fit for the A) left calibration and B) right calibration. The left linear fit produced a

slope= 0.12 V/Nm and  $R^2 = 0.987$ . The right linear fit produced a slope= 0.25 V/Nm and an  $R^2 = 0.979$ .

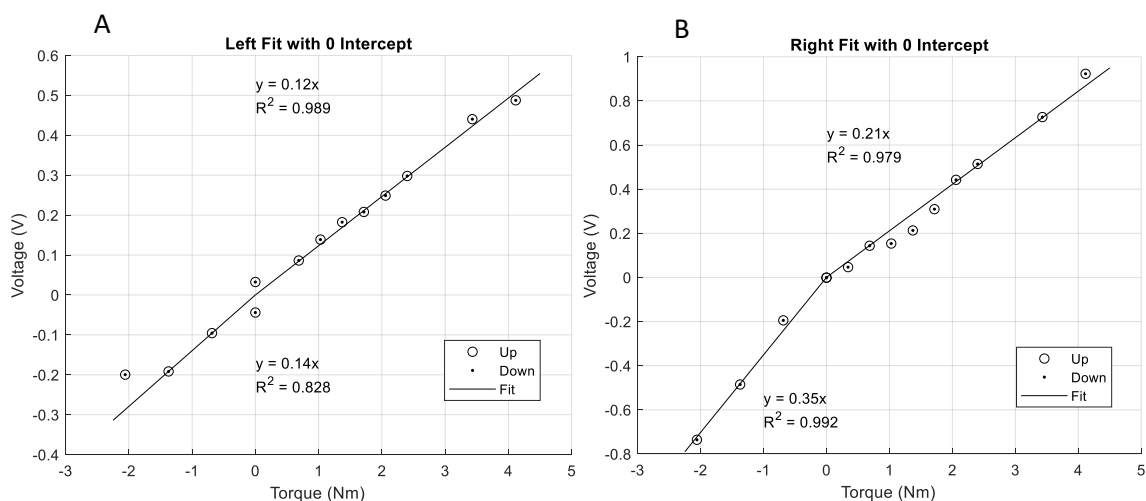


**Figure 2.17: Linear fit with intercept forced through zero.** The zero intercept linear fit shows the A) left fit with a slope= 0.12 and  $R^2=0.989$  for the positive values and slope= 0.14 and  $R^2=0.828$  for the negative values. B) right fit with a slope= 0.21 and  $R^2=0.979$  for the positive values and slope= 0.35 and  $R^2=0.992$  for the negative values

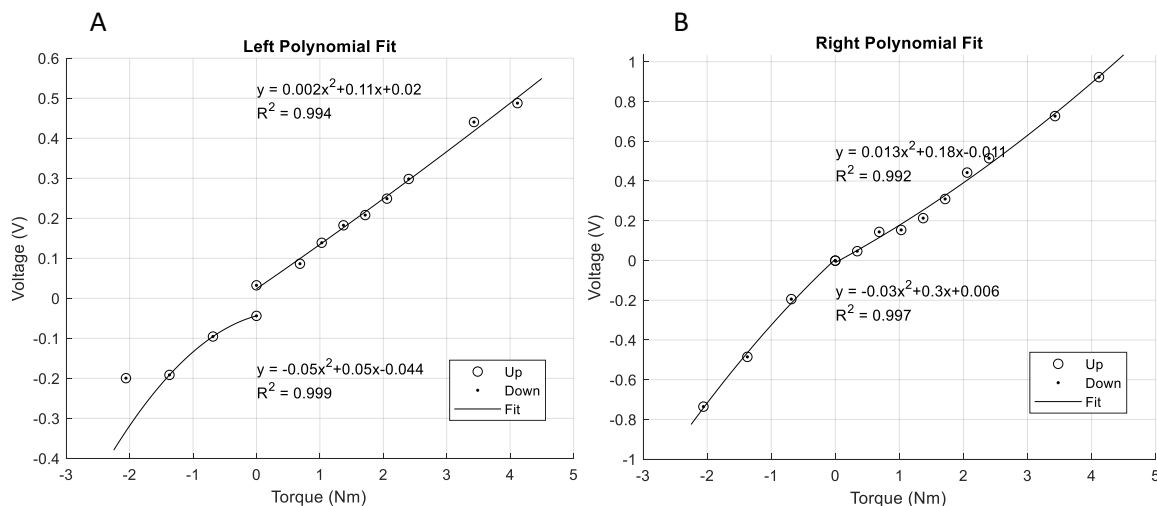


**Figure 2.18: Polynomial fit for calibration curve.** The polynomial fit shows a second order fit for the A) left and B) right values. The left fit produced  $R^2 = 0.994$  for the positive values and  $R^2 = 0.999$  for the negative values. The right fit produced  $R^2 = 0.992$  for the positive values and  $R^2 = 0.997$  for the negative values.

Measurement	Non- Linearity Error (%)	Coefficient of Determination ( $R^2$ )	Total Accuracy	Conversion from voltage to torque
Left Linear Fit	-11%	+Nm 0.987 -Nm 0.987	98.7%	+1V= 8 Nm -1V= 8 Nm
Right Linear Fit	10%	+Nm 0.979 -Nm 0.979	97.3%	+1V= 6.3 Nm -1V= 6.3 Nm
Left 0 Intercept	-11%	+Nm 0.989 -Nm 0.989	95.7%	+1V= 8.3 Nm -1V= 7.14 Nm
Right 0 Intercept	10%	+Nm 0.979 -Nm 0.992	94.8%	+1V= 4.8 Nm -1V= 2.9 Nm
Left Polynomial	Non Linear	+Nm 0.994 -Nm 0.999	98.5%	+1V= 7.6 Nm -1V= 10 Nm
Right Polynomial	Non Linear	+Nm 0.992 -Nm 0.997	95.1%	+1V= 5.5 Nm -1V= 3.6 Nm

**Table 2.2: Error measurements for unused calibration fits.** The error measurements for the calibration fits that are shown are the errors that change when the curve changes. The conversion from voltage to torque, total accuracy,  $R^2$ , and non-linearity are shown.

### *Calibration 2: Left*

The second calibration of the left transducer six months after the first was based on known torque inputs is seen in Figure 2.19. The five day calibration showed low repetition error of loops and low day to day variability (slope = 0.2, 0.27, 0.24, 0.26, and 0.25). The conversion of the torque and voltage for voltage as the independent variable is in Figure 2.22. The averaged calibration of the device is represented in Figure 2.20. The

left calibration conversion resulted in a voltage to torque conversion of 0.134V per Nm for positive torque values. The conversion from voltage to torque resulted in 4.113 Nm per V. The negative torque calibration found a voltage to torque conversion of 0.287 V per Nm and inversely 3.241 Nm per V (Figure 20 and 22). The left transducer was maxed out at -0.8 V on the low end causing no voltage increase even after increases in torque.

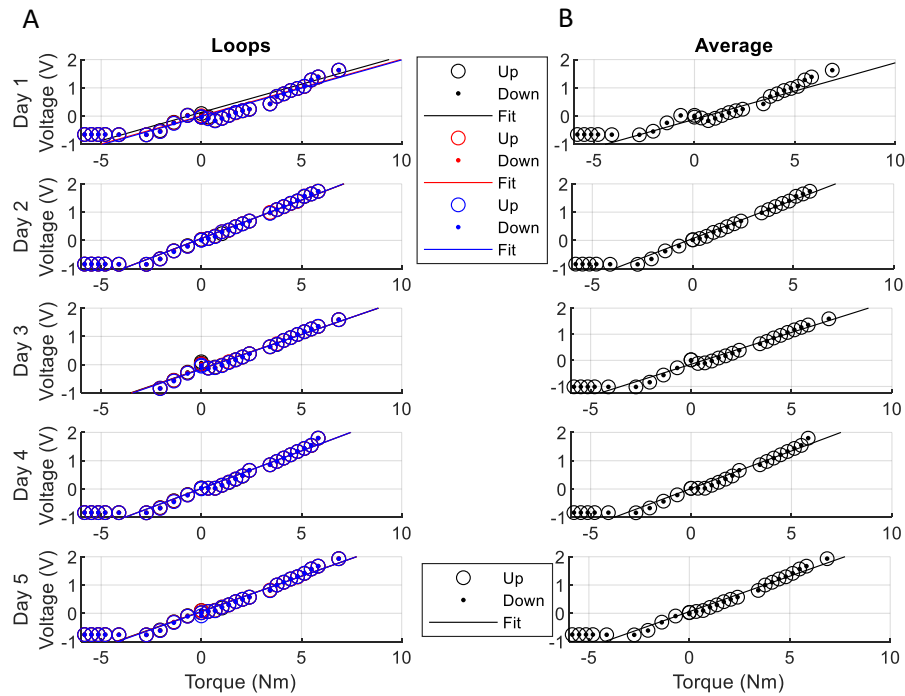


**Figure 2.19: Left torque transducer calibration.** 5 consecutive day calibration of the left torque transducer showing A) each day of loops and B) the average of all the loops for that day. Each day had 3 loops and the average of each day is the combined average of all 3 loops.

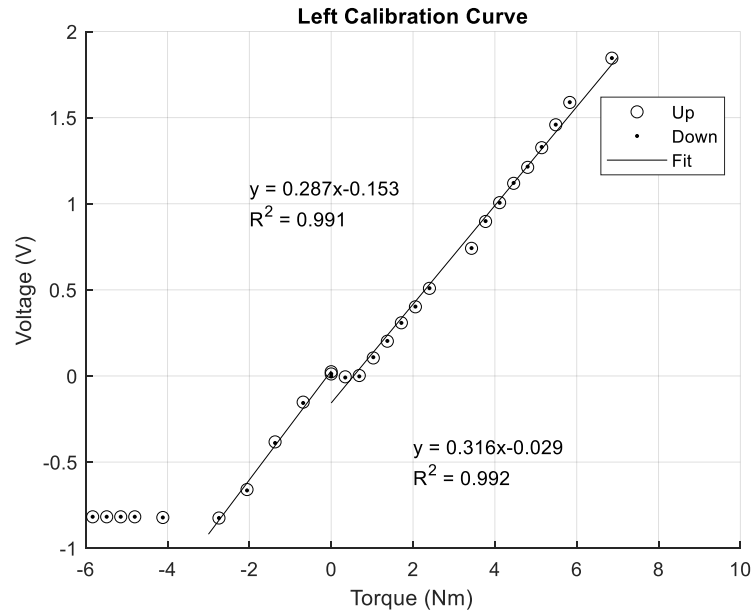


**Figure 2.20: Overall left calibration.** Averaged calibration of all 5 days of calibrating. The positive and negative torques provide separate linear fits for differences in sides. The bottom side linear fit corresponding to negative torques is completed without the lower limit bounds to keep linearity.

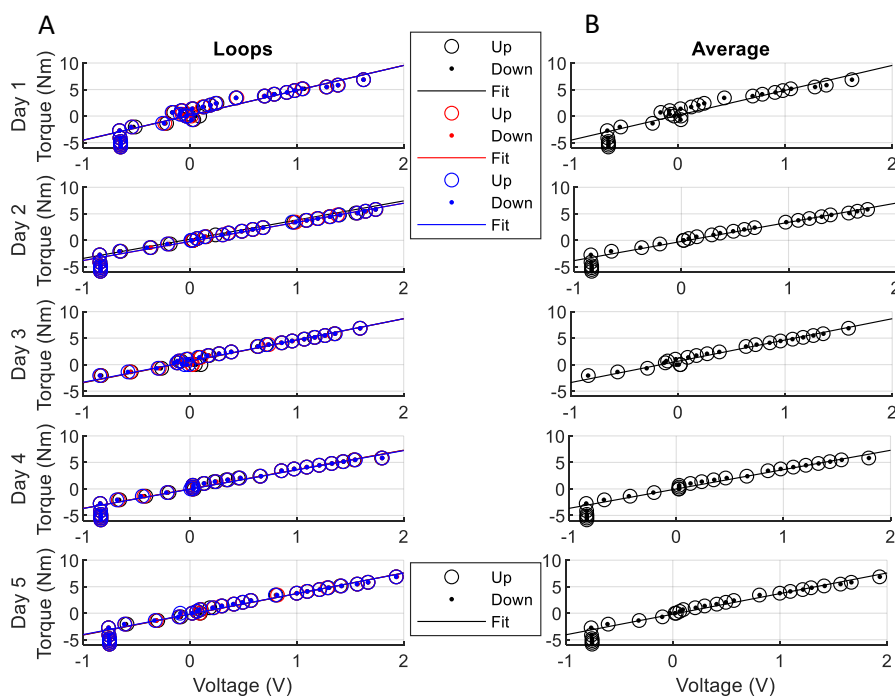


**Figure 2.21: 5 day calibration conversion: left.** The conversion of voltage to torque showing A) the loops each day and B) the day by day average of that day's loops. This is the inverse of Figure 2.18.

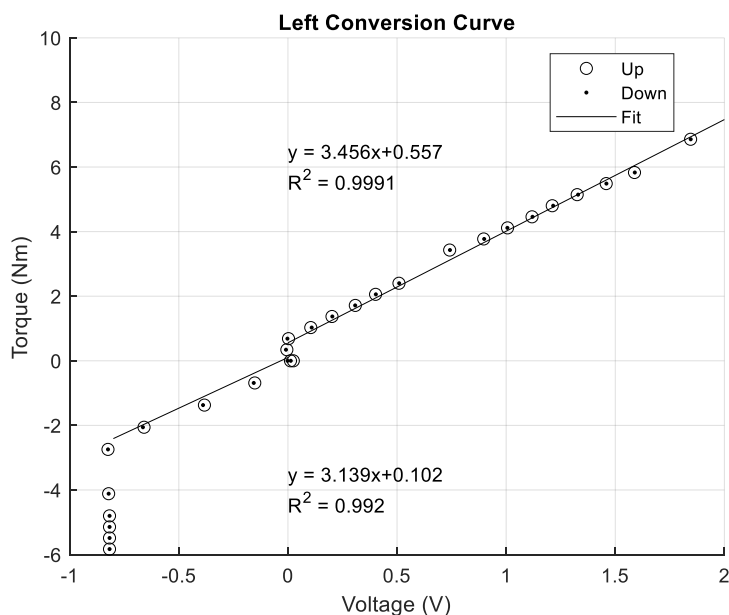


**Figure 2.22: Total calibration conversion of the left torque transducer.** This is an inverse of the Figure 2.19. The lower bounds threshold is not included in the linear fit.

### Calibration 2: Right

The right transducer calibration over 5 consecutive days can be seen in Figure 2.23. Each day has 3 loops of calibration runs and the loops are averaged to produce the averaged graph  $A$  each day. The right calibration resulted in a voltage to torque conversion of 0.146 V per Nm for positive torque values (Figure 2.24). The conversion from voltage to torque resulted in 5.25 Nm per V (Figure 2.25, 2.26). The negative torque calibration found a voltage to torque conversion of 0.546 V per Nm and inversely 1.56 Nm per V (Figure 2.25, 2.26). The five day calibration showed minimal repetition error of loops and low day to day variability (slope = 0.3, 0.31, 0.22, 0.24, and 0.25) similar to the left transducer calibration.

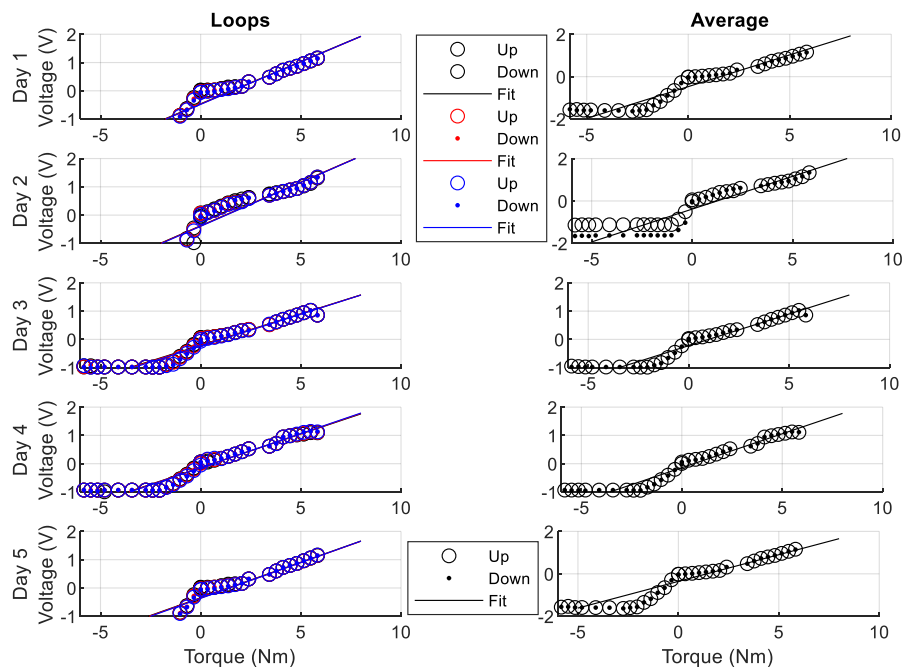


**Figure 2.23: Right torque transducer calibration.** 5 consecutive day calibration of the right torque transducer showing A) each day of loops and B) the average of all the loops for that day. Each day had 3 loops and the average of each day is the combined average of all 3 loops.

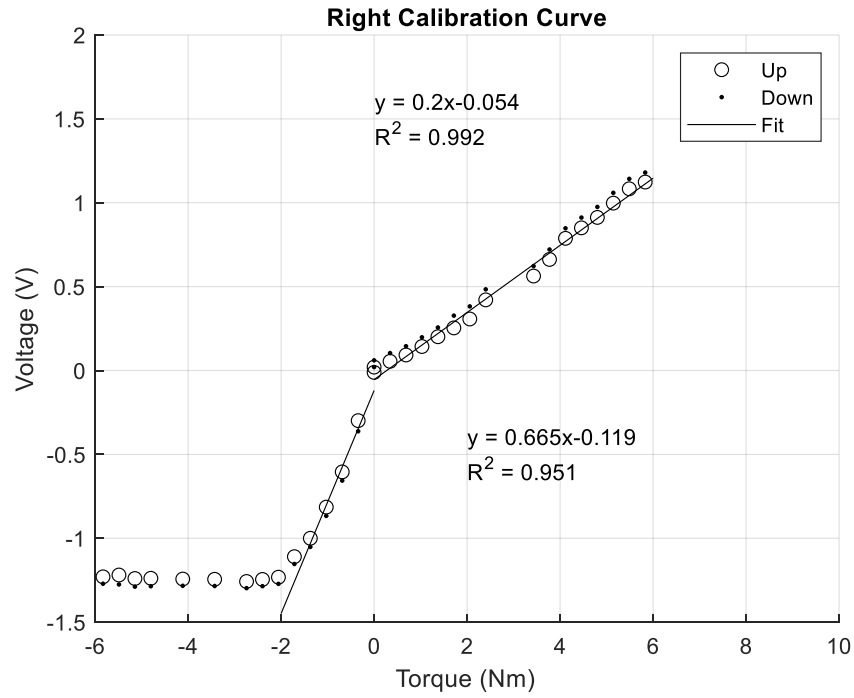


**Figure 2.24: Overall right calibartion.** Averaged calibration of all 5 days of calibrating. The positive and negative torques provide separate linear fits for differences in sides. The bottom side linear fit corresponding to negative torques is completed without the lower limit bounds to keep linearity.

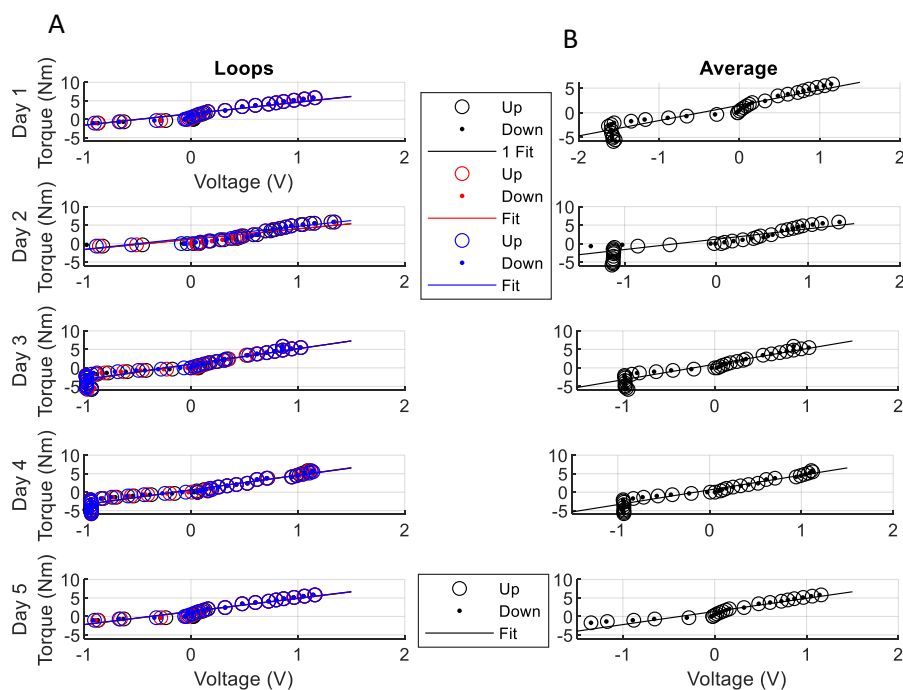


**Figure 2.25: 5 day calibration conversion: right.** The conversion of voltage to torque showing A) the loops each day and B) the day by day average of that day's loops. This is the inverse of Figure 2.22.

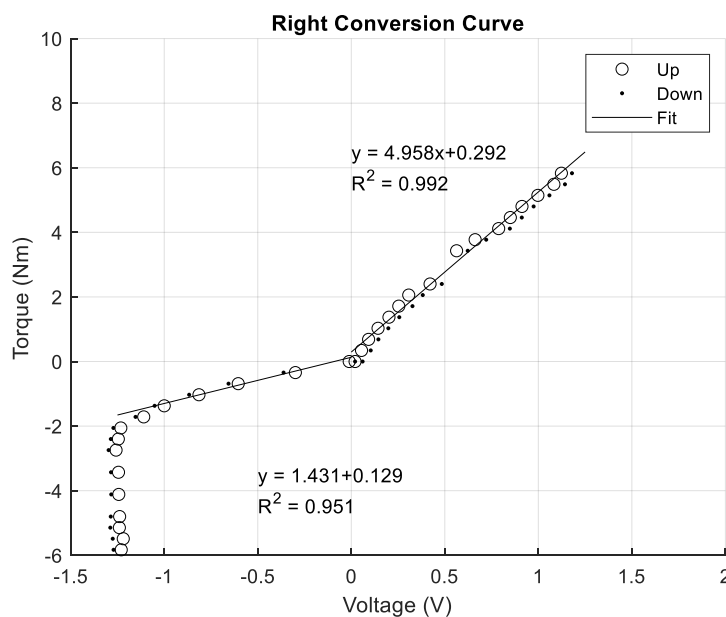


**Figure 2.26: Total calibration conversion of the right torque transducer.** This is an inverse of the Figure 2.23. The lower bounds threshold is not included in the linear fit.

### *Analysis of Torque Transducer*

The conversion from voltage to torque provided by the end calibration results in 1 V being equal to 4.11 Nm and 5.25 Nm for the left and right transmitters, respectively for the positive torques. Negative torque provided a conversion of 3.24 Nm and 1.56 Nm per volt for the left and right. The conversion is needed to find the amount of torque and work that is done during pedaling by a subject. These measurements are calculated based on the piece-wise linear regression fit to the averaged final calibration data.

The statistical analysis of the left and right calibration produced a high total accuracy at 99.48% and 97.06%. Error in the torque transducer was measured across the same areas as the beginning calibration. The left calibration error was below 5% for all error measurements. The analysis of the right transducer produced error below 5% similarly to the left transducer. The difference being a lower hysteresis, but a higher non-linearity error. There was a low total error in the transducer.

Measurement	Left Calibration	Right Calibration
Conversion from voltage to torque	+1V = 4.11 Nm -1V = 3.24 Nm	+1V = 5.25 Nm -1V = 1.56 Nm
Total Accuracy	99.48%	97.06%
Coefficient of Determination ( $R^2$ )	+Nm = 0.987 -Nm = 0.992	+Nm = 0.984 -Nm = 0.951
Repeatability Error	2%	3%
Hysteresis Error (%)	3.13%	1.75%
Non-Linearity Error (%)	1.36%	3.5%
Maximum Deviation	0.038V	0.042V

**Table 2.3: Measurement system error for end calibration.** The error measurements provide the conversion from voltage to torque, total accuracy,  $R^2$ , repeatability, hysteresis, non-linearity, and maximum deviation errors.

Device Fabricator	Total Accuracy (%)	R <sup>2</sup>	Repeatability	Hysteresis (%)	Torque Measurement	MR Compatible
Gusso et al.*	-	0.999	-	-	Load Cells	Y
Pedersen et al.;	97%	-	-	-	MRI cardiac	Y
Roest et al.*					ergometer,	
					Lode BV	
Rappaport and Schindler-Ivens	98%	0.983	98%	2.44%	Strain Gauge	Y
Chinworth and Zimmermann	96%	-	-	-	Strain Gauge	N
Duinen	>95%	0.999	0.065N	-	Strain Gauge	Y
Broker and Gregor*	-	-	-	-	Piezoelectric force pedal system	N
Cheng et al.	-	-	-	-	Deflection of pendulum corresponding to flywheel friction	Y, open magnet
Brown and Kautz; Davis and Hull	-	-	-	-	Plantar five-bar linkage model for crank and pedal rotation	N
Jeneson et al.	-	-	-	-	No torque	Y

**Table 2.4: Comparison of other devices to the designed device.** The comparisons are based on total accuracy, R<sup>2</sup>, repeatability, and hysteresis. Devices are ranked from top to bottom as most accurate to least accurate based on total accuracy. If there is no total accuracy the device is then compared by the next item. Comparison includes devices designed by private companies designed in research labs. All devices are pedaling devices except for van Dunman. This was the device the torque transducer was based on. \*Denotes the device was designed and fabricated by a private company.

## Discussion

Accurate torque measurements in and out of the MRI scanner are important for understanding torque symmetry in pedaling. Especially, in stroke survivors where the use of the affected limb is typically lower than that of the non-affected limb (Kautz and Brown 1998). A torque transducer capable of measuring applied torque to a pedaling device has been designed in this study. Torque measurement should be both accurate and

precise. Accurate refers to the closeness of the torque values to the measured standard and precise is referring to the closeness of the torque values at the same voltage.

Measuring torque using the torque transducers is shown to be both accurate and precise. The torque transducers were redesigned for improvements in design and functionality. Design improvements were focused on circuit board components and layout. The functionality of the device is based on high accuracy and precision.

### *Circuit Board Components and Layout*

Improvements to circuit board components and layout is shown to improve the accuracy of the device while providing a more robust system. The improved accuracy is seen by the high total accuracy and low error values. Resistor and capacitors were chosen with increased tolerance from 5% to 1%. All components which could be found as surface mount were used to provide smaller lead lengths from component to component. Shorter lead lengths decrease potential interference in the circuit because longer connecting leads have greater chance of picking up noise. The noise in the signal is minimized shown in Figure 2.7. The clean square wave generated by the transmitter circuit frequency converter from the applied voltage shows the frequency converter in the circuit before transmission to the receiver is not contaminated with noise. The frequency spectrum (Figure 2.8) after passing through the receiver circuit and being converted back to a voltage signal shows low frequencies in the signal. Noise contamination in the receiver would show an increase in power at higher frequencies, which is not the case because there is low power at higher frequencies.. The filter in the receiver is a low pass filter at 200 Hz. The majority of frequencies being passed through the receiver for

recording are less than 100 Hz with no torque applied and less than 50 Hz with applied torque. The circuitry of the transmitter and receiver circuits with improved components is shown to increase the accuracy and precision of the transducer.

The transducer redesign improved the robustness of the device. The transmitter and receiver circuit board layouts were designed to be more robust and reduce potential for componentry breakage. The change from Delrin and copper to stainless steel for the crank shaft improved the strength of the shaft. The strain gauge and battery supply wires were moved closer to the outside of the device to not allow them to lay across all the other componentry. Moving the wires allowed for easier attaching and removing of the transducer from the pedaling device. A new optical transmitter mounting system was introduced to hold the optical transmitter tighter to the circuit board and reduce the potential of bending to the connecting wires or movement of the optical transmitter. The new mounting system provided better stabilization of the optical transmitter and allowed for easy connection with the fiber optic cable. The new design of the receiver circuit board with rotary potentiometers attached to the top along with banana plugs for test points removed the need to open the housing unit. Not opening the housing unit kept all the componentry inside safe from external factors because the components were not exposed to the outside. This robust design did not need the box to be opened and all gain and voltage settings to be applied from the outside of the housing unit. The layout of both the transmitter and receiver circuit boards have been improved for better long term use.

### *Transducer Calibration*

The torque transducer has been successfully designed to be both accurate and precise, which is consistent with the intent of the redesign for this device. The calibration suggests that the torque transducer can accurately and precisely measure torque during pedaling. The transducer was calibrated for measuring the torque production of pedaling with the device. Despite magnetic fields in an MR environment, the transducer should maintain its range and accuracy and the MR environment should not have any effects on the device (Duinen 2007, Turkseven and Ueda 2013). Duinen showed that their device, which this device was based on, was unaffected by an MRI scanner. The noise spectrum of the scanner with and without the device were not significantly different. Similar results have shown the use of these types of devices can increase the amount of data received from MR environments. The transducer produced a linear calibration curve represented by near 1  $R^2$  values for the specified range, which is expected for this device because of the linear properties of the strain gauges. The transducer was non-linear at the bottoming out point. This was not included in the calibration curve. The bottoming out was not linear due to the frequency range of the oscillator in the transmitter circuit. The oscillator is set at 7 kHz with a minimum of 6 kHz and maximum of 10 kHz. Outside of this range, the device cannot measure torque. As torque is applied to the device, the frequency increases with positive torque and decreases with torque values in the opposite direction. The bottoming out happened in the 6 kHz and below range. Strain gauges linearly change their electrical resistance in response to applied torque, so the strain gauge resistance still changes outside of the

frequency range (Omega 1999, Cimbala 2013). The device has been demonstrated to measure torques and correlates voltage with torque.

The strain gauges of the torque transducer accurately respond to increases and decreases in torque on the top and bottom sides of the device. It is shown that there is a difference in sensitivity between the two sides of the device and between the two transducers (Figure 2.20, 2.22 and Figure 2.25, 2.26). Differences in sensitivity between sides of the transducer or between transducers may be a product of the strain gauge attachment to the Delrin crank arm. Assuming the Delrin is uniform across the crank arms, the sensitivity difference may be due to how the strain gauges are directly attached to and placed on the crank arm. All gauges were placed at the center of the top and bottom sides of both devices parallel to the length of the crank arm. The gauges being placed off center in either the parallel or perpendicular direction to the crank arm would cause a change in the gauge sensitivity in relation to the crank arm and thus cause different torque-voltage relationships. As well, since the gauges are attached with glue, the difference in amount of glue used to attach the gauge would provide a difference in the sensitivity affecting the torque-voltage relationship. More glue being used would decrease the sensitivity of the strain gauge because the glue is malleable. The amount of glue used was not controlled for attaching the strain gauges to the crank arm.

The two calibrations show a bottoming out, previously mentioned, in regards to voltage clipping of the calibration below 1.25 Nm and 2 Nm for the left and right, respectively. The bottoming out of the calibration on the low end is due to the design of the frequency oscillator of the transmitter circuit. The oscillator operates between 6 kHz and 10 kHz. The circuit was set to 7 kHz because that was what was done by Duinen and

the original designer of the first iteration of this device (Duinen 2007). The frequency increases as loads are added to the top side while the frequency decreases while loads are applied to the bottom side, so the bottoming out of the calibration is due to an excess of load on the bottom side of the device that causes the frequency to cross below 6 kHz. The transmitter circuit could be set higher than 7 kHz, but it is unknown what frequency corresponds to a certain load. If the circuit was set too high, the calibration could have topped out causing the same circumstance on the upper side. Increasing the set point would be recommended if the device was calibrated a third time for the new set point. It is unknown if there is a better set point or if 7 kHz is the best option. The bottoming out effect causes the loss of quantifiable torque beyond the minimum voltage. During pedaling, this could make a minimum value not as low as it actually is meant to be. This is only a problem if a user is pedaling and produces torques below the minimum amount.

The first calibration provided the calibration that will be used for the pedaling studying in Chapter 3 (Figure 2.14, 2.15). The calibration had largely different calibration curves for the left and right transducers. This difference may present a sensitivity difference where the right transducer is more sensitive than the left because of the right transducer has a wider range of voltages for the applied torques. The two calibrations are similar in the torque measurement range for maximum torque and linearity. Both transducers are capable of accurately producing the torque traces seen during pedaling. The end calibration resulted in a different calibration curve compared to the beginning calibration. Prior to the second calibration, the strain gauge wires on the left transducer had to be repaired due to damage during attachment of the transducer to the pedaling device. As well, the optical transmitter on the right transducer was replaced because of a

shorted LED and the transistor was replaced because it is the corresponding component that drives the optical transmitter. Chinworth and Zimmermann reported similar issues with a wear and tear effect of using a similar strain gauge device. They mentioned making changes and fixing componentry on their device. They described repairing wires and cable-to-cable connections which were subject to floor contact. The wear and tear they had caused them to cease data collection and with continued use, problems became progressively worse (Chinworth and Zimmermann). Changes to components and fixing the device may have been the cause of the difference in the calibration changes from the first to second calibrations. Chinworth and Zimmermann found similar results with changes in equations from different calibrations but maintaining similar slopes. They attested their differences to the device design and fabrication they could not control (Chinworth and Zimmermann). This may lead to the possibility that the left transmitter had a non-functioning strain gauge causing the first calibration to be twice the second calibration slope with the gauge being fixed at the second calibration. The right transducer did not change significantly between the first and second calibration with the new optical transmitter.

### *Comparison to Similar Devices*

Torque measuring devices used during pedaling have been designed by a number of research laboratories and by fewer companies. The devices designed have been both safe and not for use in an MR environment. A comparative layout (Table 2.4) of the different pedaling devices can be found. The different devices each have their own specific qualities and designs but are all used for the same purpose: to measure torque

while pedaling. The method of device measurement of torque includes using load cells, strain gauges, piezoelectric force sensors, pendulum deflection and calculation of torque, and a plantar five-bar linkage model. The devices from Gusso, Pedersen, Roest, and Broker are all developed by private companies (Gusso et al. 2012, Pedersen et al. 1999, Roest et al. 2001, Broker and Gregor 1994). The devices from Chinworth, Cheng, Brown, Davis, and Jeneson are fabricated in a research lab setting (Chinworth and Zimmermann, Cheng et al. 2003, Brown and Kautz 1998, Davis and Hull 1981, Jeneson et al. 2010). The devices used by Pedersen and Roest were the same device and Brown and Davis used the same device as well. The device used by Duinen is not a pedaling device. It is a finger individuation device used to measure maximal force output of the index finger. It is compared because it is the design that the designed torque sensor described is based on.

The devices mentioned have little to no calibration data reported. For the devices that have calibrations that are reported on, there is minimal description of how the calibration was completed. The Duinen device has the most calibration statistics reported mentioning the total accuracy,  $R^2$ , and repeatability. The fabricated torque transducer has similar total accuracy being above 95% but with a lower  $R^2$ , though both are well about 0.95. The repeatability of the Duinen cannot be compared because it is reported differently (Duinen 2007). Both devices are accurate, and it is difficult to say if one is better than another. Other devices that report their accuracy all have above 95% accuracy as well (Pedersen et al. 1999, Roest et al. 2001, Chinworth and Zimmermann). The devices are reported to complete their intended task without issue. The device from Gusso and colleagues reports an  $R^2$  of 0.999 similar to Duinen (Gusso et al. 2012). This is not significantly different compared to the fabricated device. The device used by Gusso

is designed by a private company potentially providing a more robust calibration. The devices from Broker, Cheng, Brown, Davis, and Jeneson have no calibration data reported (Broker and Gregor 1994, Cheng et al. 2003, Brown and Kautz 1998, Davis and Hull 1981, Jeneson et al. 2010). It is difficult to compare similar devices' accuracy measurements when they are not reported. It was aimed to be fully transparent for the design and calibration of the torque transducer.

### *Measure of Pedaling Asymmetry*

The redesign enabled the device to accurately and precisely measure changes in torque. The improved components and device design improve the accuracy of the device, so the torque data measured will be true to the produced torque during pedaling. The minimal variability in the device relating to high precision produces a pedaling system that will measure the same torque under the same load. The new redesigned device was able to measure torque differences down to a scale of 0.2 Nm. The resolution of the measurements suggests that the device can measure pedaling asymmetry. Having high resolution allows for more of an understanding of the asymmetries because the asymmetries can be more distinct. Quantifying asymmetries during pedaling is possible using this torque measuring device.

This device had similar accuracy and  $R^2$  values to devices from other studies that have discussed and shown asymmetries in pedaling (Gusso et al. 2012, Pedersen et al. 1999, Roest et al. 2001, Chinworth and Zimmermann, Kautz and Brown 1998). The other studies mentioned have described differences in pedaling asymmetries and the differences in the torque and work production during pedaling using other devices. The

redesigned device is similarly capable of measuring torque, so the device may similarly be able to measure the pedaling asymmetries. Chinworth and Zimmermann designed a similar strain gauge transducer torque measuring pedaling device which was reported to measure pedaling asymmetries, so the device described here would be able to do the same. The described device is able to quantify the torque produced during pedaling, which will provide pedaling asymmetry.

#### *When a New Calibration is Needed*

In the event of one of the following scenarios, a new calibration should be completed. A new calibration should be completed similarly to the previous calibration but does not need to be completed over multiple days. It has been shown that there is minimal day to day variation, so any new calibration does not need to be calibrated over successive days. A new calibration should be completed if any component of the transmitter circuit board is replaced. Most likely, the replacement of the LED transmitter would be the case. If any connecting wire from the strain gauges to the circuit board breaks and needs to be soldered for connection purposes, a new calibration should be completed. A new calibration does not need to be completed for any changes done to the receiver circuit board because the receiver circuit does not affect the torque transducer's functionality. If there are no problems pertaining to the torque transducer for an extended period of time, it is recommended to calibrate the transducer every one to two years for verification of the accuracy and calibration curves.

### *Limitations*

There were several limitations to the design of this device. First, the size of the transmitter receiver was limited to the internal space of the crankshaft where the transmitter circuit was housed. The transmitter circuit could not be placed somewhere else due to the design of the pedaling device. Second, the torque measuring device was limited to two strain gauges per circuit because of the number of wires and size. More strain gauges would accumulate more wires which would be too large to fit on the circuit board and into the crank shaft. Therefore, only two strain gauges were used for each circuit. Third, the maximum load for the calibration of the device was limited by the calibrated masses that were available. 10kg was the maximum amount of mass calibrated because of the limited calibrated masses. This device is used in a pedaling study, so it has to be assumed that torques above the maximum measured torque are continued to be linear. Lastly, the frequency oscillator of the device was limited to the 6 kHz to 10 kHz band, so there is the bottoming out problem associated with going below 6 kHz. Bottoming out is limited by the lower end of the frequency band. The device is used in the pedaling study so the device is limited by the minimum voltage it can accurately collect and it was found that no voltages go below the minimum measured voltage. The bottoming out problem could be addressed by a completely different circuit design with a larger frequency range, but it is unknown if the larger frequency range would reduce the problem or just increase the frequency band for each torque.

## Conclusion

Measuring torque symmetry while pedaling is possible using strain gauge torque transducers in an MR environment. It was demonstrated that the transducer design and fabrication is a functional torque transducer that is both accurate (98%) and precise (98%). The device is calibrated to measure a wide range of torques (-3 to 8 Nm) and is accurate down to 0.13 Nm intervals. The device has similar statistical error qualities to other devices similar in design which proves for accurate torque recordings. The device is not day to day or trial by trial dependent making it consistent over time. The torque transducer has been updated and improved from the previous design and is a more robust system. The application of this device with respect to the device functionality should be interpreted in light of limitations of the fabrication. The device is not the same as high priced devices designed by large companies but is well designed for research use. The need of a cautious interpretation of the device is warranted.

## CHAPTER 3: ASYMMETRY IN PEDALING AFTER STROKE

### Introduction

In people with stroke, primary functional movements that require bilateral movement such as walking, standing, or pedaling, and behaviors are completed by the non-paretic lower limb. The increased use of the non-paretic leg and the decreased movement in the paretic leg are leading causes of asymmetric movement patterns in stroke survivors. Bowden and colleagues demonstrate that 60 percent of forward locomotion is completed with the non-paretic lower limb and Kautz and colleagues show that the non-paretic limb does a majority of the work in pedaling too (Bowden et al. 2006, Kautz and Brown 1998). Asymmetric movements allow for stroke survivors to functionally move. These asymmetric movements are a strategy for stroke survivors to get around paralysis or weakness in their affected limb in acute stages. The overuse and prolonged use of these strategies is associated with decreased movement of the paretic limb and limited recovery. Decreased use of the paretic limb, limiting recovery, leads to a decreased quality of life in survivors (Allred et al. 2005, Allred and Jones 2008, Mayo et al. 2002, Nadeau et al. 1999). The asymmetric movements remain beyond their usefulness in the acute stages.

Asymmetric movements are persistent in chronic stroke even when the affected limb has improved motor function (Brown, Kautz and Dairaghi 1997, Brown and Kautz 1998). One problem that causes the non-paretic limb to complete functional movements is the inability to appropriately time the excitation of their muscles in the paretic limb. Inaccurate timing of muscles is apparent during cyclical locomotor movements (Kautz and Brown 1998). Muscle activation timing is difficult because of the complexity of

multijoint movements. Kautz and Brown were able to quantify the amount of mechanical work completed by the paretic leg compared to the non-paretic leg and the timing of the EMG during a cycling paradigm. They showed two abnormalities that were correlated with less work completed by the paretic leg. First, they showed prolonged excitation in the vastus medialis and second, phase-advanced excitation in the rectus femoris and semimembranosus (Kautz and Brown 1998). This suggests that muscles are affected differently based on their function.

In our laboratory, there have been studies aiming to quantify the pedaling symmetry in people with stroke. Previous studies have quantified the asymmetries in pedaling comparing stroke survivors with health age matched controls in terms of muscle activity and cortical activation and volume (Cleland 2018, Promjunyakul et al. 2015). Cleland measured asymmetry during three pedaling conditions: conventional, unilateral, and bilateral uncoupled pedaling. Cleland found that during bilateral uncoupled pedaling, stroke survivors were unable to maintain the same velocity or smoothness compared to conventional pedaling (Cleland et al. 2016). Stroke survivors had to develop different strategies to complete the task. Cleland showed that the paretic limb produced less torque than the non-paretic limb using a separate pedaling device and that the muscle activity of the rectus femoris, medial gastrocnemius, and biceps femoris were all significantly less modulated in the paretic limb compared to the non-paretic limb and control limbs (Cleland et al. 2016). This reinforces what is found by Kautz and Brown with impaired muscle activity in the paretic limb. Promjunyakul demonstrated reduced cortical activation and volume in the stroke survivors compared to controls. Promjunyakul suggested that impaired locomotion was associated with decreased volume of activation

(Promjunyakul et al. 2015). While both studies measured asymmetry in stroke, neither had the ability to measure torque and work. Torque and work could have helped relate the asymmetry with muscle activity and cortical activation.

This study examined the impairments of the paretic limb and impaired interlimb symmetry using torque and work during pedaling. Impairments of the paretic limb and interlimb symmetry are related because of the effects the paretic limb can have on the non-paretic limb causing impaired movements (Arene and Hidler 2009). Pedaling symmetry was compared during conventional bilateral coupled pedaling in chronic stroke survivors and age matched controls in both the laboratory setting and MRI scanner. Pedaling involves continuous, reciprocal, multijoint movement of both limbs, and therefore is a useful model of functional lower limb movement. During conventional pedaling, the two crank shafts are mechanically coupled allowing torques from each side transfer to the other. Conventional pedaling exposes asymmetries because bilateral coupled pedaling can be completed with minimal contributions from the paretic limb. The purpose of this study is to describe the pedaling symmetry of stroke survivors and compare pedaling with healthy age matched controls. The study aims to describe the differences in pedaling between the two groups. As well, the study aims to quantify the differences between pedaling in the laboratory and during MRI scanning.

## **Methods**

### *Participants*

This study recruited 15 individuals with chronic stroke and 19 age-matched controls participated. All were free of neurological disease or injury other than stroke.

The participants were consented in accordance with the Institutional Review Boards at Marquette University and the Medical College of Wisconsin. Participant demographics are found in Table 3.1.

	Control (n=19)	Stroke (n=15)
Age (years)	60 (8.4)	57 (12.5)
Sex (M/F)	8/11	6/9
Time since stroke (years)		6.5 (4.5)
Stroke location (cortical/subcortical)		9/6
Stroke type (ischemic/hemorrhagic)		6/9
Paretic limb (L/R)		0/15
Fugl-Meyer <sub>total</sub> (max = 96)		81 (39-96)
FM <sub>motor</sub> (max = 34)		24 (1-34)
FM <sub>sens</sub> (max = 12)		9 (0-12)
FM <sub>bal</sub> (max = 10)		8 (6-10)
FM <sub>rom</sub> (max = 20)		19 (10-20)
FM <sub>pain</sub> (max = 20)		19 (16-20)
Berg Balance (56)		49 (18-56)
Gait Speed (m/s)		0.98 m/s (0.24-1.5)

**Table 3.1: Participant demographics.** Characteristics for the control and stroke groups. All values are Mean (SD|range). FM: Fugl Meyer. Each subcategory of the FM lower extremity is noted.

### *Clinical Measures*

People with stroke underwent clinic assessments including the Fugl-Meyer (FM) Assessment, Berg Balance test, and 8 meter walk test to characterize their impairment of the lower limbs. The Fugl-Meyer Assessment consisted of motor, sensory, balance, range of motion, and pain components. Values are reported in Table 3.1.

### *Equipment and Procedures*

The data collection for this study was part of a larger study meant to measure and characterize resting state and functional connectivity in stroke for motor, language, and memory tasks. This larger study consisted of a familiarization and scanning session where the pedaling tasks were completed along with the language and memory tasks.

All participants completed, to the best of their ability, a familiarization and an MRI scanning session. During which, participants performed conventional pedaling. Tasks were enabled by the custom designed split crank bike. See Figure 3.1. The split crank bike has a split crank shaft that was fastened together with a coupler to allow conventional bilateral pedaling. Both sides of the pedaling device had the eccentric pulley that enabled the participant to pedal with no contribution from the opposite limb. During bilateral pedaling, the coupler was in place to fix the two halves into a 180 degree apart position. Removal of the coupler elicited the ability to pedal unilaterally. The participant's body was placed close enough to the device, so they would not hyperextend their knees and far enough, so they were not bringing their knees too close to their upper body. Their placement was chosen by visual inspection by the experimenters and by verbal feedback from the participant. Their feet were secured to the pedals with a strap around the heel and forefoot of each foot. The feet were secured to the pedals because many stroke survivors could not otherwise keep their paretic foot on the pedal. The ankle could still move freely.

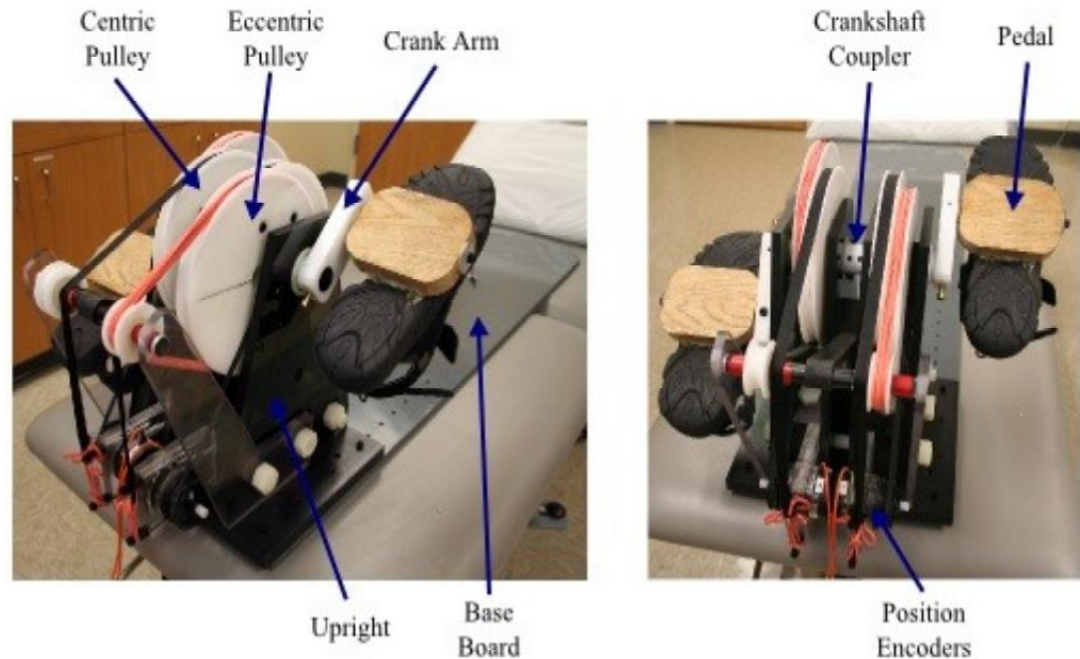


**Figure 3.1: Novel Pedaling Device.** The device shown is capable of pedaling bilaterally, unilaterally, or unilaterally uncoupled. The device is outfitted with recording measurements of torque, velocity, and crank position.

During the familiarization session, participants were outfitted with EMG sensors on seven muscles on each lower limb for 14 muscles total: rectus femoris (RF), semimembranosus (SM), biceps femoris (BF), vastus medialis (VM), tibialis anterior (TA), medial gastric (MG), and soleus (SOL). The skin was prepped by cleaning the skin with isopropyl alcohol and cotton. The electrodes were placed in the middle of each muscle along the longitudinal fiber direction. Muscle activity was recorded using an 8-channel EMG system (DS-80-IM/1009, Delsys, MA, USA). The EMG system was connected to amplifiers (DS-80-IM/1098, Delsys, MA, USA) and amplified 1000 times before the signal was sent to the analog to digital converter (CED Micro1401 mkII, Cambridge Electronic Design, Cambridge, UK). The EMG signal was recorded in Spike2 (Cambridge Electronic Design, Cambridge, UK) and sampled at 2 kHz. These muscles

were selected based on research done by Ting and group (Ting et al. 1999). The muscles selected are used during some or all parts of the pedaling cycle, regardless of forward or backward pedaling and are prime movers in pedaling. The muscles move in three pairs of alternating antagonistic functions. The extensor and flexor pair accelerates the limb into extension or flexion, the planter flexor and dorsiflexor pair stabilizes the ankle so it does not relax during extension or flexion, and the anterior and posterior movement pair accelerates the foot anteriorly or posteriorly relative to the pelvis. Reference electrodes were placed on the medial malleolus.

The purpose of the familiarization session was to collect asymmetry data and create a baseline symmetry profile of the control group to compare with the stroke group. As well, the first session was used for familiarizing the participant to the setup of the pedaling device and the tasks they would complete during the scanning session. Participants performed bilateral coupled pedaling. They were asked to pedal forward at a comfortable rate using both limbs. The pedaling conditions had a 45 second exposure period, then 180 seconds of data collection. During the 180 second trial, neither instructions nor feedback were provided.

During the scanning session participants performed bilateral pedaling to the best of their ability. Tasks were enabled by the same device used for the first session and the setup of the participant was the same. No EMG was recorded in this session.

Participants performed two pedaling conditions while in the scanner. The conditions were both bilateral coupled pedaling. Both pedaling conditions consisted of a total of four minutes of pedaling. The first bilateral coupled condition had participants pedal for 60 seconds and then rest for 40 seconds, which was repeated four times. The

second condition had participants pedal for four to eight seconds and rest for six to two seconds. This was repeated 40 times.

### *Data Analysis*

Position and velocity data were low pass filtered at 20 Hz. The first calibration was used for converting the voltage data to torque. The torque data was low pass filtered at 12 Hz. The root mean square (RMS) of the EMG was taken and the EMG was smoothed at 1 ms intervals equal to a window of 200 data points. The velocity, torque, and EMG data were referenced to the position of the crank in 1 degree increments described previously (Schindler-Ivens, Brown and Brooke 2004). Ensemble averages were created for all participants. From the ensemble averages, we computed the mean and coefficient of variation (COV) of pedaling velocity. These values acted as measures of pedaling performance. COV of velocity provided a measure of smooth, continuous pedaling.

From pedaling, positive work was calculated as the sum of the positive torque values under the torque curve and negative work was calculated as the sum of the negative torque values from the area under the curve. Negative work values are absolute valued and shown as positive values. The net work is the sum of the positive and non-absolute valued negative values. Symmetry was calculated for the symmetry index (SI) shown by Linder and colleagues (i.e.  $[T_{\text{non-paretic}} - T_{\text{paretic}}] / \{[T_{\text{non-paretic}} + T_{\text{paretic}}] / 2\}$ ) (Linder et al. 2018). In symmetry index, T represents the average torque for the down stroke or upstroke. Downstroke is defined as the area from top dead center to bottom dead center (0-180 degrees) and upstroke is characterized by bottom dead center to top dead center

(180-360 degrees). A positive SI indicated a greater contribution from the non-paretic or right limb and a negative SI indicated a greater contribution from the paretic limb or left limb. The SI was calculated for the downstroke and upstroke separately.

Mean EMG amplitude and the modulation index (MI) of EMG were calculated for each muscle for all participants. MI was calculated as the difference between the maximum and minimum amplitude divided by the maximum amplitude and measured as a percent (i.e.  $[EMG_{\max} - EMG_{\min}] / EMG_{\max} * 100$ ). Between-group and between-limb comparisons of the EMG amplitude are different from each other in pedaling because a normalization factor is not possible due to background EMG signals (Cleland 2018). MI was used because it was able to compare the modulation of the muscle activity. Since muscles are active in a phasic manner during pedaling, it was reasoned that higher muscle output would have higher MI values. Mean EMG amplitude and MI were important for within-limb comparisons of muscle activity.

### *Statistics*

All data were tested for normality using the Shapiro Wilk test. Data used for between-group comparisons were tested for equality of variances using the Levene's test. Non-parametric statistics were used for non-normal data or data with unequal variances. All statistical tests used MATLAB (R2018b, The Mathworks Inc., Natick, MA) and  $P < 0.05$  was accepted as significant.

Within and between group comparisons were achieved for mean and COV of velocity, torque characteristics, EMG MI, and mean EMG amplitude. Between group comparisons were performed with independent sample t-tests. Within group comparisons

were performed with paired sample t-tests. In controls, there were no differences between limbs for any measure of torque, velocity, or EMG, so the average of the limbs was used. One sample t-tests were used to compare mean velocity and torque production. Correlations were used to examine the relationships between the torque, work completed, COV of velocity, and clinical measures.

## **Results**

Group mean (SD) values and tests for significance for torque, work, velocity, and EMG are provided in Tables 3.5, 3.8, 3.9 and 3.10. Examples of pedaling behaviors in the laboratory across groups are shown in Figures 3.4 and 3.6 and pedaling behaviors during fMRI as shown in Figures 3.11 and 3.14. Additional figures are shown in Appendix A.

### *Pedaling data*

During conventional pedaling, both groups displayed continuous, forward progression of the crank arm (Figure 3.2). There was a between-group difference in the COV of pedaling velocity: control COV= 8.5 (3.3) and stroke= 13.5 (7.2) with  $p < 0.05$ . In both groups, mean pedaling velocity was not significantly different: control= 434 (110) and stroke= 406 (80) with  $p > 0.1$ .

The control group pedaled symmetrically with an average SI of -0.07 for the downstroke and 0.12 for the upstroke (Table 3.2). The control group showed 10 participants pedaling with more net work completed on their right limb compared to left and 6 participants pedaling with more net work with their left limb (Figure 3.3). The control group tended to have symmetrical torque and work values (Figure 3.4). The peak

torque was significantly correlated with positive work and net work for both limbs. Net work and positive work are significantly correlated as well. Minimum torque and negative work are not correlated with any torque or work parameters and the right and left limbs are not correlated with one another (Figure 3.5).

Consistent with asymmetric contributions, in the stroke group, there was more asymmetry shown by a greater SI value in the upstroke (1.04), but a similar SI value for the down stroke (-0.04) (Table 3.3). The stroke group showed 5 participants pedaled with more net work on their non-paretic limb than their paretic limb and 6 participants with more net work on their paretic limb than their non-paretic (Figure 3.6). The non-paretic and paretic limb tended to have similar torque and work values (Figure 3.7). The peak torque is significantly correlated with positive work and net work on both limbs. The net work is significantly correlated with the positive work for both limbs and negative work for the non-paretic limb. The positive work is significantly correlated with the negative work for the non-paretic limb. Minimum torque, negative work and net work are all not significantly correlated between the non-paretic and paretic limbs (Figure 3.8).

A multilinear regression was used to determine the torque and work components that drove the net work values which produced the symmetry (Table 3.4 and 3.5). The regression analysis showed the positive work ( $p_L < 0.001$ ,  $p_R < 0.001$ ) in the control group and peak torque ( $p_{NP}=0.023$ ,  $p_P=0.009$ ) and positive work ( $p_{NP} < 0.001$ ,  $p_P=0.003$ ) in the stroke group significantly contribute to net work when compared with the opposite limb minimum torque and negative work.

The control and stroke groups differed in the torque and work produced during pedaling (Table 3.6 and Figures 3.9 and 3.10). There were significant differences

between the peak torque, minimum torque, and negative work between the control group and the paretic limb of the stroke group ( $p < 0.05$ ). There were significant differences with the minimum torque and negative work between the non-paretic and paretic limbs of the stroke group ( $p < 0.05$ ). There were no differences between the control group and the non-paretic limb of the stroke group ( $p > 0.1$ ). The total positive and net work contribution was not different between the control group and either the paretic or non-paretic limbs ( $p > 0.1$ ). The non-paretic limb and paretic limb were not significantly different for total positive or net work production ( $p > 0.05$ ). The SI was not significantly different for the control and stroke group for the upstroke or downstroke, but the upstroke trended toward significantly less symmetric (0.1).

This can be viewed in Figure 3.4 with C09 who had a large peak torque and small minimum torque which resulted in an average positive work of 30.2 J and negative work of -0.4 J. The significant difference between the positive and negative work is an example of the positive work driving the net work. Similarly, S05 had large peak torque and positive work, but minimal minimum torque and negative work. These two examples show that both control and stroke participants mainly rely on the positive work for dictating the symmetry and the difference in methods used for coordinating work.

The control and stroke groups pedaling with different timing of positive and negative work (Table 3.7). The control group spend 294 degrees producing positive work with the left limb and 270 degrees producing positive work with the right limb. The stroke group spent 294 degrees producing positive work with the non-paretic limb and 262 degrees producing positive work with the paretic limb. The left and right limbs of the control group are significantly different:  $p = 0.03$ . The left limb of the control group and

non-paretic limb of the stroke group are not different ( $p>0.1$ ) but the left limb and paretic limb are significantly different ( $p= 0.003$ ). The right limb is significantly different than the non-paretic limb ( $p= 0.04$ ) and not different than the paretic limb ( $p= 0.07$ ). The non-paretic limb is significantly different than the paretic limb:  $p= 0.008$ . The right limb and non-paretic limb are producing positive work for longer durations than the right limb and paretic limb but there are not differences in the positive work completed. The differences in timing of negative work being produced may lead to the differences in total negative work.

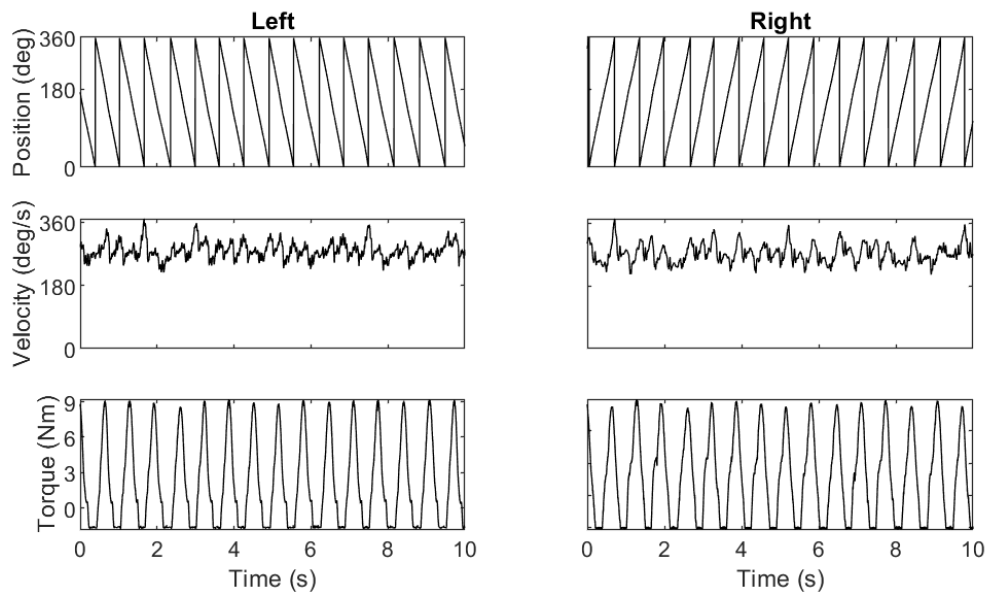


**Figure 3.2: Position, velocity, and torque over time.** Position, velocity, and torque data are shown over a 10 second interval. Position is measured from 0 to 360 degrees. The right position increases from 0 to 360 while the left position decreases. Position and velocity are recorded from the optical encoder on the pedaling device. Torque is measured from the designed torque sensors.

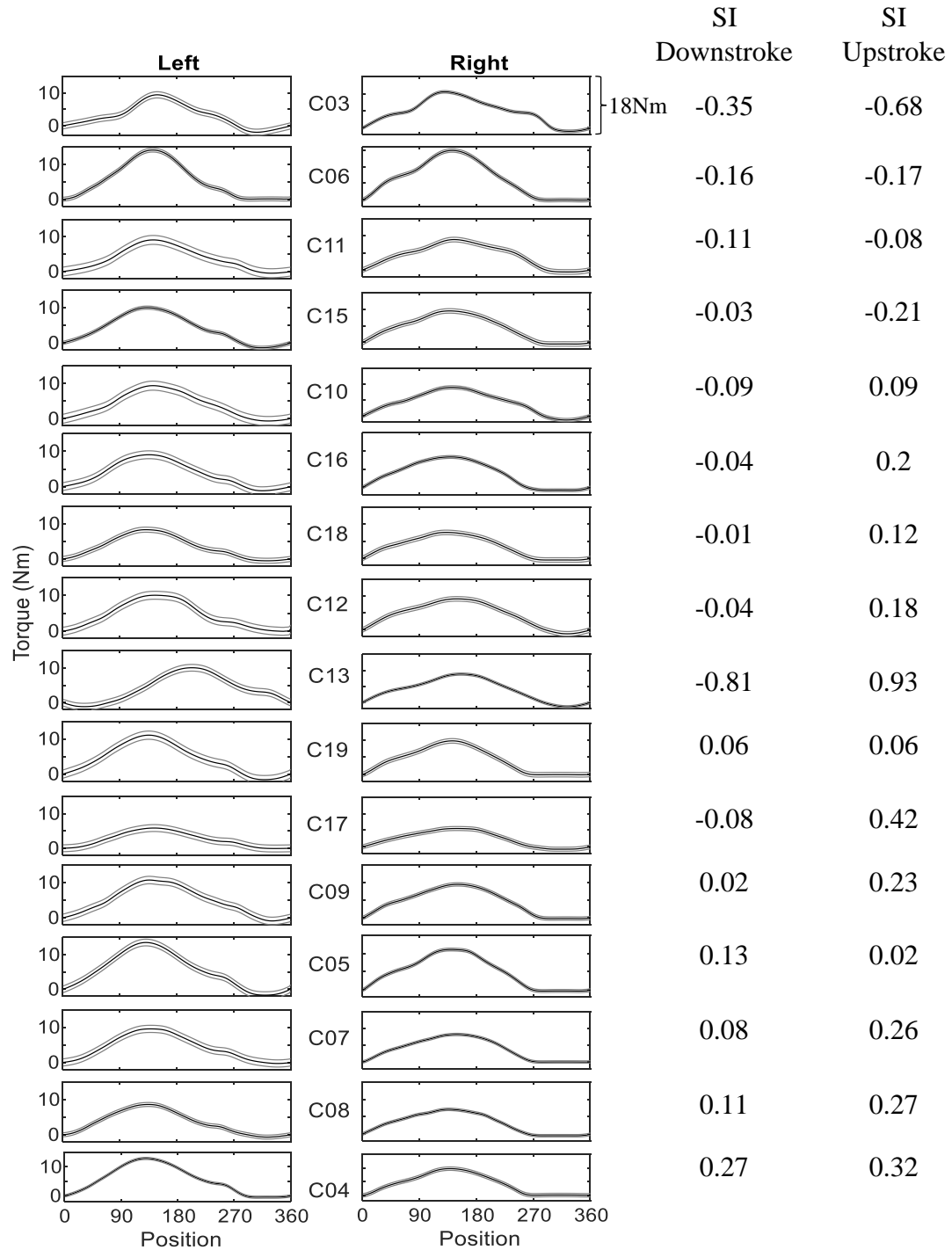


**Figure 3.3: Symmetry of control participants.** Symmetry index is based on the average torque completed in either the downstroke or upstroke. Solid black lines are the average torque curve for all revolutions during pedaling and the gray lines are one standard deviation from the mean.

	Left			Right			SI Down- stroke	SI Up- stroke
	Max Min Torque (Nm)	Positive Work (J)	Negative Work (J)	Max Min Torque (Nm)	Positive Work (J)	Negative Work (J)		
C03	9.5 -2.0	20.7	-1.8	11.3 -1.0	32.3	-0.8	-0.35	-0.68
C06	14.2 0	33.2	-0.0	16.0 -0.2	42.1	-0.2	-0.16	-0.17
C11	9.1 -0.5	23.6	-0.3	9.5 -0.6	28.2	-0.6	-0.11	-0.08
C15	10.0 -1.4	26.0	-1.3	10.2 -0.5	29.2	-0.7	-0.03	-0.21
C10	9.4 -0.6	24.9	-0.5	9.7 -1.3	28.4	-1.2	-0.09	0.09
C16	9.0 -1.2	23.5	-1.0	8.9 -0.8	25.2	-1.3	-0.04	0.2
C18	8.3 -0.5	21.6	-0.5	8.1 -0.5	23.0	-0.8	-0.01	0.12
C12	10.0 -0.1	27.9	-0.0	9.8 -1.2	30.2	-1.1	-0.04	0.18
C13	10.1 -1.1	26.5	-0.9	9.4 -1.4	27.0	-1.3	-0.81	0.93
C19	11.0 -1.6	28.3	-1.4	10.5 -0.2	27.2	-0.2	0.06	0.06
C17	5.8 -0.1	16.0	-0.1	5.9 -0.7	16.7	-0.9	-0.08	0.42
C09	10.7 -0.9	30.6	-0.5	10.1 -0.2	29.8	-0.3	0.02	0.23
C05	13.5 -1.7	34.8	-1.5	11.9 -0.3	32.5	-0.5	0.13	0.02
C07	9.5 -0.3	26.5	-0.2	8.7 -0.1	24.8	-0.1	0.08	0.26
C08	8.6 -0.7	22.3	-0.5	7.6 -0.5	21.1	-0.8	0.11	0.27
C04	12.9 -0.5	34.6	-0.5	10.4 0	27.4	-0.0	0.27	0.32
Avg	10.1 -0.8	26.3	-0.7	9.9 -0.6	27.8	-0.7	-0.07	0.122
std	2.1 0.6	5.2	0.6	2.2 0.4	5.6	0.4	0.24	0.34

**Table 3.2: Individual torque and work data for all control participants.** Control participants are listed based on work percentage comparison from the symmetry of Figure 3.4. All torque and work measures are separated and shown above.

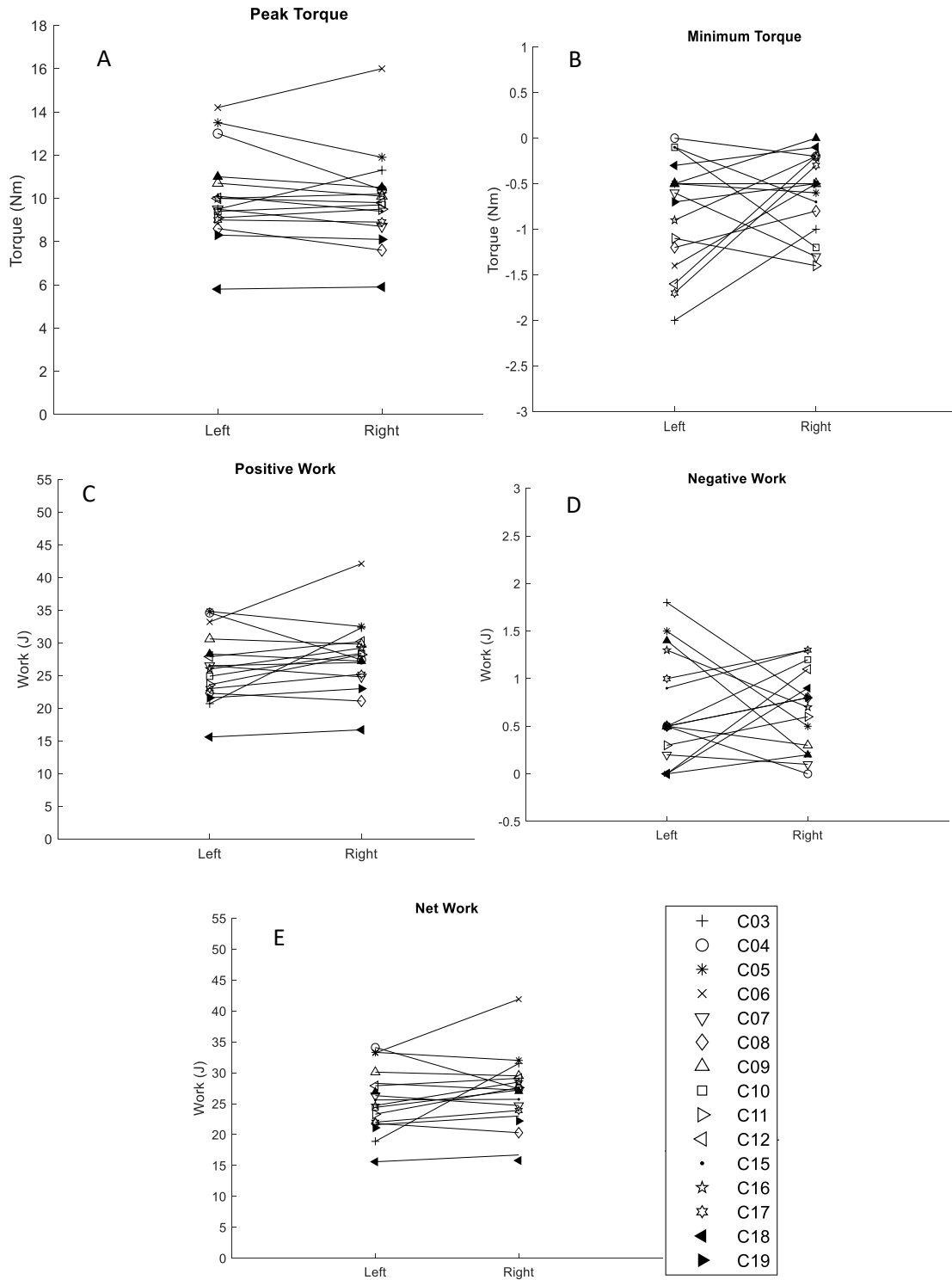


**Figure 3.4: Magnitude of the left and right torque and work data for controls.** Visual representation of Table 3.2 for comparison of left and right A) peak torque ( $R^2 = 0.869$  and  $p = 0.0$ ), B) minimum torque ( $R^2 = 0.067$  and  $p = 0.8$ ), C) positive work ( $R^2 = 0.668$  and  $p = 0.005$ ), D) negative work ( $R^2 = 0.066$  and  $p = 0.8$ ) and E) net work ( $R^2 = 0.678$  and  $p = 0.007$ ).

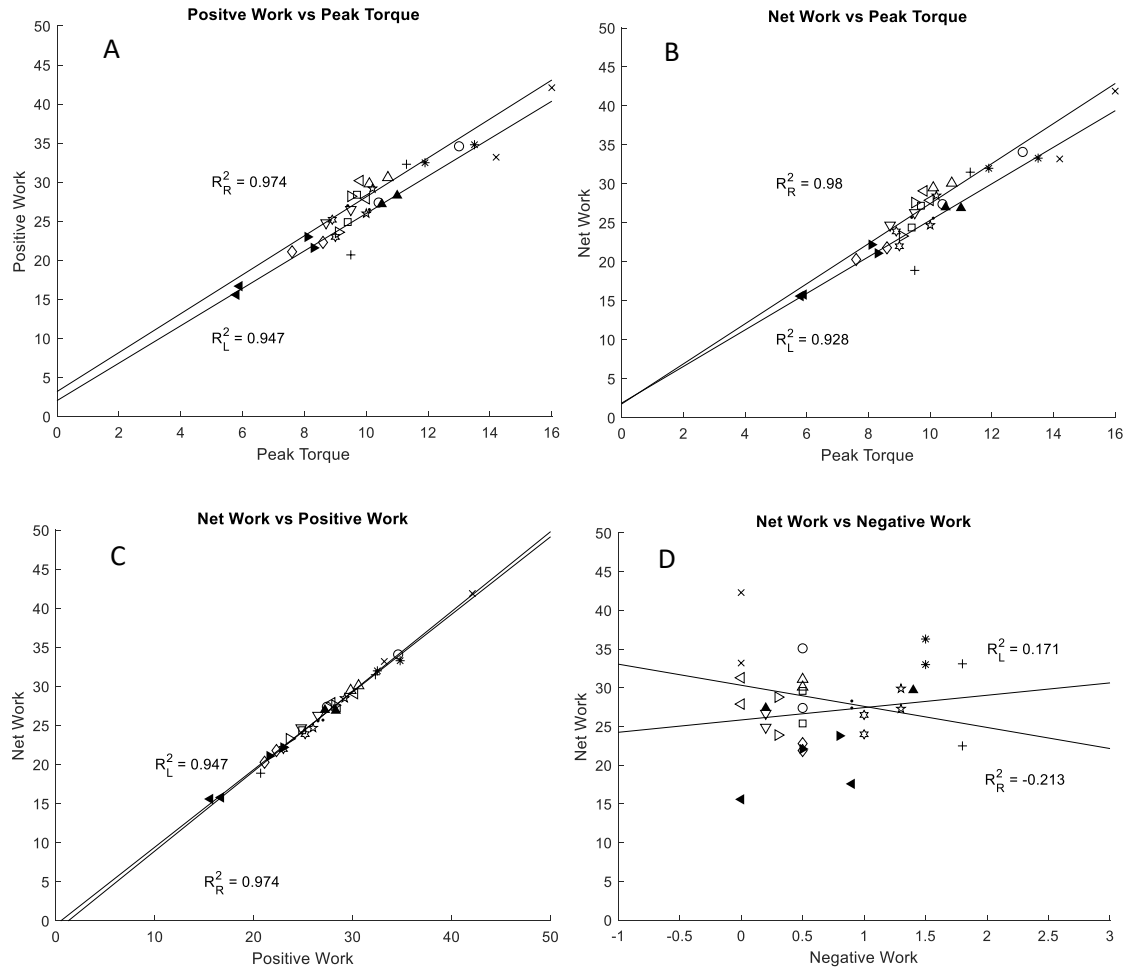


**Figure 3.5: Torque and work correlations for control participants.** A) Positive work and peak torque are highly correlated at  $R^2 = 0.974$  and  $0.974$  for the left and right respectively ( $p < 0.001$ ). B) The net work and peak torque are significantly correlated ( $R^2 = 0.98$ ,  $R^2 = 0.928$  and  $p < 0.001$ ). C) Net work and positive work are significantly correlated ( $R^2 = 0.947$ ,  $R^2 = 0.974$  and  $p < 0.001$ ). D) Net work and negative work are not correlated at  $R^2 = 0.171$  and  $R^2 = -0.213$  ( $p = 0.5$  and  $p = 0.4$ ).

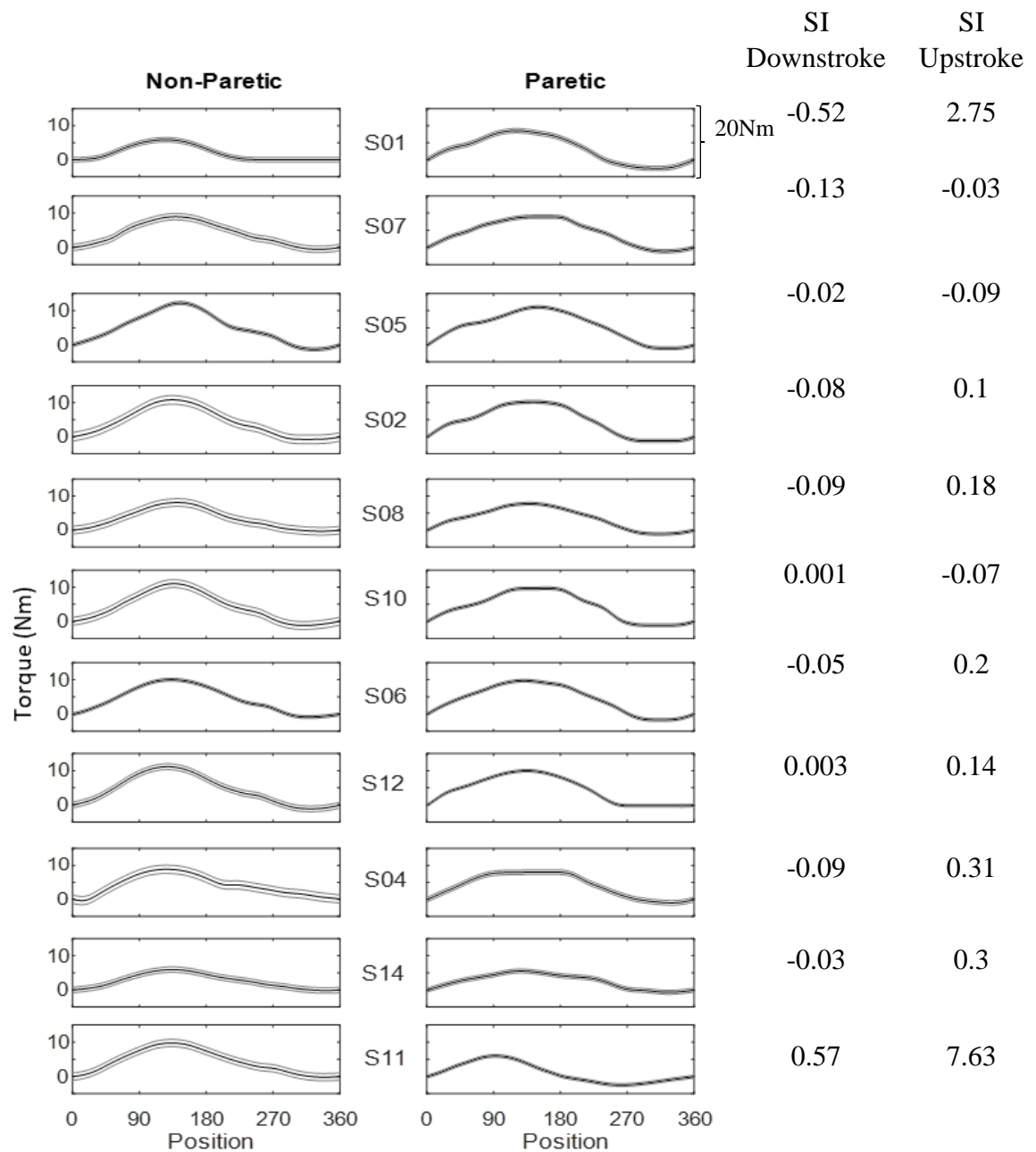


**Figure 3.6: Symmetry of stroke participants.** Ordered from most work completed with the non-paretic limb compared to the paretic limb to the least work completed with the non-paretic limb compared to the paretic limb. Symmetry index is based on the average torque completed in either the downstroke or upstroke. Solid black lines are the average torque for all revolutions and gray lines are one standard deviation from the average.

	Non-Paretic			Paretic				
	Max Min Torque (Nm)	Positive Work (J)	Negative Work (J)	Max Min Torque (Nm)	Positive Work (J)	Negative Work (J)	SI Down- stroke	SI Up- stroke
S01	5.7 -0.2	12.2	-0.0	8.5 -0.7	22.2	-3.7	-0.52	2.75
S07	9.0 -0.4	24.6	-0.4	8.9 -1.0	27.9	-1.0	-0.13	-0.03
S05	12.2 -1.2	31.3	-1.0	11.1 -0.3	33.2	-0.9	-0.02	-0.09
S02	10.8 -0.9	27.2	-0.8	10.2 -1.7	29.3	-1.7	-0.08	0.1
S08	8.1 -1.2	20.6	-0.2	7.8 -1.2	22.2	-1.3	-0.09	0.18
S10	11.1 -0.3	27.0	-1.1	9.7 -1.2	27.9	-1.5	0.001	-0.07
S06	10.0 -0.8	27.5	-0.7	9.7 -1.2	28.6	-1.9	-0.05	0.2
S12	11.2 -1.3	28.7	-1.0	10.0 -1.0	27.8	-0.4	0.003	0.14
S04	8.8 -0.6	25.9	-0.1	8.0 -1.2	26.0	-0.9	-0.09	0.31
S14	6.0 0	16.6	-0.1	5.5 -2.5	16.2	-0.6	-0.03	0.3
S11	9.7 -0.2	27.2	-0.1	5.6 -2.5	10.8	-4.5	0.57	7.63
Avg	9.3 -0.6	24.4	-0.5	8.6 -1.3	24.7	-1.7	-0.04	1.04
std	2.1 0.5	5.7	0.4	1.8 0.7	6.5	1.3	0.25	2.33

**Table 3.3: Individual torque and work data for all stroke participants.** Stroke participants are listed based on work percentage comparison from the symmetry of Figure 3.6. All torque and work measures are separated shown above.

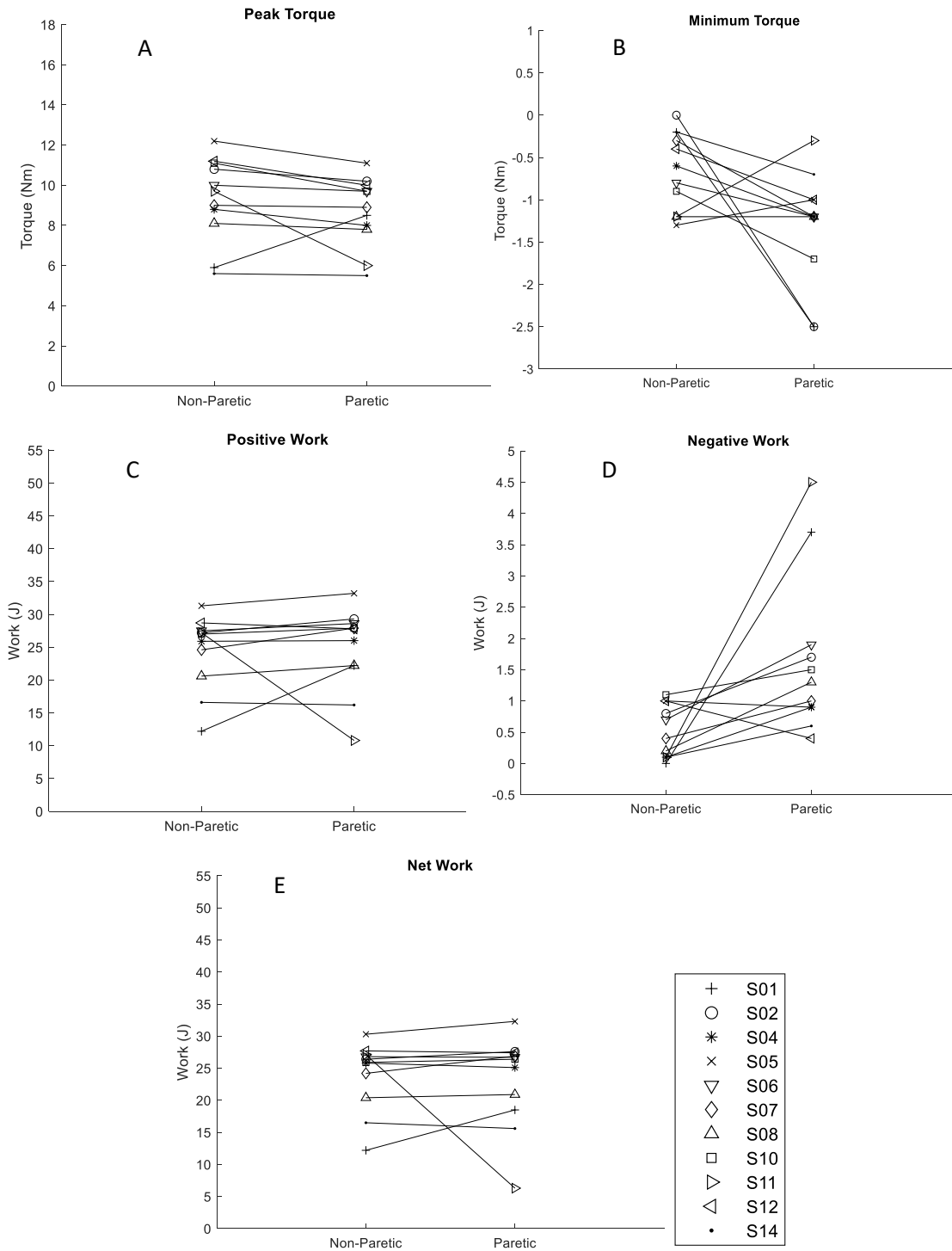


**Figure 3.7: Magnitude of the paretic and non-paretic torque and work data for stroke participants.** Visual representation of Table 3.3 for comparison of the paretic and non-paretic A) peak torque ( $R^2 = 0.726$  and  $p=0.01$ ), B) minimum torque ( $R^2 = -0.526$  and  $p=0.1$ ), C) positive work ( $R^2 = 0.476$  and  $p=0.1$ ), D) negative work ( $R^2 = -0.417$  and  $p=0.2$ ), and E) net work ( $R^2 = 0.437$  and  $p=0.1$ ).

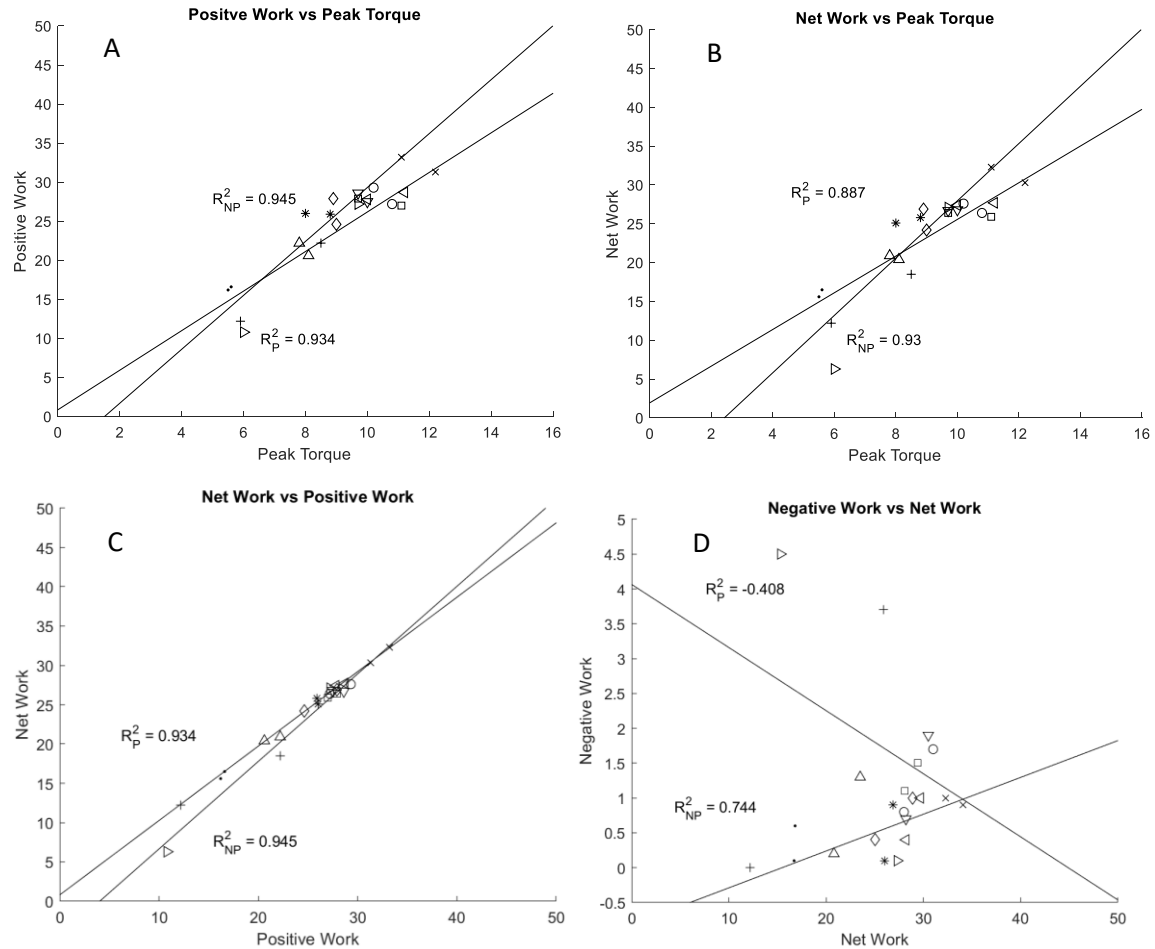


**Figure 3.8: Torque and work correlations for stroke participants.** A) positive work and peak torque are significantly correlated for the paretic ( $R^2 = 0.945$  and  $p = 0.0$ ) and non-paretic ( $R^2 = 0.934$  and  $p = 0.0$ ) limbs. B) the net work is significantly correlated with peak torque for both limbs (Non-paretic:  $R^2 = 0.93$  and  $p = 0.0$ . Paretic:  $R^2 = 0.887$  and  $p = 0.0$ ). C) net work is significantly correlated with positive work for both limbs (Non-paretic:  $R^2 = 0.945$  and  $p = 0.0$ . Paretic:  $R^2 = 0.934$  and  $p = 0.0$ ). D) negative work is not correlated with the paretic limb ( $R^2 = -0.408$  and  $p = 0.2$ ) but is significantly correlated with the non-paretic limb ( $R^2 = 0.744$  and  $p = 0.009$ ).

	Estimate	Coeff	t-Stat	p-value
Intercept	0		N/A	N/A
X1	0.28		0.74	0.49
X2	-1.45		-0.49	0.64
X3	0.93		6.34	0.001
X4	-1.43		-0.45	0.67
R <sup>2</sup>	0.993			

**Table 3.4: Multilinear regression model for control group.** X1 = peak torque, X2 = minimum torque, X3 = positive work, and X4 = negative work. The inputs are compared to net work.

	Estimate	t-Stat	p-value
Intercept	-0.42	N/A	N/A
X1	-0.03	-0.05	0.96
X2	-0.86	-0.46	0.67
X3	1.03	5.79	0.002
X4	-0.6	-0.31	0.77
R <sup>2</sup>	0.989		

**Table 3.5: Multilinear regression model for stroke group.** X1 = peak torque, X2 = minimum torque, X3 = positive work, and X4 = negative work. The inputs are compared to net work.

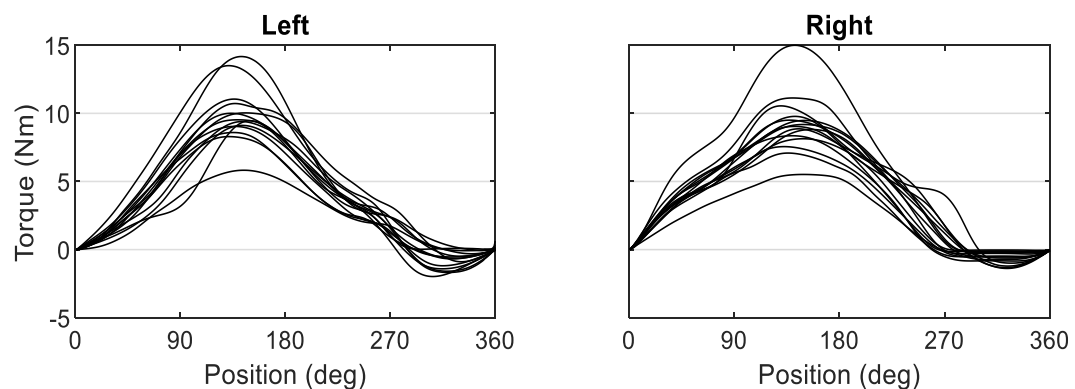


**Figure 3.9: Overlaid torque curves for control group.** The left and right limbs can be seen to have different magnitudes between participants. Overall, the two limbs are similar when compared ( $p=0.2$ ).

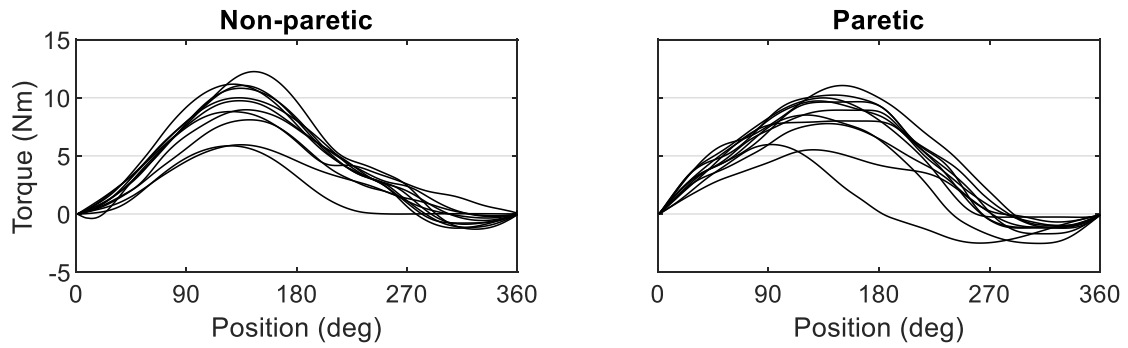


**Figure 3.10: Overlaid torque curves for the stroke group.** The non-paretic and paretic limbs are shown for all stroke participants. The two groups have a variety of magnitudes but are not different when averaged.

	Control	Stroke	
		NP	P
Velocity (deg/s)	434 (110)	406 (80)	
COV (%)	8.5 (3.3)	13.5 (7.2) <sup>a</sup>	
Max Torque (Nm)	10 (2.1)	9.3 (2.1)	8.6 (1.8) <sup>a</sup>
Min Torque (Nm)	-0.7 (0.5)	-0.6 (0.5)	-1.3 (0.7) <sup>ab</sup>
Positive Work (J)	27.1 (5.4)	24.4 (5.7)	24.7 (6.5)
Negative Work (J)	-0.7 (0.5)	-0.5 (0.4)	-1.7 (1.3) <sup>ab</sup>
Net Work (J)	26.4 (5)	23.9 (5.5)	23.1 (5.5)
SI Downstroke	-0.07 (0.24)	-0.04 (0.24)	
SI Upstroke	0.12 (0.34)	1.04 (2.33)	

<sup>a</sup>  $p < 0.05$  vs control

<sup>b</sup>  $p < 0.05$  vs non-paretic

**Table 3.6: Group average control and stroke torque and work kinetics.** Values are shown for all torque and work measurements for the average of the limbs for the controls and the non-paretic and paretic for the stroke group.

	Left	Right		Non-Paretic	Paretic
C03	275	299	S11	320	183
C06	360	280	S14	321	280
C11	306	289	S04	299	282
C15	281	277	S12	285	258
C10	295	285	S06	289	271
C16	286	259	S10	277	264
C18	290	266	S08	304	271
C12	339	288	S02	282	263
C13	287	285	S05	293	289
C19	284	264	S07	304	285
C17	318	267	S01	256	239
C09	308	281			
C05	284	269			
C07	273	316			
C08	291	260			
C04	287	288			
Mean	294	270		294	262
SD	(18)	(15)		(19)	(30)

**Table 3.7: Degrees of positive work.** Values represent the degrees where the torque trace is aiding to increase the amount of positive work completed by the limb. Left and Right are significantly different at a p-value of 0.03 of controls. Left is not significantly different than the non-paretic limb. The right limb is significantly different than the non-paretic limb with a p-value of 0.04. The right limb is not significantly different than the paretic limb at a p-value of 0.07. The left and non-paretic limbs are significantly different than the paretic at a p-value of 0.003 and 0.008 respectively.

### *MRI Pedaling Data*

The control group pedaled symmetrically in the scanner with an average SI value of -0.08 for the downstroke and -0.01 for the upstroke. The control group showed 6 participants pedaling with more work completed on their right limb compared to left limb and 5 participants pedaling with more net work with their left limb (Figure 3.11 and Table 3.8). The left and right limbs were significantly correlated with one another for peak torque, positive work, and net work ( $p < 0.01$ ) but the negative work and minimum torque were not correlated ( $p > 0.05$ ) (Figure 3.12). In the control group, the peak torque,

positive work and net work are all significantly correlated:  $p < 0.001$ . The negative work is not correlated with peak torque, positive work, or net work:  $p > 0.05$  (Figure 3.13).

The stroke group pedaled comparably symmetric with the control group with a SI value of -0.08 for the downstroke, but a greater SI value for the upstroke (0.21). The stroke group showed 3 participants pedaling with more work completed on their paretic limb compared to non-paretic limb and 5 participants pedaling with more net work with their non-paretic limb (Figure 3.14 and Table 3.9). The non-paretic and paretic limbs were significantly correlated with one another for peak torque, positive work, and net work ( $p < 0.01$ ) but the negative work and minimum torque were not correlated ( $p > 0.05$ ) (Figure 3.15). In the control group, the peak torque, positive work and net work are all significantly correlated:  $p < 0.001$ . The negative work is not correlated with peak torque, positive work, or net work:  $p > 0.05$  (Figure 3.16). The peak torque is significantly correlated between the non-paretic and paretic limbs of the stroke group and minimum torque, positive work, negative work, and net work are all not significantly correlated between the non-paretic and paretic limb.

During pedaling in the fMRI, both groups displayed continuous, forward progression of the device (Table 3.10). There was no between-group difference in COV in pedaling. Both groups showed no significant differences in pedaling velocity. There were significant differences between the control group and the stroke group for both the non-paretic and paretic limbs for minimum torque and negative work:  $p < 0.05$ . There were no differences between the non-paretic limb and paretic limb for any torque or work measure. There was no difference in the SI between the control group and stroke group.

A multilinear regression was used to determine the torque and work components that drove net work while pedaling in the MRI scanner (Table 3.11 and 3.12). The multilinear regression analysis showed the positive work in the control group and positive work and the opposite limb minimum torque in the stroke group significantly contribute to net work when compared with the peak torque and the opposite limb negative work.

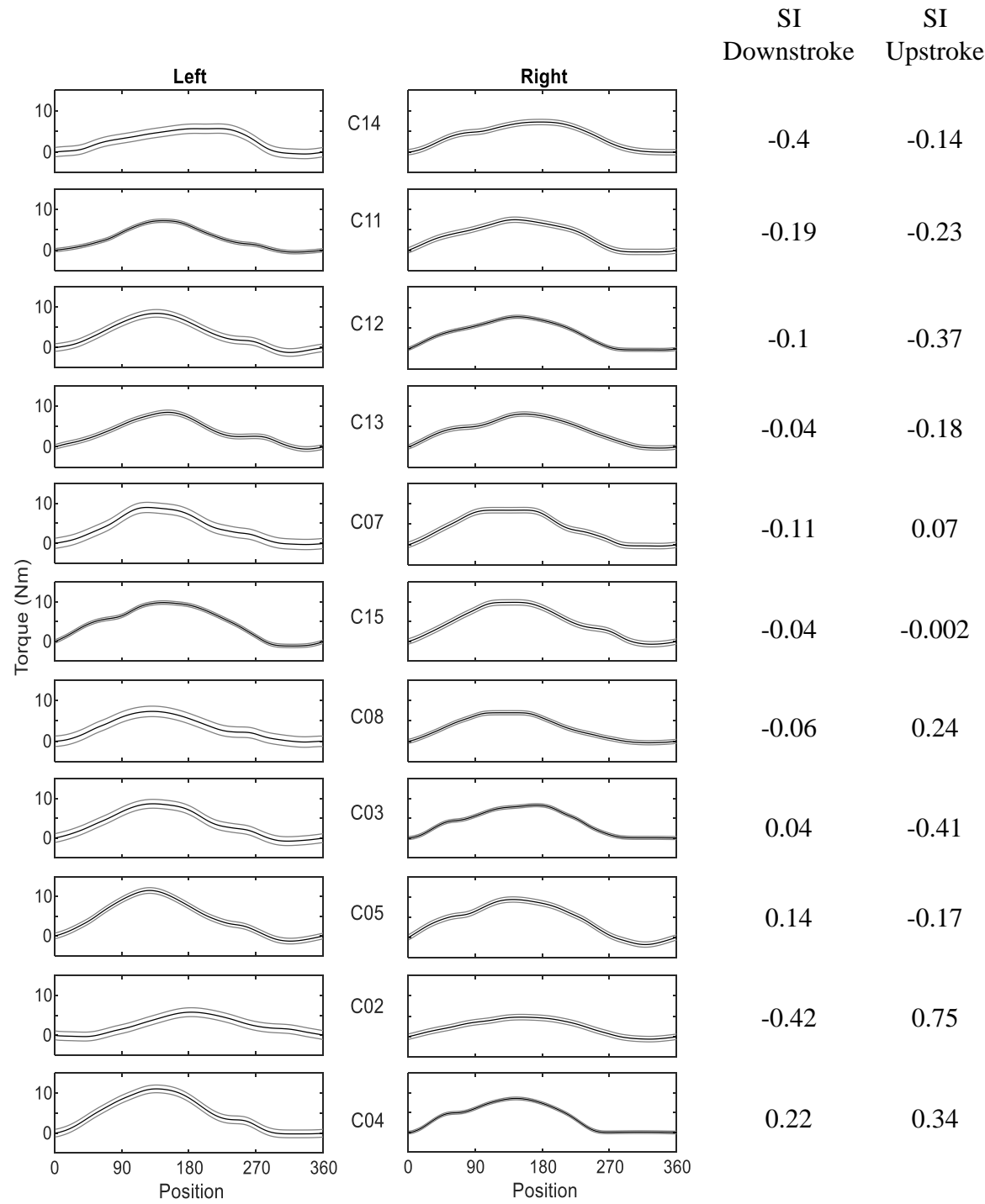


**Figure 3.11: Symmetry of control participants during fMRI pedaling.** ordered from most work completed with the right limb to least work completed in comparison to the left limb. Symmetry index is based on the average torque completed in either the downstroke or upstroke. Solid black lines are the ensemble averaged torque and gray lines are one standard deviation from the mean.

	Left			Right			SI Down- stroke	SI Up- stroke
	Max Min Torque (Nm)	Positive Work (J)	Negative Work (J)	Max Min Torque (Nm)	Positive Work (J)	Negative Work (J)		
C14	5.7 -0.5	18.0	-0.3	7.3 0	23.7	0	-0.4	-0.14
C11	7.2 -0.5	17.9	-0.4	7.5 -0.4	22.0	-0.5	-0.19	-0.23
C12	8.4 -1.3	20.9	-1.0	7.7 -0.3	22.2	-0.3	-0.1	-0.37
C13	8.4 -0.6	22.6	-0.3	8.0 -0.3	24.6	-0.2	-0.04	-0.18
C07	9.0 -0.3	23.8	-0.2	8.4 -0.3	25.4	-0.3	-0.11	0.07
C15	9.8 -1.2	29.3	-0.7	9.9 -0.7	29.4	-0.5	-0.04	-0.002
C08	7.3 -0.2	20.1	-0.1	7.0 -0.4	20.1	-0.3	-0.06	0.24
C03	9.0 -1.4	22.4	-1.4	7.5 0	20.7	0	0.04	-0.41
C05	11.5 -1.3	28.9	-0.2	9.3 -1.8	27.5	-1.7	0.14	-0.17
C02	5.8 -0.3	15.6	-0.2	4.8 -0.6	15.6	-0.2	-0.42	0.75
C04	11.1 -0.2	29.8	-0.2	8.6 0	23.1	0	0.22	0.34
Avg	8.5 -0.7	22.7	-0.6	7.8 -0.5	23.0	-0.4	-0.08	-0.01
std	1.9 0.5	4.9	0.5	1.3 0.5	4.0	0.5	0.2	0.34

**Table 3.8: Individual torque and work values for control participants during fMRI pedaling.** Control participants are listed based on work percent of the right limb in decreasing order. All torque and work measures are separated and shown above.

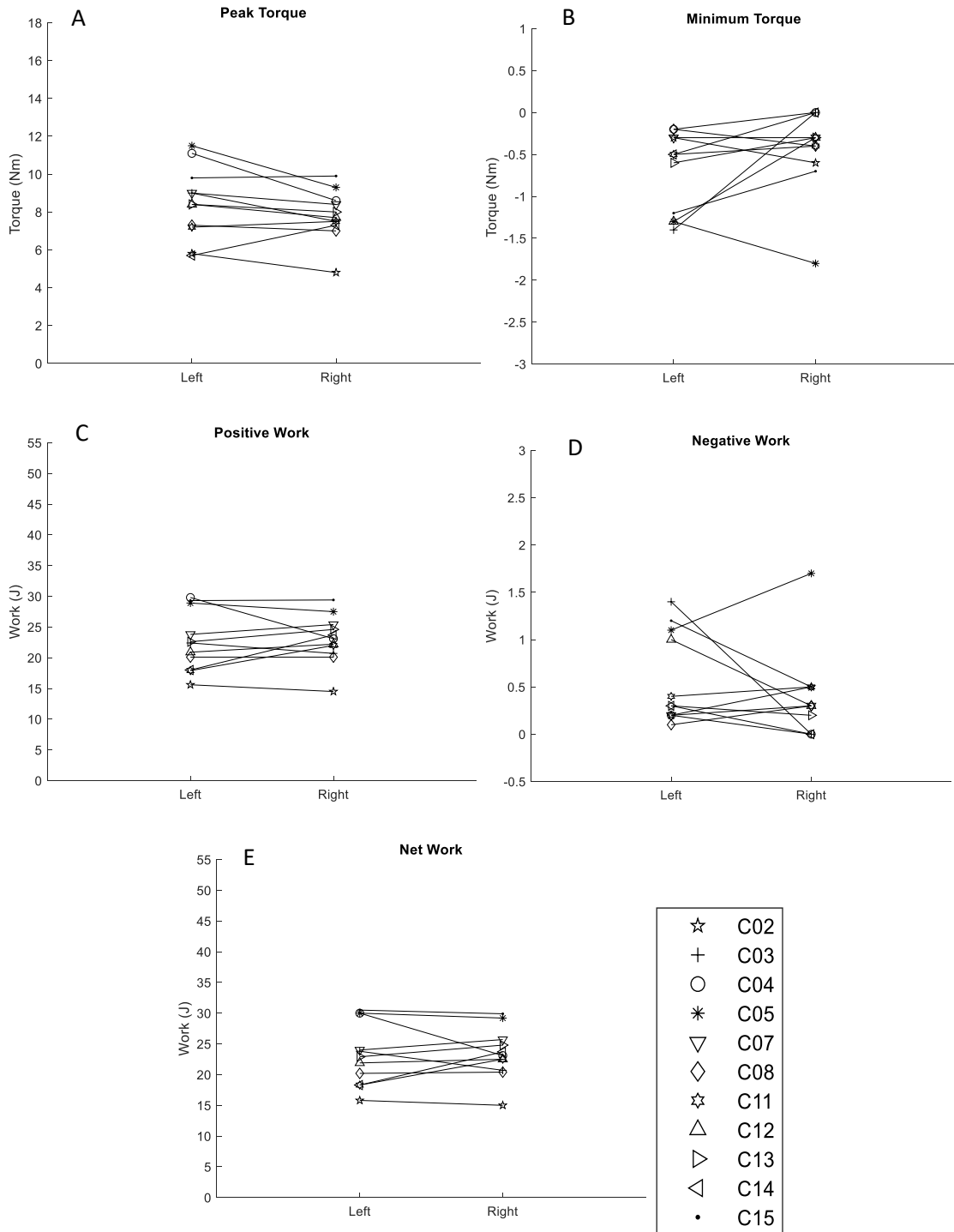


**Figure 3.12: Magnitude of the left and right limbs for torque and work values for controls during fMRI pedaling.** Visual presentation of Table 3.6 for comparison of the left and right A) peak torque ( $R^2 = 0.8$  and  $p = 0.003$ ), B) minimum torque ( $R^2 = 0.362$  and  $p = 0.3$ ), C) positive work ( $R^2 = 0.746$  and  $p = 0.008$ ), D) negative work ( $R^2 = 0.311$  and  $p = 0.4$ ), and E) net work ( $R^2 = 0.756$  and  $p = 0.007$ ).

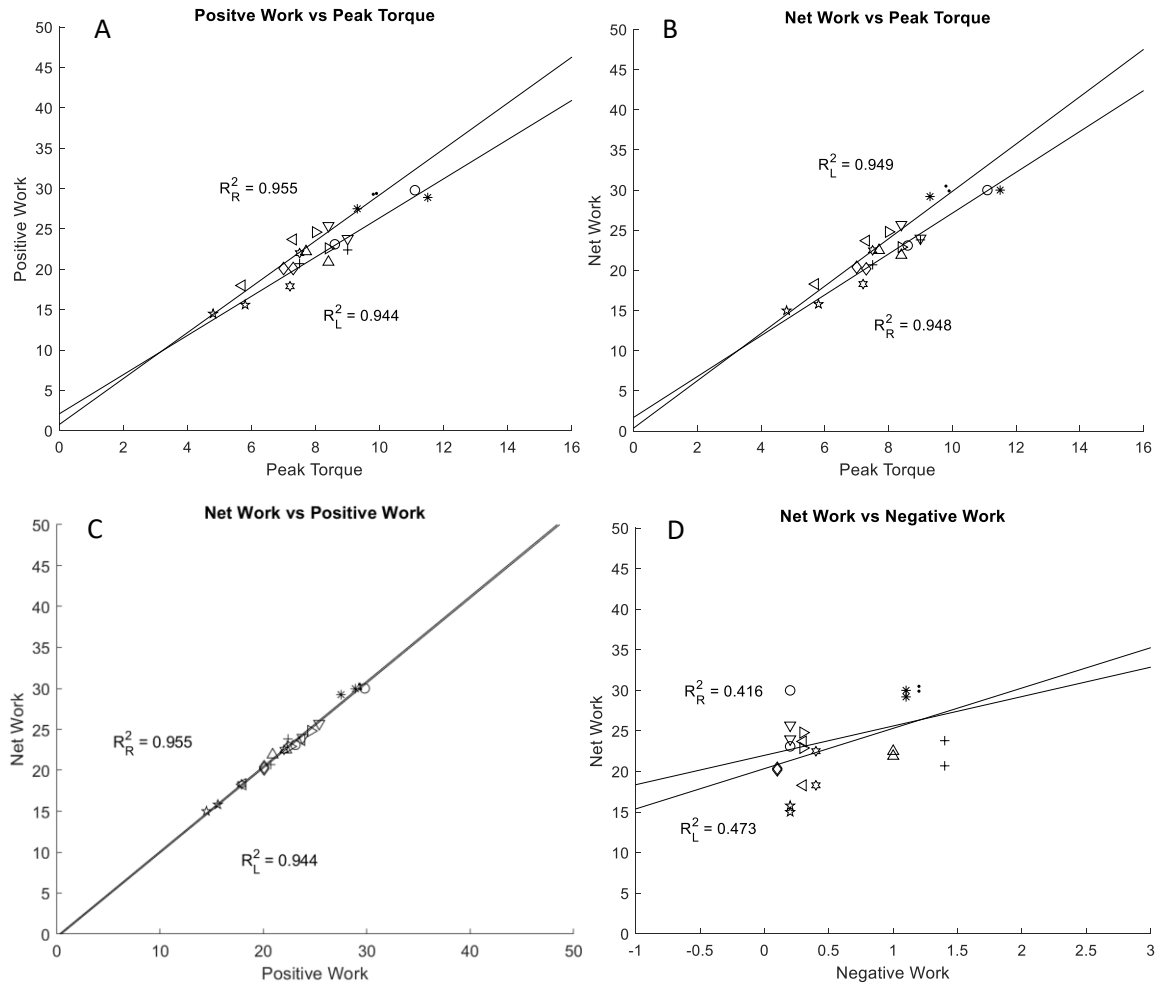


**Figure 3.13: Torque and work correlations for control participants during fMRI pedaling.** A) positive work and peak torque are significantly correlated for the left ( $R^2=0.955$  and  $p=0.0$ ) and right ( $R^2=0.944$  and  $p=0.0$ ) limbs. B) the net work is significantly correlated with peak torque for both limbs (left:  $R^2=0.949$  and  $p=0.0$ , right:  $R^2=0.948$  and  $p=0.0$ ). C) net work is significantly correlated with positive work for both limbs (left:  $R^2=0.955$  and  $p=0.0$ , right:  $R^2=0.944$  and  $p=0.0$ ). D) negative work is not correlated with either limb (left:  $R^2=0.473$  and  $p=0.14$ , right:  $R^2=0.416$  and  $p=0.2$ ).

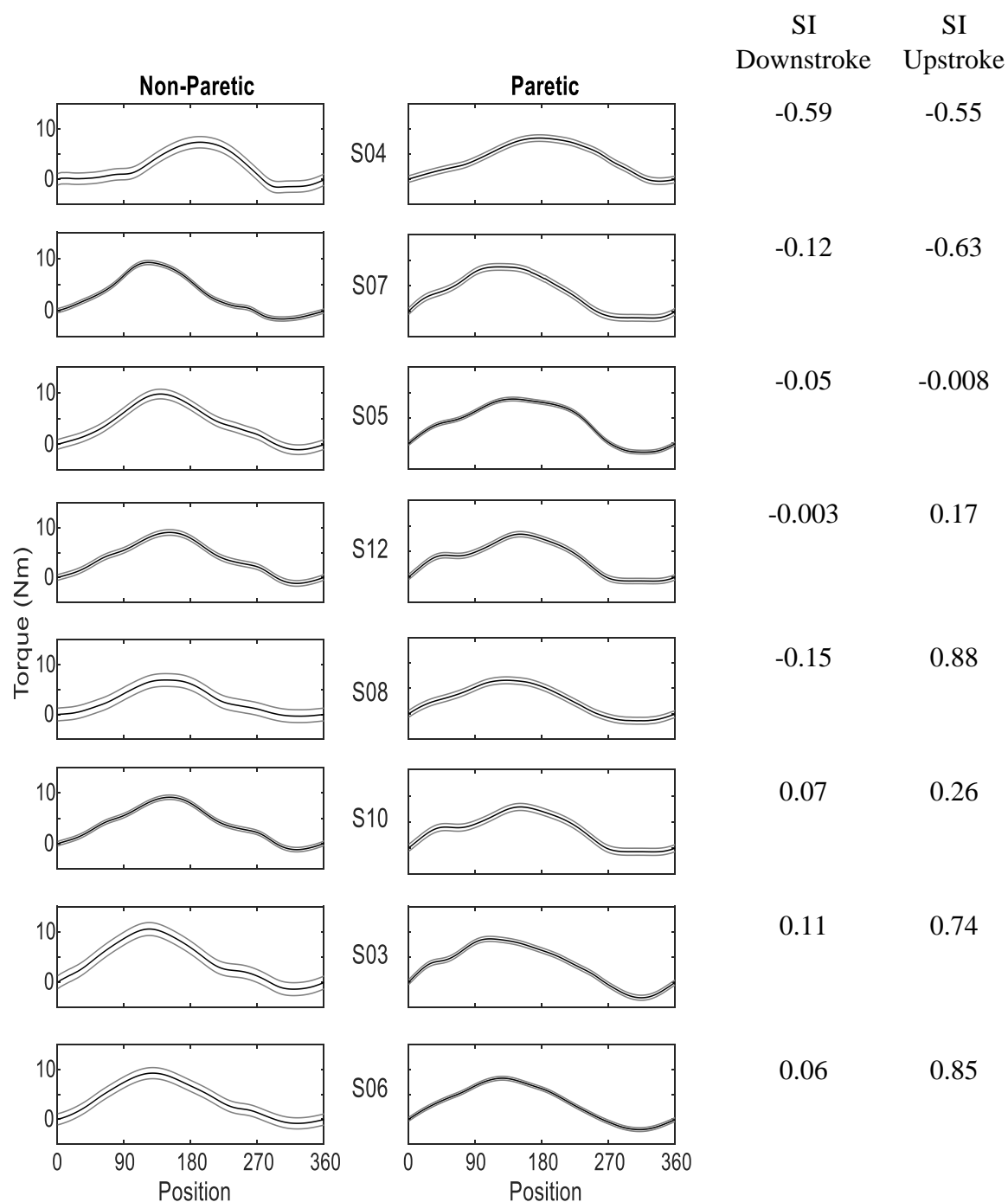


**Figure 3.14: Symmetry of stroke participants during fMRI pedaling.** Ordered from most work completed with the non-paretic limb compared to the paretic limb to the least work completed with the non-paretic limb compared to the paretic limb. Symmetry index is based on the average torque completed in either the downstroke or upstroke. Solid black lines are the average torque for all revolutions and gray lines are one standard deviation from the average.

	Non-Paretic			Paretic			SI Down-stroke	SI Up-stroke
	Max Min Torque (Nm)	Positive Work (J)	Negative Work (J)	Max Min Torque (Nm)	Positive Work (J)	Negative Work (J)		
S04	7.4 -1.6	15.8	-1.7	8.2 -0.4	25.6	-0.2	-0.59	-0.55
S07	9.2 -1.6	20.2	-1.8	8.7 -1.3	23.8	-2	-0.12	-0.63
S05	9.8 -1	24.7	-0.8	8.7 -1.7	26.7	-1.9	-0.05	-0.008
S12	9.1 -1.2	23.9	-0.9	8.4 -0.8	23.2	-1.1	-0.003	0.17
S08	6.9 -0.4	17.1	-0.3	6.6 -1.3	17.7	-1.8	-0.15	0.88
S10	9.1 -1.2	24.2	-0.8	7.8 -0.8	21.7	-1	0.07	0.26
S03	10.5 -1.4	26.6	-1.2	8.6 -3.1	24.3	-3.3	0.11	0.74
S06	9.3 -0.8	24.5	-0.6	8.3 -2.1	21.9	-2	0.06	0.85
Avg	8.9 -1.1	22.1	-1	8.2 -1.4	23.1	-1.7	-0.08	0.21
std	1.2 0.4	3.9	0.5	0.7 0.9	2.8	0.9	0.22	0.59

**Table 3.9: Individual torque and work data for all stroke participants during fMRI pedaling.** Stroke participants are listed based on work percentage comparison from the symmetry of Figure 3.14. All torque and work measures are separated shown above.

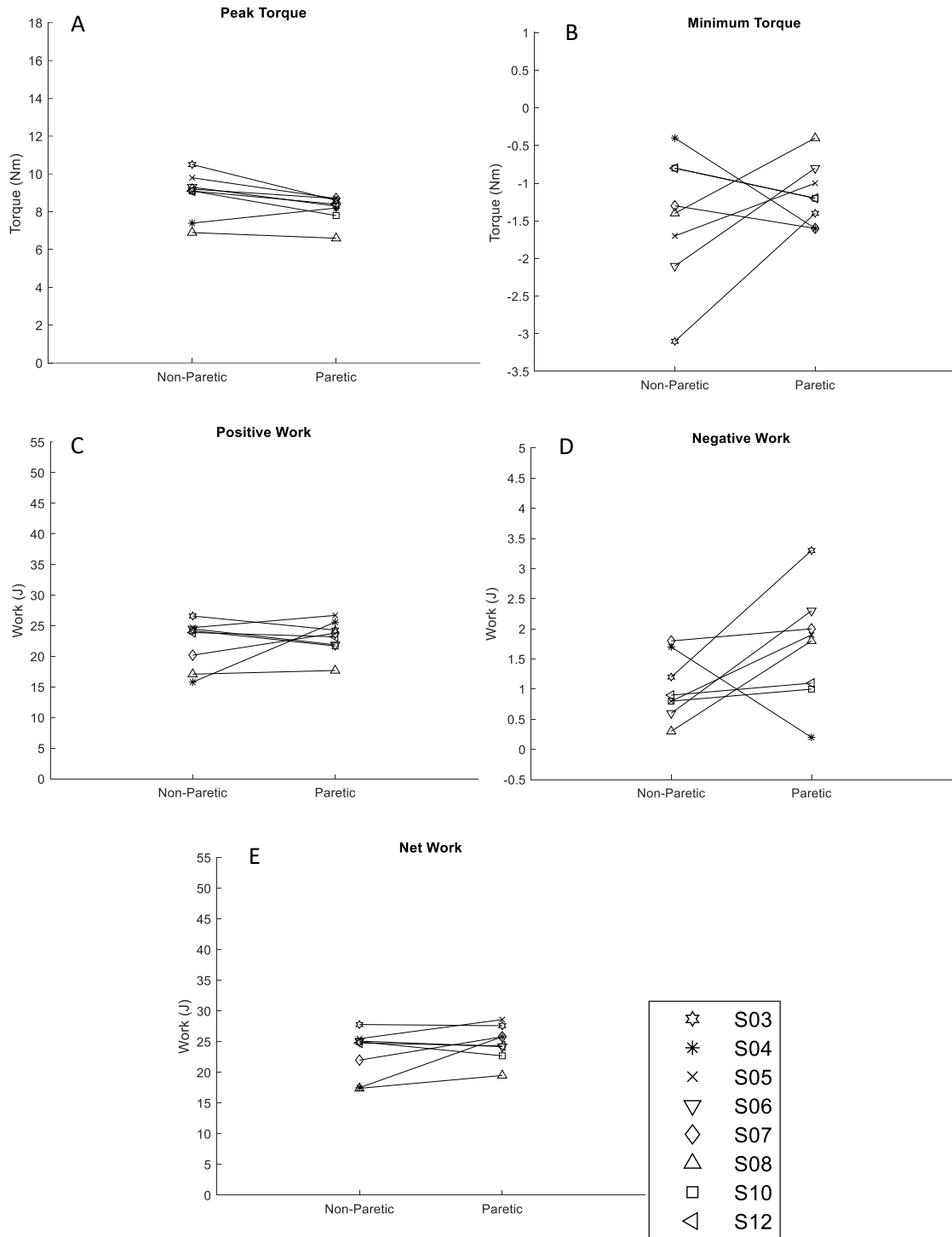


**Figure 3.15: Magnitude of the paretic and non-paretic torque and work data for stroke participants during fMRI pedaling.** Visual representation of Table 3.3 for comparison of the paretic and non-paretic A) peak torque ( $R^2 = 0.762$  and  $p = 0.03$ ), B) minimum torque ( $R^2 = -0.17$  and  $p = 0.7$ ), C) positive work ( $R^2 = 0.249$  and  $p = 0.6$ ), D) negative work ( $R^2 = -0.187$  and  $p = 0.7$ ), and E) net work ( $R^2 = 0.516$  and  $p = 0.2$ ).

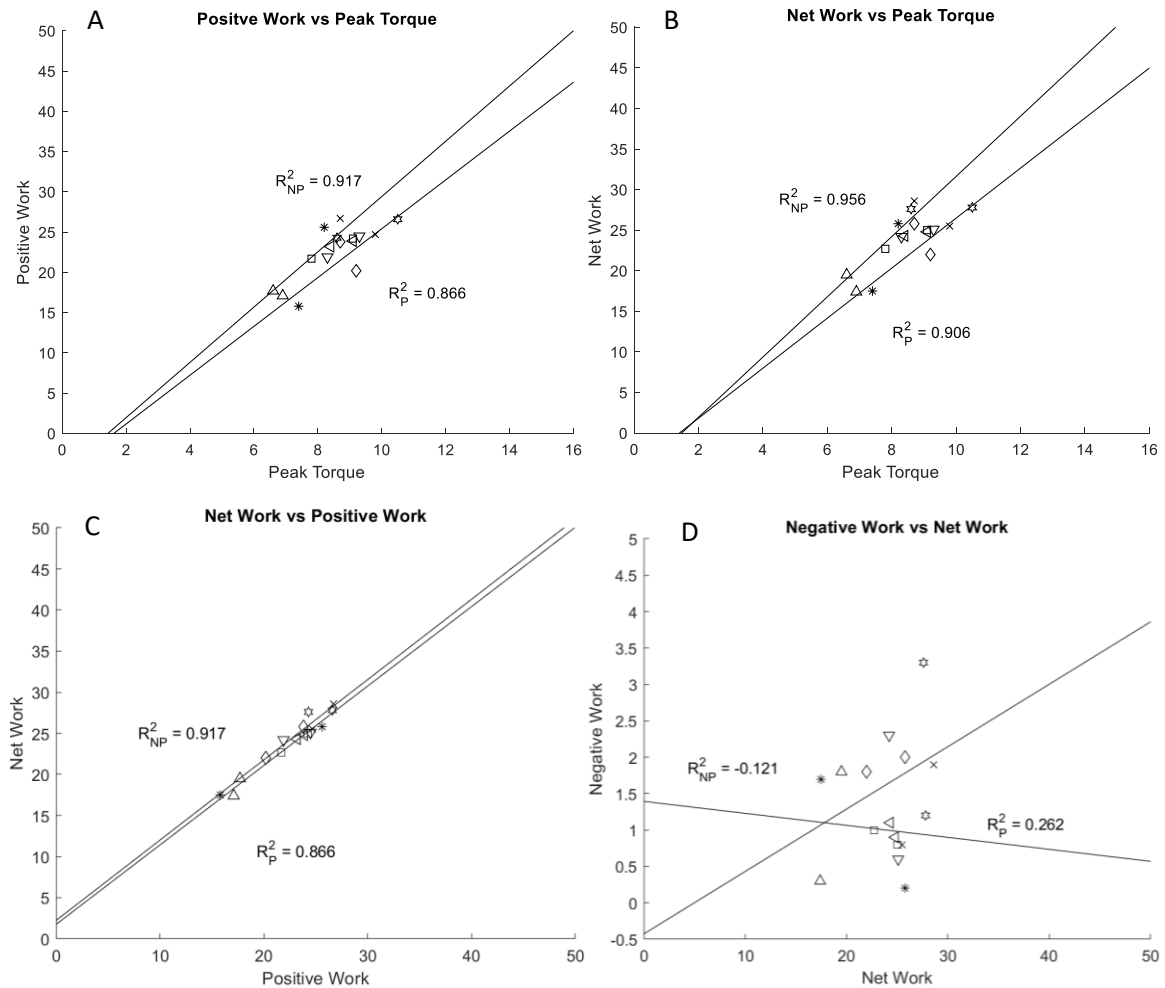


**Figure 3.16: Torque and work correlations for stroke participants during fMRI pedaling.** A) positive work and peak torque are significantly correlated for the paretic ( $R^2 = 0.866$  and  $p = 0.001$ ) and non-paretic ( $R^2 = 0.917$  and  $p = 0.005$ ) limbs. B) the net work is significantly correlated with peak torque for both limbs (Non-paretic:  $R^2 = 0.956$  and  $p = 0.0$ . Paretic:  $R^2 = 0.906$  and  $p = 0.0$ ). C) net work is significantly correlated with positive work for both limbs (Non-paretic:  $R^2 = 0.917$  and  $p = 0.0$ . Paretic:  $R^2 = 0.866$  and  $p = 0.0$ ). D) negative work is not correlated with the non-paretic limb ( $R^2 = 0.744$  and  $p = 0.121$ ) or paretic limb ( $R^2 = -0.262$  and  $p = 0.53$ ).

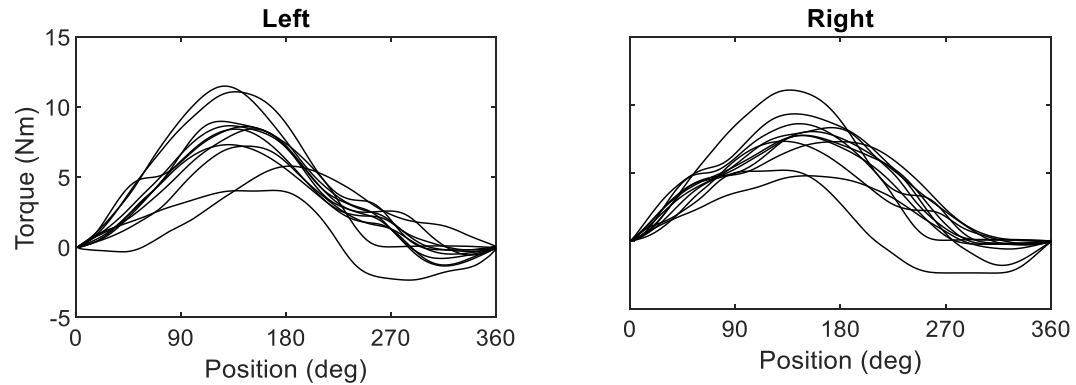


**Figure 3.17: Overlaid torque curves for control group during scanning.** The left and right limbs can be seen to have different magnitudes between participants. Overall, the two limbs are similar ( $p=0.2$ ).

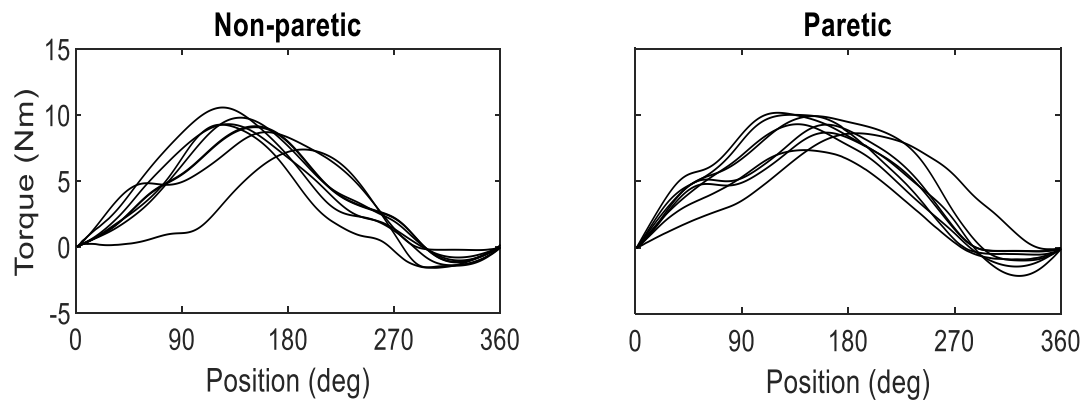


**Figure 3.18: Overlaid torque curves for stroke group during scanning.** The non-paretic and paretic limbs are shown for all stroke participants. The two groups have a relatively small variety of magnitudes but are not different when averaged.

	Control	Stroke	
		NP	P
Velocity (deg/s)	396 (108)	396 (108)	
COV (%)	27 (11)	27 (8)	
Max Torque (Nm)	8.2 (1.6)	8.9 (1.2)	8.2 (0.7)
Min Torque (Nm)	-0.6 (0.5)	-1.1 (0.4) <sup>a</sup>	-1.4 (0.9) <sup>a</sup>
Positive Work (J)	22.9 (4.4)	22.1 (3.9)	23.1 (2.8)
Negative Work (J)	-0.5 (0.5)	-1 (0.5) <sup>a</sup>	-1.7 (0.9) <sup>a</sup>
Net Work (J)	22.4 (3.9)	21.1 (3.4)	21.4 (1.9)
SI Downstroke	-0.08 (0.2)	-0.08 (0.22)	
SI Upstroke	-0.01 (0.34)	0.21 (0.59)	

<sup>a</sup> p<0.05 vs control<sup>b</sup> p<0.05 vs non-paretic

**Table 3.10: Control and stroke pedaling kinetics for fMRI pedaling.** Values are shown for all torque and work measurements as the average of the limbs for the control group and the non-paretic and paretic for the stroke group.

	Estimate	t-Stat	p-value
Intercept	-0.14	-0.53	0.65
x2	0.33	2.87	0.1
x3	-0.91	-6.99	0.02
x4	0.87	31.72	0.001
x5	0.03	0.65	0.58
R <sup>2</sup>	1		

**Table 3.11: Multilinear regression model for control group during fMRI.** X1 = peak torque, X2 = minimum torque, X3 = positive work, and X4 = negative work. The inputs are compared to net work.

	Estimate	t-Stat	p-value
Intercept	-0.01	-0.008	0.99
x2	0.38	1.09	0.39
x3	-1	-6.89	0.02
x4	0.87	10.53	0.009
x5	0.1	0.37	0.75
R <sup>2</sup>	0.996		

**Table 3.12: Multilinear regression model for stroke group during fMRI.** X1 = peak torque, X2 = minimum torque, X3 = positive work, and X4 = negative work. The inputs are compared to net work.

### *Familiarization versus fMRI pedaling*

Comparisons of the familiarization and fMRI scanning sessions of the study resulted in differences in pedaling torque and work between the two, but no differences in the symmetry in any of the groups or the velocity (Table 3.9). The control and stroke groups pedaling during fMRI had significantly greater COV compared to the control ( $p<0.001$ ,  $p<0.001$ ) and stroke ( $p<0.001$ ,  $p<0.001$ ) groups during familiarization. There were no differences in velocity between groups ( $p>0.1$ ).

The torque and work between groups had changed between the two groups but the symmetry did not significantly change in the upstroke or downstroke, but the upstroke in the stroke group is less symmetric than the control group (Figure 3.19 and 3.20). The control group in the MRI had significantly different peak torque ( $p=0.02$ ) and net work ( $p=0.006$ ) compared to the control group in the familiarization and significantly different min torque ( $p=0.007$ ) and negative work ( $p=0.008$ ) compared to the paretic limb of the stroke group in the familiarization. The non-paretic limb of the stroke group during fMRI pedaling had significantly different min torque ( $p=0.02$ ), positive work ( $p=0.02$ ), and net work ( $p=0.006$ ) compared to the controls in the familiarization, significantly different min torque ( $p=0.02$ ) compared to the non-paretic limb in the familiarization, and significantly different net work ( $p=0.04$ ) compared to the paretic limb in the familiarization session. The paretic limb of the stroke group had significant differences in all measures of torque and work ( $p<0.05$ ) compared to the familiarization controls, min torque ( $p=0.02$ ) and negative work ( $p=0.001$ ) compared to familiarization of the non-paretic limb, and net work ( $p=0.04$ ) compared to the paretic limb in the familiarization.

	Familiarization			fMRI		
	Control	Stroke NP	P	Control	Stroke NP	P
Velocity (deg/s)	434 (110)	406 (80)		396 (108)	396 (108)	
COV (%)	8.5 (3.3)	13.5 (7.2)		27 (11) <sup>abc</sup>	27 (8) <sup>abc</sup>	
Max Torque (Nm)	10 (2.1)	9.3 (2.1)	8.6 (1.8)	8.2 (1.6) <sup>a</sup>	8.9 (1.2)	8.2 (0.7) <sup>a</sup>
Min Torque (Nm)	-0.7 (0.5)	-0.6 (0.5)	-1.3 (0.7)	-0.6 (0.5) <sup>c</sup>	-1.1 (0.4) <sup>ab</sup>	-1.4 (0.9) <sup>ab</sup>
Positive Work (J)	27.1 (5.4)	24.4 (5.7)	24.7 (6.5)	22.9 (4.4) <sup>a</sup>	22.1 (3.9) <sup>a</sup>	23.1 (2.8) <sup>a</sup>
Negative Work (J)	-0.7 (0.5)	-0.5 (0.4)	-1.7 (1.3)	-0.5 (0.5) <sup>c</sup>	-1 (0.5) <sup>b</sup>	-1.7 (0.9) <sup>ab</sup>
Net Work (J)	26.4 (5)	23.9 (5.5)	23.1 (5.5)	22.4 (3.9) <sup>a</sup>	21.1 (3.4) <sup>ac</sup>	21.4 (1.9) <sup>ac</sup>
SI Downstroke	-0.07 (0.24)	-0.04 (0.24)		-0.08 (0.2)	-0.08 (0.22)	
SI Upstroke	0.12 (0.34)	1.04 (2.33)		-0.01 (0.34)	0.21 (0.59)	
<sup>a</sup> p<0.05 vs control familiarization <sup>b</sup> p<0.05 vs non-paretic familiarization <sup>c</sup> p<0.05 vs paretic familiarization						

**Table 3.13: Comparison of familiarization and fMRI pedaling values.** All values are averaged across participants for all groups. Values are shown for all torque and work measurements.

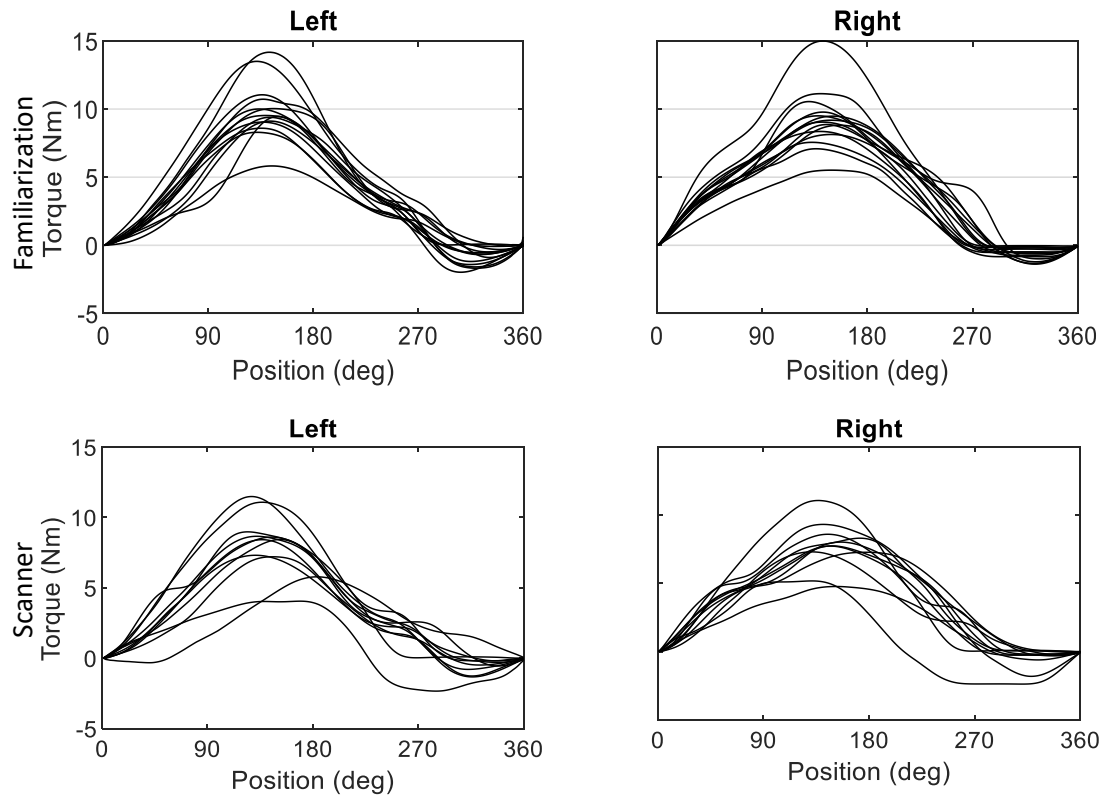


**Figure 3.19: Comparison of the familiarization and scanning pedaling for the control group.** Visual overlay of control group pedaling from both sessions.

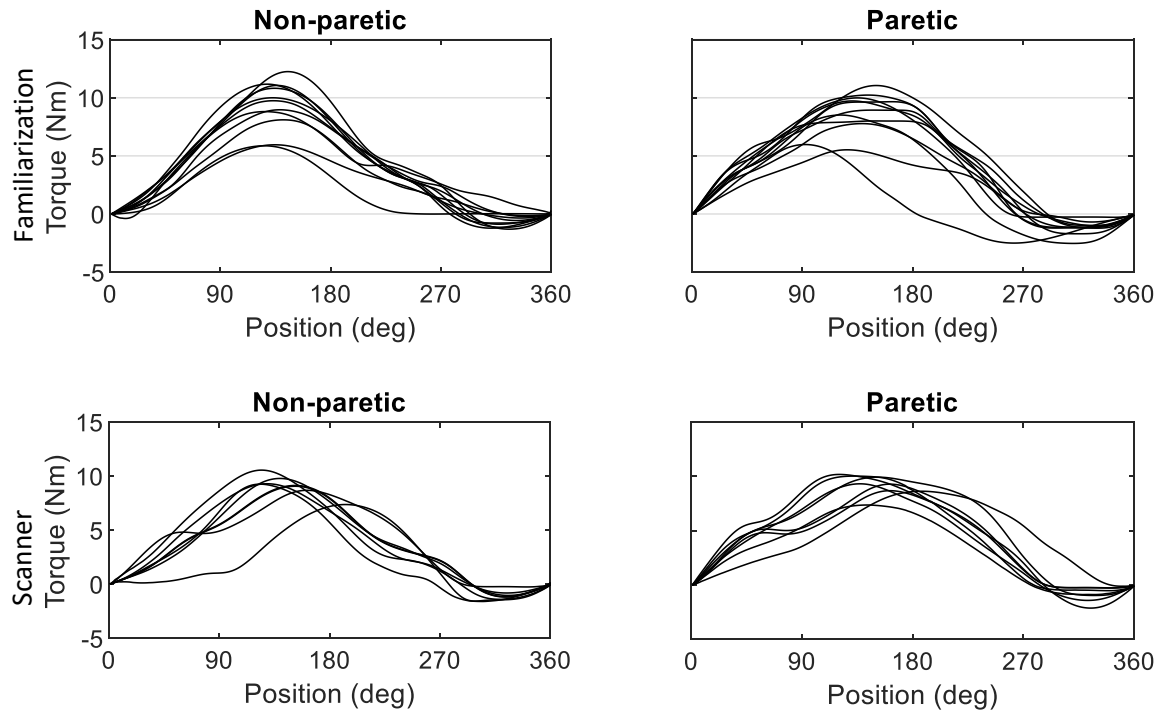


**Figure 3.20: Comparison of the familiarization and scanning pedaling for the stroke group.** Visual overlay of stroke group pedaling for both sessions.

### *EMG activity*

During conventional pedaling, controls participants showed no significant between limb differences for MI or mean EMG (Table 3.10 and Figure 3.21) for any muscle examined ( $p < 0.05$ ). In people with stroke, the MI in all muscles tended to be lower in the paretic limb than the control limb (Figure 3.22). The paretic limb had a lower MI in all muscles except the TA compared to the control limb. There were no significant differences between the TA and SOL for MI between the control group and the paretic limb. There was a significant difference between the SM of the paretic and non-paretic but, otherwise, no differences between the non-paretic and paretic groups for MI.

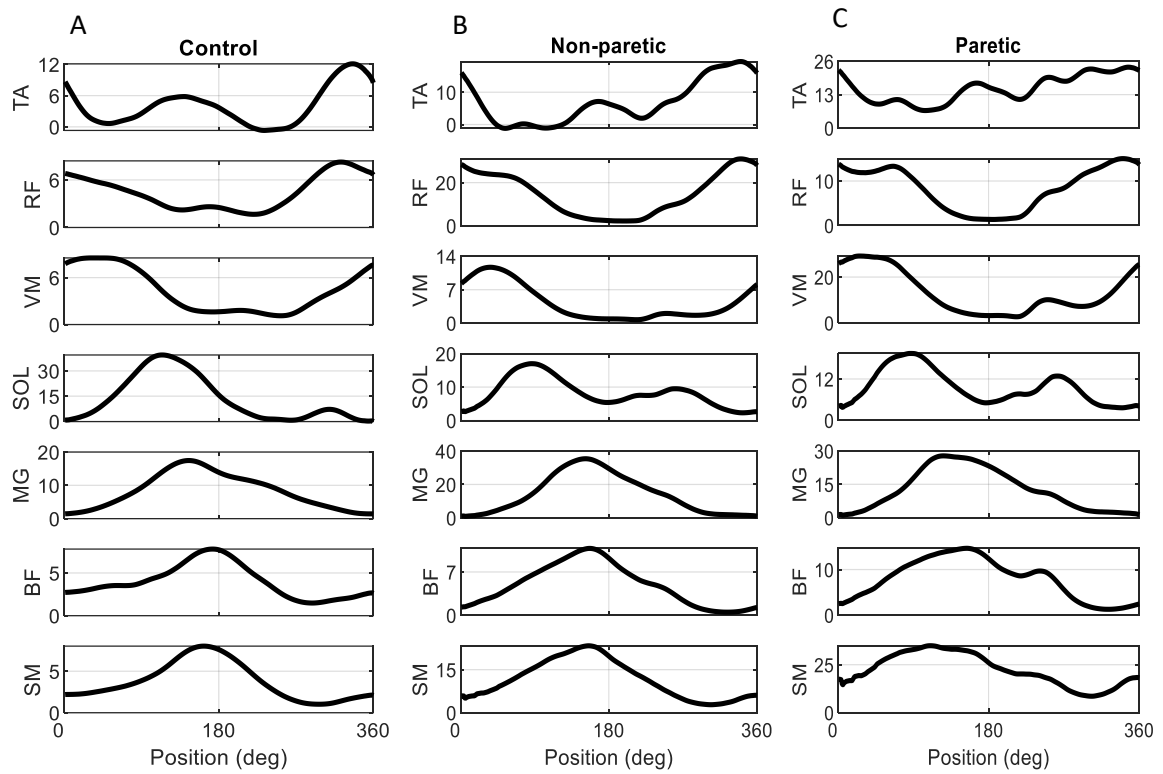


**Figure 3.21: EMG amplitude data averaged across cycle for control and stroke participants.** EMG is collected from both limbs during conventional pedaling and averaged across all cycles. A) averaged control participants, B) non-paretic limb of stroke group, and C) paretic limb of stroke group.

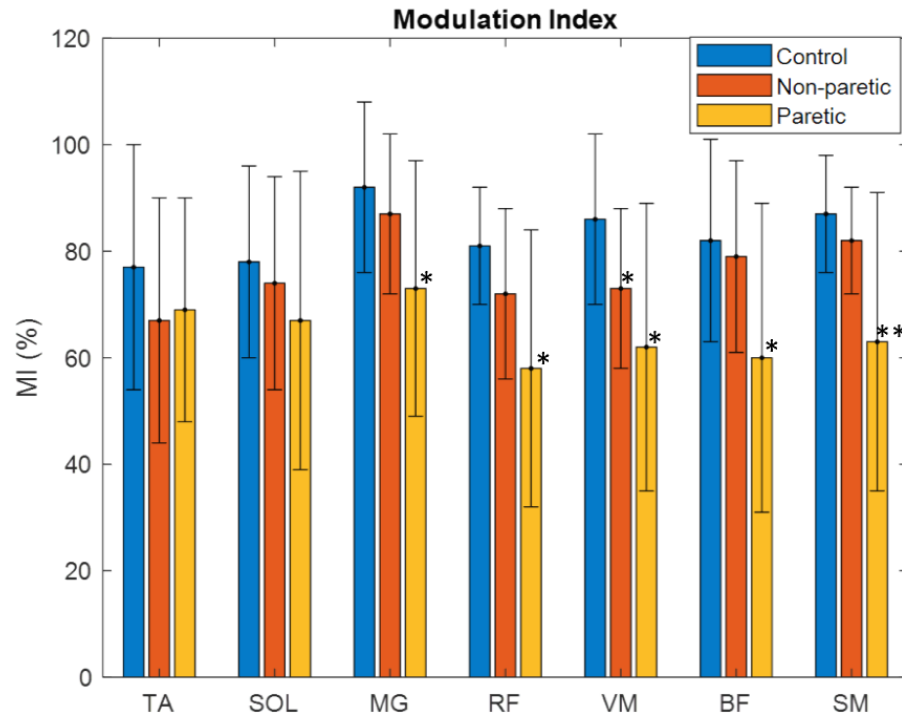


**Figure 3.22: EMG modulation index differences across muscles.** The differences between the control limb, non-paretic, and paretic limb are shown. \* denotes significant differences compared to the control group ( $p < 0.05$ ), and \*\* denotes the significant differences compared to both the control and non-paretic groups ( $p < 0.05$ ).

Conventional Pedaling			
		Control	Stroke
			Non-Paretic      Paretic
EMG			
	TA	77 (23)	67 (23)
	SOL	78 (18)	67 (28)
	MG	92 (16)	73 (24) <sup>a</sup>
MI (%)	RF	81 (11)	58 (26) <sup>a</sup>
	VM	86 (16)	62 (27) <sup>a</sup>
	BF	82 (19)	60 (29) <sup>a</sup>
	SM	87 (11)	63 (28) <sup>ab</sup>
Mean Amplitude (uV)			
	TA	6.7 (5.2)	13 (16.3) <sup>ab</sup>
	SOL	20.9 (41.9)	10.4 (9.7) <sup>a</sup>
	MG	11 (7)	17.5 (36.4) <sup>b</sup>
	RF	4.9 (2.6)	7.2 (11.5) <sup>ab</sup>
	VM	5.5 (3.2)	17.5 (40) <sup>b</sup>
	BF	4.4 (1.7)	8.9 (11.9) <sup>ab</sup>
	SM	4.7 (2.3)	21.2 (46.6) <sup>ab</sup>

<sup>a</sup> p<0.05 vs control

<sup>b</sup> p<0.05 vs non-paretic

**Table 3.14: Muscle activity for control and stroke groups during familiarization session.** The top section shows MI (SD) for both groups for all seven muscles. The bottom section shows the mean (SD) EMG for both groups for all seven muscles. TA: tibialis anterior, SOL: soleus, MG: medial gastrocnemius, RF: rectus femoris, VM: vastus medialis, BF: biceps femoris, SM: semimembranosus.

#### *Relationships between mechanical work and clinical measures*

The Fugl Meyer had correlations with torque and work in some cases, but the Berg Balance and walking speed were not correlated with any measure of torque or work. In the stroke group, positive work of the paretic limb was significantly correlated with the total Fugl Meyer ( $R^2=0.712$ ,  $p=0.01$ ) and the motor component of the Fugl Meyer ( $R^2=0.69$ ,  $p=0.02$ ). Positive work was not significantly correlated with the sensory component of the Fugl Meyer, Berg Balance, or walking speed. The negative work completed of the paretic limb was not significantly correlated with any part of the Fugl

Meyer, Berg Balance, or walking speed. The stroke group symmetry was significantly correlated with the total Fugl Meyer ( $R^2=0.888$ ,  $p=0.0$ ) and both the sensory ( $R^2=0.766$ ,  $p=0.002$ ) and motor ( $R^2=0.805$ ,  $p=0.006$ ) components. The berg balance and walking speed were not significantly correlated with symmetry.

## **Discussion**

The purpose of this study was to describe the pedaling symmetry of stroke survivors and compare pedaling with healthy age matched controls. The study aimed to describe the differences in pedaling between the two groups. As well, the study aimed to quantify the differences between pedaling in the laboratory and during MRI scanning. Torque, work, and symmetry index were considered for measuring impairment in symmetry. A novel, pedaling device enabled conventional bilateral pedaling for the study. The bilateral pedaling provided measures of asymmetry during continuous, reciprocal, flexion and extension movements involving both lower limbs. While evidence was found that there were differences in pedaling in both torque and work, results suggest that there may not be any significant differences in pedaling symmetry index in this study even though some results trended toward significance. Below, the findings are discussed in the context of prior work and implications.

### *Pedaling in Laboratory Setting*

Consistent with prior reports (De Marchis et al. 2015, Kautz and Brown 1998), the paretic lower limb is unable to produce the same amount of torque as the control limb of healthy age-matched controls. It is shown that the paretic limb has a lower peak torque

during pedaling, but does not have a difference in positive work. Prior work has shown there to be differences in the positive work completed by the control, non-paretic, and paretic lower limbs. This work used a different pedaling set up with a fly wheel which provided extra resistance (Kautz and Brown 1998, Kautz and Neptune 2002, De Marchis et al. 2015). The previous studies examined pedaling at different work levels which were shown to be greater than this study. For instance, Kautz and Brown aimed to have participants pedal at a moderate workload of 135 J and a cadance of 40 rpm (Kautz and Brown 1998). This study did not control for workload or cadence and allowed participants to pedal at a comfortable rate. The workload may not be specified but is known to be comparatively low. The work completed during this study was less than the work done in other studies (Kautz and Brown 1998, Chen et al. 2005, Lin, Chen and Lin 2013, Gusso et al. 2012, Jang et al. 2005, Turkseven and Ueda 2013). There were differences in the minimum torque production and negative work. Both the minimum torque and negative work were significantly different in the paretic limb compared to the non-paretic and control limbs. The minimum torque in the paretic limb was lower than the non-paretic and control limb with no differences between the non-paretic and control limbs. Similarly, there was significantly more negative work completed by the paretic limb than the non-paretic or control limbs. This is consistent with Kautz and Brown who show how the VM and RF muscles were being excited while lengthening during the upstroke, which produces negative work during pedaling (Kautz and Brown 1998). While minimum torque and negative work at different than the non-paretic and control limbs there is no difference in the symmetry between the stroke survivors and age-matched controls.

In the current study, the control group SI for the downstroke was -0.07 and 0.12 for the upstroke while the stroke group SI was -0.04 for the downstroke and 1.04 for the upstroke. The symmetrical pedaling of the controls is consistent with symmetry measured in other studies (Liu and J. 2010, Dorel et al. 2010, Patterson and Moreno 1990, Linder et al. 2018). The symmetry between the two groups was not significantly different, but the upstroke of the stroke group was considerably more asymmetric. The increase in asymmetries in the stroke group was driven by two participants who were more asymmetric than the other participants in the stroke group. In the case of net work, the net work is primarily driven by the positive work completed. The positive work is significantly correlated with the net work while the negative work is uncorrelated and plays a minimal role in effecting the net work. Comparisons using an multilinear regression analysis between the different measures of torque and work to the net work resulted in positive work influencing the net work the most with some influence from the peak torque as well. The minimum torque and negative work were not major components of the net work. The lack of differences in the multilinear regression suggest that at low loads, the positive work and peak torque greatly outweigh the negative work and minimum torque.

The ability to coordinate work for symmetric pedaling is needed. This study agrees with previous studies that the negative work, as a result of pedaling strategy, produced while pedaling is increased in the stroke group (De Marchis et al. 2015, Kautz and Brown 1998, Kautz and Neptune 2002). The paretic limb moves differently than the non-paretic limb and the differences cause a larger negative work completed. This is demonstrated by S07 whose negative work on the paretic limb was over twice the negative work of the non-paretic limb.

The peak and minimum torque do not directly affect the symmetry of pedaling. A large peak torque could be accompanied by lower positive work and similarly for minimum torque and negative work. The non-paretic limb of S04 and S08 are good examples for what may happen with the peak torque and positive work. S04 has a comparatively smaller peak torque than the stroke group but a larger positive work while S08 has a smaller peak torque and positive work. This suggests that the peak torque is not the only variable that affects positive work, but the amount of time positive work is generated. In this case, S04 and S08 have a similar amount of time for positive work to be generated, so the larger peak torque adds to the increased positive work. Similarly, the non-paretic limbs of S08 and S10 are a good example for minimum torque and negative work. S08 had a minimum torque much less than zero but a small negative work while S10 has a minimum torque close to zero and large negative work. The negative work is related to the amount of time negative work is being produced. S10 is producing negative work longer than S08 and, even though S10 has a minimum torque closer to zero, it produces more negative work.

Muscle activity in the MG, RF, VM, BF, and SM of the paretic limb were less modulated than the control limb. Only the SM was significantly less modulated in the paretic limb compared to the non-paretic limb. While quantitative comparisons of EMG amplitude between the paretic and non-paretic limb were not made, visual inspections of the data revealed many examples in which no task-related EMG was observed in the paretic limb during conventional pedaling. These observations support the conclusion that conventional pedaling is accomplished primarily by the non-paretic limb in people with stroke. However, these results differ from some of the kinetic results of torque and

work because the kinetic results do not describe large asymmetrical difference between the stroke and control groups even though there are differences in some of the kinetic values. The EMG results also suggest that pedaling is a useful model for functional lower limb movements, such as walking, in which the non-paretic limb generates more work (Bowden et al. 2006, Turns, Neptune and Kautz 2007). This supports what is found in the torque and work completed for the stroke group because the non-paretic limb tends to be larger than the paretic limb even if the symmetry is not different.

### *Pedaling During fMRI*

Use of an fMRI pedaling paradigm to test for pedaling symmetry while in an MRI scanner resulted in no differences in the symmetry index between groups, but the upstroke in the stroke group was lower than the upstroke or downstroke in either group. Differences were seen between the control and stroke groups for minimum torque and negative work. There were no differences between the max torque, positive work, or net work between groups. This suggests that the work completed by the paretic limb is different from the control limb but the max torque and positive work are not where the differences lay. Paretic limb work production has been shown by other studies to be decreased compared to the non-paretic or control limbs but this was studied outside of an MRI scanner (De Marchis et al. 2015, Kautz and Brown 1998). In scanner pedaling was studied by a few groups (Gusso et al. 2012, Pedersen et al. 1999, Roest et al. 2001, Jeneson et al. 2010, Promjunyakul et al. 2015) but not all measured pedaling torques or asymmetry. In the scanner, it has been seen that brain activation is lateralized in the stroke group in the cerebellum to the damaged hemisphere and there is a decrease in

activation volume. The amount of reduction in brain action volume may suggest pedaling asymmetries with increased reduction. The other studies cannot be compared because they measured cardiac output at specific power levels, 90-145w, but did not provide work or symmetry.

The two participants in the stroke group who were most impaired, S01 and S11, are not part of the scanning values because torques were unable to be measured for S01 in the scanner and S11 was not scanned. The two most impaired subjects not being part of the scanning data increases the max torque, positive work, net work, and symmetry index values. These two subjects had lower pedaling kinetic values which potentially could have brought down the average to a significant difference. A multilinear regression analysis showed that the net work of pedaling is primarily composed of the positive work from pedaling. The stroke group did show that the minimum torque of the opposite limb did play a role in the net work as well. A minimum work farther from 0 of the opposite leg would suggest that more positive work needs to be completed by the leg in the downstroke to overcome the resistance of the upstroke. The minimum torque was not a factor in the control group.

#### *Differences Between Familiarization and fMRI Pedaling*

No previous studies have examined the comparison of pedaling on the same device between a laboratory setting and MRI scanning. It was found that there are no differences in pedaling symmetry between the familiarization session or MRI scanning session. Differences were found in all measures of torque and work for all groups, as well as, a difference in COV. There were no differences in the velocity between either session,

but the velocity trended lower in the scanning session. The results suggest that pedaling velocity becomes less consistent and more variable during scanning, which may be related to the setup of pedaling in the scanner. The participants are laying supine, similar to the familiarization, but were strapped down. A chest strap was used to restrict upper body movement and the head was placed in the MRI coil with a vacuum pillow to stabilize the head. Participants were unable to see their feet during the scanning trials. Participants tended to be farther from the device in the scanner than in the laboratory because of the scanner's bore. As well, this may be due to the lack of continuous pedaling, which instead was shorter bouts of pedaling. These differences may have led to the differences shown in torque and work between the two sessions. The scanning session had lower peak torque, positive work, and net work values for the control group but no differences in the minimum torque or negative work. The non-paretic limb in the stroke group had no differences between sessions for peak torque, positive work, or net work but had a lower minimum torque and negative work values. The paretic limb for the stroke group had a significantly lower net work in the MRI scanning session compared to the familiarization, but no other differences. This suggests that both groups in the two sessions produced similar amounts of work but may overall be lowered in the scanner. The decrease in work may be caused by the previously mentioned setup differences, as well as, the less participation in the scanning session, and decreased velocity. Less participation in the scanning session may suggest that differences in torque and work are caused by participants who had greater torque and work in the familiarization session not being scanned. This would decrease the average of the torque and work values for the scanning values.

The scanning session reinforces the conclusion about net work from the familiarization session. The scanning session shows that the net work is composed of the positive work by majority with minimal addition of the negative work. The peak torque shown to contribute in the familiarization session is not as important during the scanning session but both focus on the positive work as the primary contributor.

Pedaling strategies between the groups did not visually change between sessions as a whole. S04 was the only subject who showed differences in their pedaling strategy between sessions. The participant showed significantly lowered peak torque and positive work in their non-paretic limb but no differences in their paretic limb. They began to increase their torque at a later degree in the scanning session and returned towards 0 much more rapidly. This suggests that there may have been other factors outside of the pedaling that affected their work contribution on the non-paretic limb. This may have caused for skewed symmetry measures and increased the symmetry measure of the stroke group in the scanning session resulting in no differences and a lower symmetry index value than in the familiarization session.

### *Pedaling Symmetry*

Asymmetries persist in both healthy adults and stroke survivors. The asymmetries of healthy adults may be due to aging or to dissimilarities in their lower limbs. On the other hand, stroke related asymmetry is related to their level of impairment (Sacchetti et al. 2010, De Marchis et al. 2015). The participants of the stroke group of this study were of higher level and lower impairment. This may relate to the minimal differences between the symmetry of the work produced of the two groups. There were asymmetrical

differences between groups for EMG. The paretic limb was less modulated than the control limb. Deficits during unilateral pedaling seen by Cleland suggest that both paretic motor impairment and deficiencies in interlimb coordination may contribute to reduced use of the paretic limb during conventional pedaling (Cleland 2018). Difficulties during the posterior transition with the paretic limb in pedaling may contribute to asymmetry. Higher functioning stroke survivors may have little trouble with this transition during conventional pedaling because there is less need for interlimb coordination, but still show asymmetrical differences in their MI of EMG. The ability to view their lower limbs, during the familiarization task, gives them the chance to use visual feedback to aid in pedaling and decrease pedaling asymmetry. Many participants noted that being able to see their limb helped them pedal more efficiently. Larger pedaling asymmetries have been seen in other studies (Alibiglou and Brown 2011b, Chen et al. 2005, De Marchis et al. 2015, Brown and Kautz 1998, Landin et al. 1977, Promjunyakul et al. 2015). These studies viewed EMG related pedaling asymmetries similar to what has been found here. As well, many of these studies viewed symmetry at higher workloads than this study produced. The workloads tended to be 3-5 times greater for work production. This suggests that pedaling symmetry at higher loads may exacerbate the differences between the non-paretic and paretic limbs in work asymmetry.

### *Limitations*

There were several limitations to this study. First, most of the participants with stroke who participated in this study had relatively high levels of function. Most individuals could function in the community and all were able to participate in the study.

In people who are lower functioning, paretic motor impairment may be a more important contributor to asymmetry. Second, this study was limited by being completed with another study measuring the neural connectivity in the cortex based on motor, language, and memory tasks. The second study had an inclusion criterion for only allowing left hemisphere lesioned stroke participants. This caused for all participants to have the same lesioned hemisphere and paretic limb. Third, the fMRI session of the study was limited by a participants' ability to comfortably be scanned. Non-MRI safe implants and claustrophobia gave challenge to having the same number of participants for the familiarization and fMRI sessions. During the fMRI, pedaling was limited by measures taken to protect image quality and the subject. To protect image quality, there needed to be less than 3 mm of head movements by the participants, so a vacuum bead pillow and chin strap were used to keep their head in place. As well, a large strap was used across the torso to keep their body in place. The pedaling device needed to be placed far enough from the scanner, so the participant's knees would not touch the bore while they pedaled. Fourth, measures of modulation index are an indirect measurement of the amplitude of muscle activity but was used because of the inability to normalize EMG responses.

## **Conclusion**

The primary conclusion from this study was that pedaling symmetries are not significantly different between stroke survivors and healthy age-matched controls at low levels of work production, but the stroke group had larger symmetry index values meaning they were less symmetric. This conclusion has several caveats. First, the amounts of torque produced, and work completed were different between groups

suggesting the symmetry index may not be the most important factor when looking at low loads. Second, the differences in pedaling between the familiarization and fMRI session may be due to the limitations and changes in set up causing restrictions to a participant's movements in the MRI. Third, bilateral activation may exacerbate paretic motor impairments by increasing coactivation and demands for stabilization. However, this is the author's interpretations, and thus the conclusions may be under-representing the effect of the paretic motor impairments.

## **CHAPTER 4: CONCLUSION AND FUTURE DIRECTIONS**

The purpose of this thesis was to describe the differences in pedaling symmetry between stroke survivors and healthy age matched controls. Furthermore, the thesis aimed to quantify how the stroke group pedaled differently from the controls in an MRI scanner and compared both the laboratory and MRI pedaling. A redesign of an MRI safe torque transducer was completed to test the pedaling symmetry. This purpose was tailored to improve the understanding of the differences in pedaling performance after stroke and if there are differences in pedaling performance during MRI scanning and in the laboratory. The preceding chapters provided novel information that may help address the problem of pedaling asymmetry. This thesis informs the work previously completed by Promjunyakul and Cleland (Cleland 2018, Promjunyakul et al. 2015). The results advance these studies by relating the cortical activity and interlimb coordination using torque and work. This study describes the mechanical work contributions during pedaling and aids in the understanding of the previous work. This chapter summarizes the main findings from this thesis and describes future studies that would further advance this line of research.

### **Summary of Results**

In chapter 2, a torque measuring system, safe in the MR environment, was designed for pedaling on a novel pedaling device. This device was designed to be both accurate and precise. The device was demonstrated to accurately and consistently measure torque. The results show there is a low amount of noise contaminating the system. The results demonstrate that the device can measure a wide variety of torques

and can accurately and precisely convert torques applied to the device to known torque values. The results show that the device is capable of being used for a pedaling study and is able to measure the torques produced.

In chapter 3, torque and work production were measured during conventional pedaling. Conventional pedaling was completed during both the familiarization and fMRI scanning sessions. The differences in pedaling kinetics were measured in both sessions. Pedaling kinetics were quantified by torque and work production during pedaling. There were multiple hypotheses for this study: 1) if stroke survivors have motor impairments, then they will pedal more asymmetrically than control participants; 2) the more motor impairment a stroke survivor has will relate to their level of asymmetry; 3) if participants are set up similarly in both sessions, then they will pedal in similar manners.

During conventional pedaling, evidence was found that stroke survivors pedaled differently than controls. The stroke group pedaled with a greater minimum torque and more negative work. There were no differences in peak torque, positive work, or net work between the stroke and control groups. This led to no differences in the symmetry between groups either even though the stroke group upstroke SI trended toward significance. This was the same across sessions for both groups. Furthermore, there were differences in pedaling performance between the familiarization and scanning session. The scanning session showed lower maximum torques, positive work, and net work. This may be related to the difference in the setup of the participants which was previously described. There were no differences in the symmetry index between sessions. This suggests that both groups pedaled in a similar manner during both sessions but with less torque and work in the scanning session due to limitations.

Overall, this thesis described the design of a torque measurement system used for pedaling in an MR environment and how pedaling symmetry is related between stroke survivors and healthy age matched controls. The results suggest that symmetry between groups is not different at low loads, but the pedaling performance is different. Stroke survivors produce more negative work while pedaling than controls. This is important for developing methods to measure and design future studies for rehabilitation after stroke.

### **Future Studies**

There is considerable potential for future investigation of how lower limb pedaling is related to motor function and brain activation. Some possibilities are discussed here.

This study has shown pedaling symmetry and measured torque and work during conventional pedaling. Studies can be conducted having participants pedal unilaterally and bilaterally uncoupled. The studies would compare the torque and work production during the different pedaling tasks with conventional pedaling. This would provide insight to how motor impairments affect torque production during other pedaling conditions and if interlimb coordination plays a role in the torque and work production. These tasks can be completed with brain scanning as well. This would describe the differences in brain activation location and volume during the different pedaling tasks.

## BIBLIOGRAPHY

- Alibiglou, L. & D. A. Brown (2011a) Impaired muscle phasing systematically adapts to varied relative angular relationships during locomotion in people poststroke. *J Neurophysiol*, 105, 1660-70.
- (2011b) Relative temporal leading or following position of the contralateral limb generates different aftereffects in muscle phasing following adaptation training post-stroke. *Exp Brain Res*, 211, 37-50.
- Allred, R. P. & T. A. Jones (2008) Maladaptive effects of learning with the less-affected forelimb after focal cortical infarcts in rats. *Exp Neurol*, 210, 172-81.
- Allred, R. P., M. A. Maldonado, J. E. Hsu And & T. A. Jones (2005) Training the "less-affected" forelimb after unilateral cortical infarcts interferes with functional recovery of the impaired forelimb in rats. *Restor Neurol Neurosci*, 23, 297-302.
- Ambrosini, E., S. Ferrante, G. Ferrigno, F. Molteni & A. Pedrocchi (2012) Cycling induced by electrical stimulation improves muscle activation and symmetry during pedaling in hemiparetic patients. *IEEE Trans Neural Syst Rehabil Eng*, 20, 320-30.
- Arand, B. 2013. *Supraspinal Control of Unilateral Locomotor Performance: an fMRI Study Using Custom Pedaling Device*. Milwaukee: Marquette University.
- Arene, N. & J. Hidler (2009) Understanding motor impairment in the paretic lower limb after a stroke: a review of the literature. *Top Stroke Rehabil*, 16, 346-56.
- Bowden, M. G., C. K. Balasubramanian, R. R. Neptune & S. A. Kautz (2006) Anterior-posterior ground reaction forces as a measure of paretic leg contribution in hemiparetic walking. *Stroke*, 37, 872-6.
- Broker, J. & R. Gregor. 1994. Mechanical energy management in cycling: source relations and energy expenditure. *Medical Science and Sports Exercise*.
- Brown, D. A. & S. A. Kautz (1998) Increased workload enhances force output during pedaling exercise in persons with poststroke hemiplegia. *Stroke*, 29, 598-606.
- Brown, D. A., S. A. Kautz & C. A. Dairaghi (1997) Muscle activity adapts to anti-gravity posture during pedalling in persons with post-stroke hemiplegia. *Brain*, 120 ( Pt 5), 825-37.
- . 1998. Muscle Activity Patterns Altered During Pedaling at Different Body Orientations. *Journal of Biomechanics*: Elsevier Science Ltd.
- Chen, H. Y., S. C. Chen, J. J. Chen, L. L. Fu & Y. L. Wang (2005) Kinesiological and kinematical analysis for stroke subjects with asymmetrical cycling movement patterns. *J Electromyogr Kinesiol*, 15, 587-95.

- Cheng, C. P., D. F. Schwandt, E. L. Topp, J. H. Anderson, R. J. Herfkens & C. A. Taylor (2003) Dynamic exercise imaging with an MR-compatible stationary cycle within the general electric open magnet. *Magn Reson Med*, 49, 581-5.
- Chinworth, S. & W. Zimmermann. Designing a sensor; a force pedal for the bicycle. Texas Woman's University, Denton, Texas, USA.
- Cimbala, J. 2013. Stress, Strain, and Strain Gages. Penn State University.
- Cleland, B. 2018. MOTOR COMPENSATION DURING LOWER LIMB PEDALING AFTER STROKE. Marquette University.
- Cleland, B., T. Gelting, B. Arand, J. Struhar & S. Schindler-Ivens. 2016. Split-crank pedaling reveals residual lower limb motor capacity after stroke. Society for Neuroscience National Meeting. San Diego, CA.
- Davis, R. R. & M. L. Hull. 1981. Measurement of pedal loading in bicycling: II. Analysis and Results. *Journal of Biomechanics*.
- De Marchis, C., E. Ambrosini, M. Schmid, M. Monticone, A. Pedrocchi, G. Ferrigno, T. D'Alessio, S. Conforto & S. Ferrante (2015) Neuro-mechanics of muscle coordination during recumbent pedaling in post-acute stroke patients. *Conf Proc IEEE Eng Med Biol Soc*, 2015, 246-9.
- Dorel, S., A. Couturier, J. Lacour, H. Vandewalle, C. Hautier & F. Hug (2010) Force-velocity relationship in cycling revisited: benefit of two-dimensional pedal forces analysis. *Medicine and Science in Sports and Exercise*.
- Duinen, H. v. 2007. *The interaction between motor fatigue and cognitive task performance*. University of Groningen: Print Partners Ipskamp.
- Engardt, M., E. Knutsson, M. Jonsson & M. Sternhag (1995) Dynamic muscle strength training in stroke patients: effects on knee extension torque, electromyographic activity, and motor function. *Arch Phys Med Rehabil*, 76, 419-25.
- Enzinger, C., H. Dawes, H. Johansen-Berg, D. Wade, M. Bogdanovic, J. Collett, C. Guy, U. Kischka, S. Ropele, F. Fazekas & P. M. Matthews (2009) Brain activity changes associated with treadmill training after stroke. *Stroke*, 40, 2460-7.
- Enzinger, C., H. Johansen-Berg, H. Dawes, M. Bogdanovic, J. Collett, C. Guy, S. Ropele, U. Kischka, D. Wade, F. Fazekas & P. M. Matthews (2008) Functional MRI correlates of lower limb function in stroke victims with gait impairment. *Stroke*, 39, 1507-13.
- Gusso, S., C. Salvador, P. Hofman, W. Cutfield, J. C. Baldi, A. Taberner & P. Nielsen (2012) Design and testing of an MRI-compatible cycle ergometer for non-invasive cardiac assessments during exercise. *Biomed Eng Online*, 11, 13.
- Hagberg, J., M. Mullin, M. Giese & E. Spitznagel (1981) Effect of pedaling rate on submaximal exercise responses of competitive cyclists. *Journal of Applied Physiology*.

- Jang, S. H., S. H. You, Y. H. Kwon, M. Hallett, M. Y. Lee & S. H. Ahn (2005) Cortical reorganization associated lower extremity motor recovery as evidenced by functional MRI and diffusion tensor tractography in a stroke patient. *Restor Neurol Neurosci*, 23, 325-9.
- Jansen, K., F. De Groote, W. Aerts, J. De Schutter, J. Duysens & I. Jonkers (2014) Altering length and velocity feedback during a neuro-musculoskeletal simulation of normal gait contributes to hemiparetic gait characteristics. *J Neuroeng Rehabil*, 11, 78.
- Jeneson, J. A., J. P. Schmitz, P. A. Hilbers & K. Nicolay (2010) An MR-compatible bicycle ergometer for in-magnet whole-body human exercise testing. *Magn Reson Med*, 63, 257-61.
- Jonkers, I., S. Delp & C. Patten (2009) Capacity to increase walking speed is limited by impaired hip and ankle power generation in lower functioning persons post-stroke. *Gait Posture*, 29, 129-37.
- Kautz, S. A. & D. A. Brown (1998) Relationships between timing of muscle excitation and impaired motor performance during cyclical lower extremity movement in post-stroke hemiplegia. *Brain*, 121 ( Pt 3), 515-26.
- Kautz, S. A. & R. R. Neptune (2002) Biomechanical determinants of pedaling energetics: internal and external work are not independent. *Exerc Sport Sci Rev*, 30, 159-65.
- Kautz, S. A. & C. Patten (2005) Interlimb influences on paretic leg function in poststroke hemiparesis. *J Neurophysiol*, 93, 2460-73.
- Landin, S., L. Hagenfeldt, B. Saltin & J. Wahren (1977) Muscle metabolism during exercise in hemiparetic patients. *Clin Sci Mol Med*, 53, 257-69.
- Lin, P. Y., J. J. Chen & S. I. Lin (2013) The cortical control of cycling exercise in stroke patients: an fNIRS study. *Hum Brain Mapp*, 34, 2381-90.
- Linder, S. M., A. B. Rosenfeldt, A. S. Bazyk, M. M. Koop, S. Ozinga & J. L. Alberts (2018) Improved lower extremity pedaling mechanics in individuals with stroke under maximal workloads. *Top Stroke Rehabil*, 25, 248-255.
- Liu, T. & J. J. (2010) Age-Related Differences in Bilateral Asymmetry in Cycling Performance. *Department of Health and Human Performance at Texas State University*.
- Luft, A. R., L. Forrester, R. F. Macko, S. McCombe-Waller, J. Whittall, F. Villagra & D. F. Hanley (2005) Brain activation of lower extremity movement in chronically impaired stroke survivors. *Neuroimage*, 26, 184-94.
- Madhavan, S., C. Krishnan, A. Jayaraman, W. Z. Rymer & J. W. Stinear (2011) Corticospinal tract integrity correlates with knee extensor weakness in chronic stroke survivors. *Clin Neurophysiol*, 122, 1588-94.
- Mayo, N. E., S. Wood-Dauphinee, R. Cote, L. Durcan & J. Carlton (2002) Activity, participation, and quality of life 6 months poststroke. *Arch Phys Med Rehabil*, 83, 1035-42.

- McComas, A. J., R. E. Sica, A. R. Upton & N. Aguilera (1973) Functional changes in motoneurons of hemiparetic patients. *J Neurol Neurosurg Psychiatry*, 36, 183-93.
- Nadeau, S., A. B. Arsenault, D. Gravel & D. Bourbonnais (1999) Analysis of the clinical factors determining natural and maximal gait speeds in adults with a stroke. *Am J Phys Med Rehabil*, 78, 123-30.
- Neptune, R. R. & W. Herzog (1999) The association between negative muscle work and pedaling rate. *J Biomech*, 32, 1021-6.
- Omega. 1999. Practical Strain Gage Measurements. Agilent Technologies.
- Patterson, R. & M. Moreno (1990) Bicycle pedaling forces as a function of pedaling rate and power output. *Journal of Medicine and Science in Sports and Exercise*.
- Pedersen, E. M., S. Kozerke, S. Ringgaard, M. B. Scheidegger & P. Boesiger (1999) Quantitative abdominal aortic flow measurements at controlled levels of ergometer exercise. *Magn Reson Imaging*, 17, 489-94.
- Promjunyakul, N. O., B. D. Schmit & S. M. Schindler-Ivens (2015) A novel fMRI paradigm suggests that pedaling-related brain activation is altered after stroke. *Front Hum Neurosci*, 9, 324.
- Raymer, G. H., B. L. Allman, C. L. Rice, G. D. Marsh & R. T. Thompson (2006) Characteristics of a MR-compatible ankle exercise ergometer for a 3.0 T head-only MR scanner. *Med Eng Phys*, 28, 489-94.
- Roest, A. A., P. Kunz, H. J. Lamb, W. A. Helbing, E. E. van der Wall & A. de Roos (2001) Biventricular response to supine physical exercise in young adults assessed with ultrafast magnetic resonance imaging. *Am J Cardiol*, 87, 601-5.
- Sacchetti, M., M. Lenti, A. Scotto Di Paulumbo & G. de Vito (2010) Different Effect of Cadence on Cycling Efficiency between Young and Older Cyclists.
- Schindler-Ivens, S., D. A. Brown & J. D. Brooke (2004) Direction-dependent phasing of locomotor muscle activity is altered post-stroke. *J Neurophysiol*, 92, 2207-16.
- Seo, J., D. Kim, S. Yang, D. Kang, J. Choi & G. Tack (2016) Comparison of joint kinematics and pedaling force in the young and the elderly. *The Journal of Physical Therapy Science*, 28.
- Sharafi, B., G. Hoffmann, A. Q. Tan & Y. D. Y (2016) Evidence of impaired neuromuscular responses in the support leg to a destabilizing swing phase perturbation in hemiparetic gait. *Exp Brain Res*, 234, 3497-3508.
- Stubbs, P. W., J. F. Nielsen, T. Sinkjaer & N. Mrachacz-Kersting (2012) Short-latency crossed spinal responses are impaired differently in sub-acute and chronic stroke patients. *Clin Neurophysiol*, 123, 541-9.

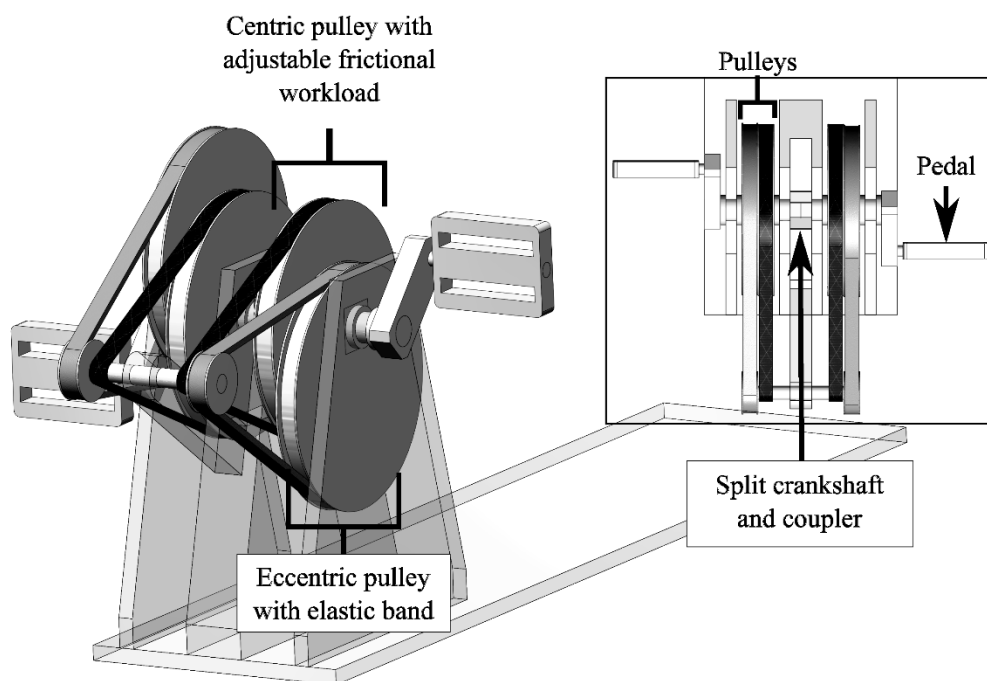
- Teixeira-Salmela, L. F., S. J. Olney, S. Nadeau & B. Brouwer (1999) Muscle strengthening and physical conditioning to reduce impairment and disability in chronic stroke survivors. *Arch Phys Med Rehabil*, 80, 1211-8.
- Ting, L. H., S. A. Kautz, D. A. Brown & F. E. Zajac (1999) Phase reversal of biomechanical functions and muscle activity in backward pedaling. *J Neurophysiol*, 81, 544-51.
- Turkseven, M. & J. Ueda (2013) Analysis of an MRI Compatible Force Sensor for Sensitivity and Precision. *IEEE Sensors Journal*, 13.
- Turns, L. J., R. R. Neptune & S. A. Kautz (2007) Relationships between muscle activity and anteroposterior ground reaction forces in hemiparetic walking. *Arch Phys Med Rehabil*, 88, 1127-35.
- van Duinen, H. 2007. The interaction between motor fatigue and cognitive task performance. University of Groningen: Print Partners Ipskamp.

## APPENDIX A: SUPPLIMENT TO CHAPTER 3

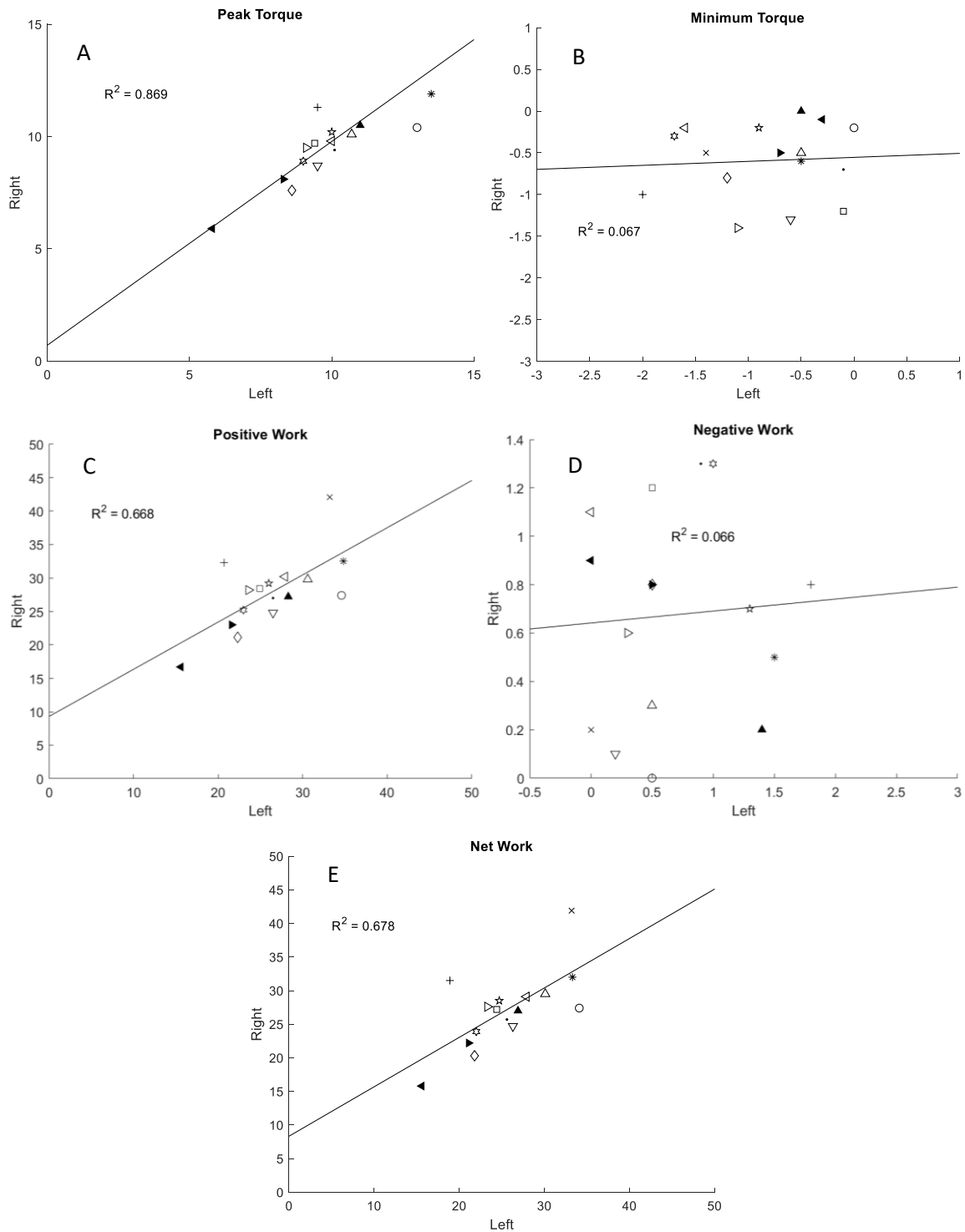
This appendix is a supplement to Chapter 3. Included is additional results and the analysis equations used to evaluate torque, work, and dependent measures of interest.

### 3/4 View

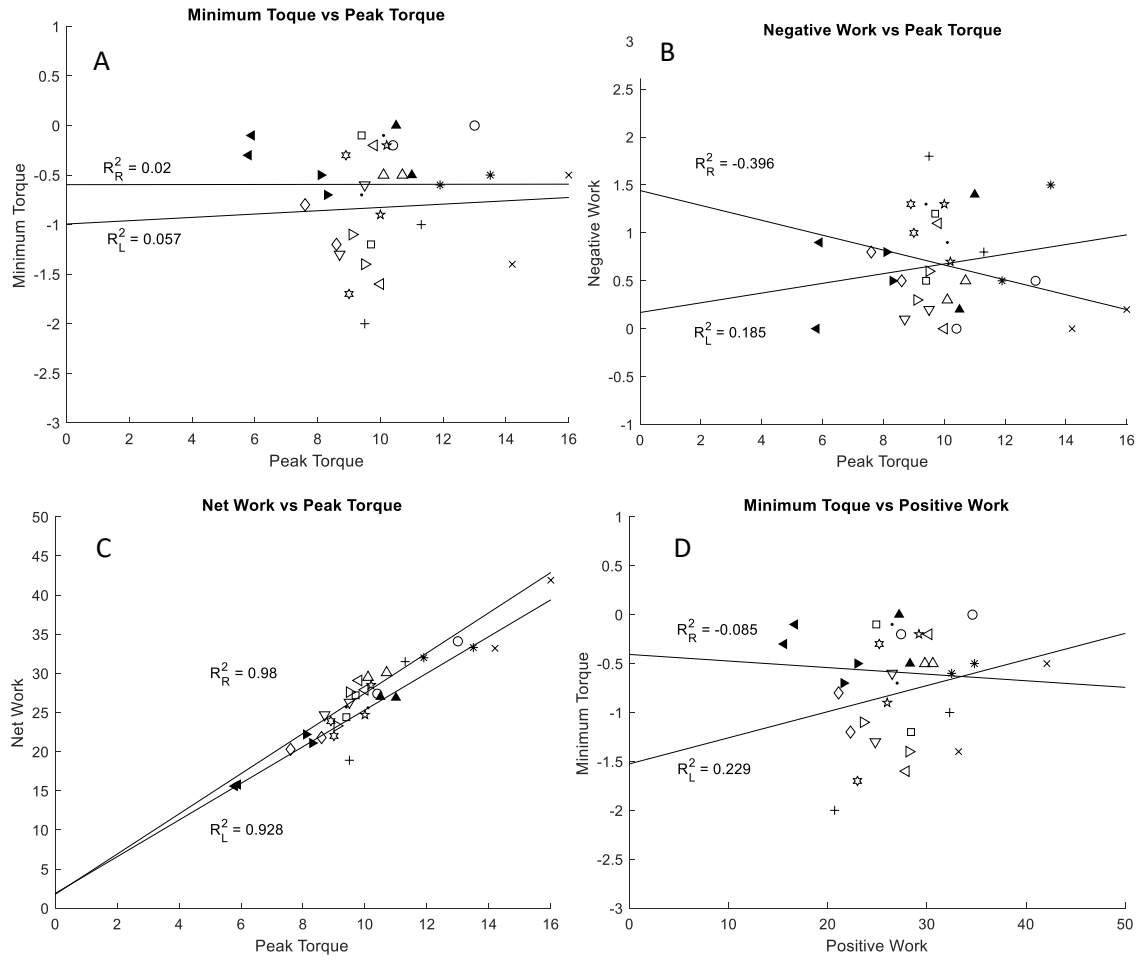
### Top View

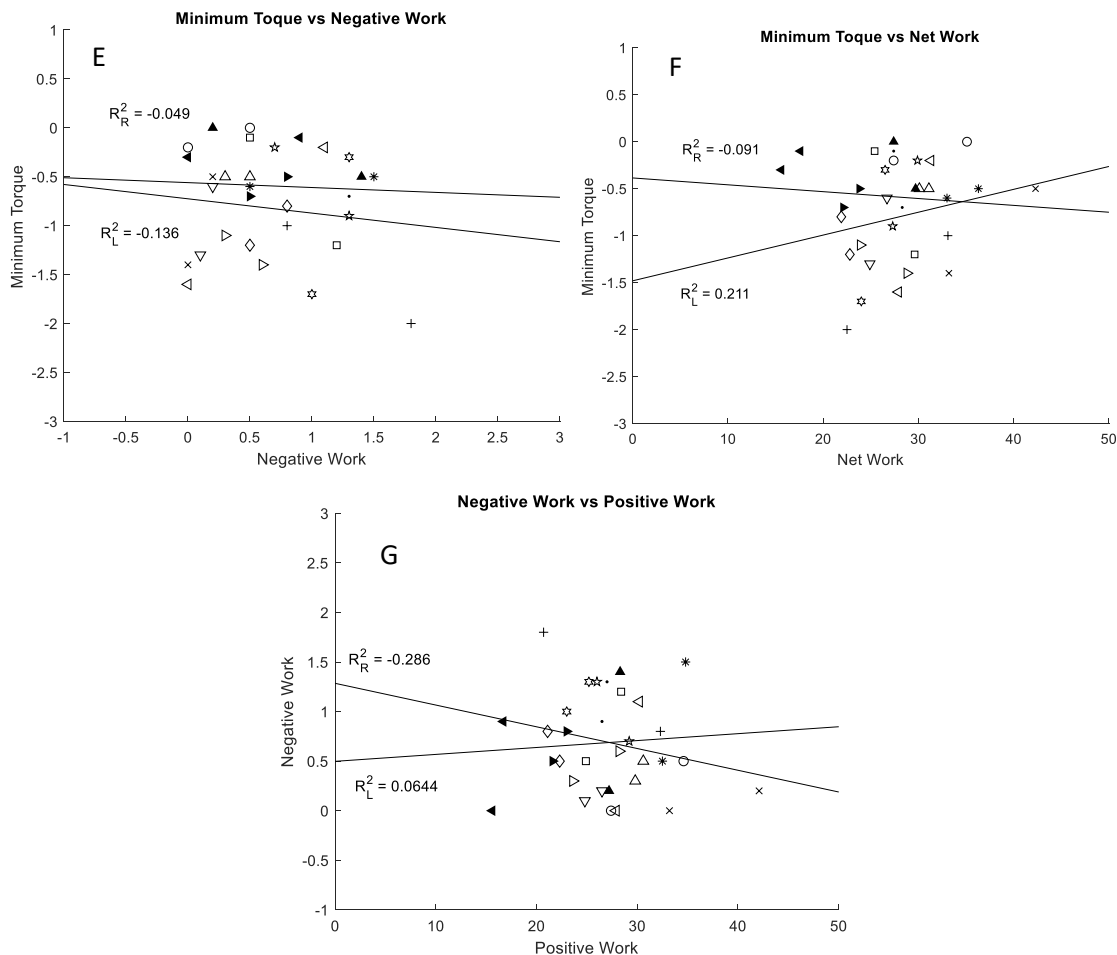


**Figure B.1: Pedaling device with split crank shaft.** The top view depicts the split crankshaft and coupler. The coupler allowed conventional pedaling when fastened in place and unilateral or bilateral uncoupled pedaling when removed. The 3/4 view depicts the pulley systems of the pedaling device. An eccentric pulley with elastic band was used during unilateral and bilateral uncoupled pedaling to simulate the contribution from the contralateral downstroke limb during conventional pedaling. The elastic band was stretched during the downstroke of the pedaling cycle, and energy stored in the band was released during the upstroke. A centric pulley applied an adjustable frictional workload

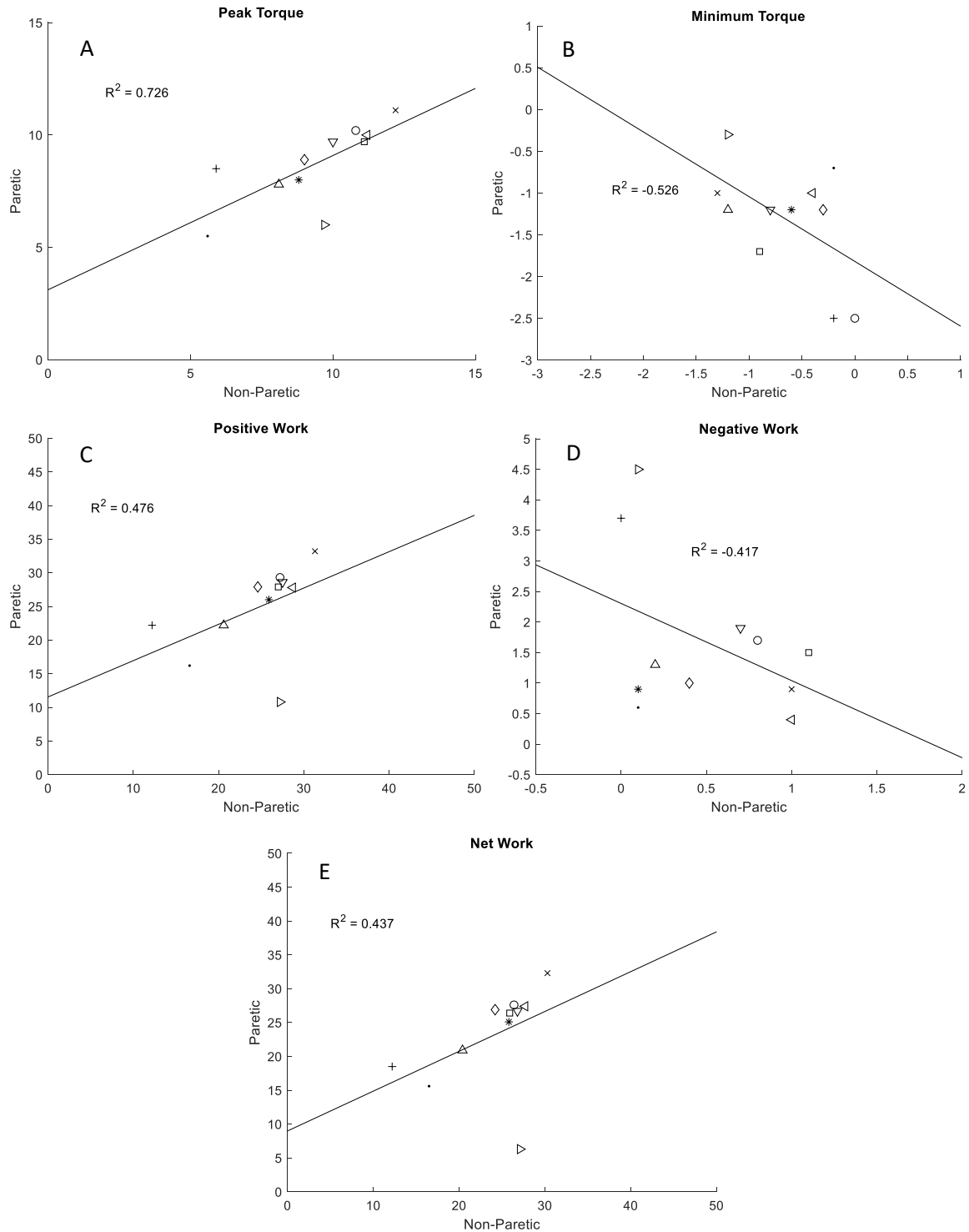


**Figure B.2: Correlations of each measure of torque and work for right versus left.** A) Peak torque measurement, B) Positive work completed, C) negative work completed, and D) net work completed.

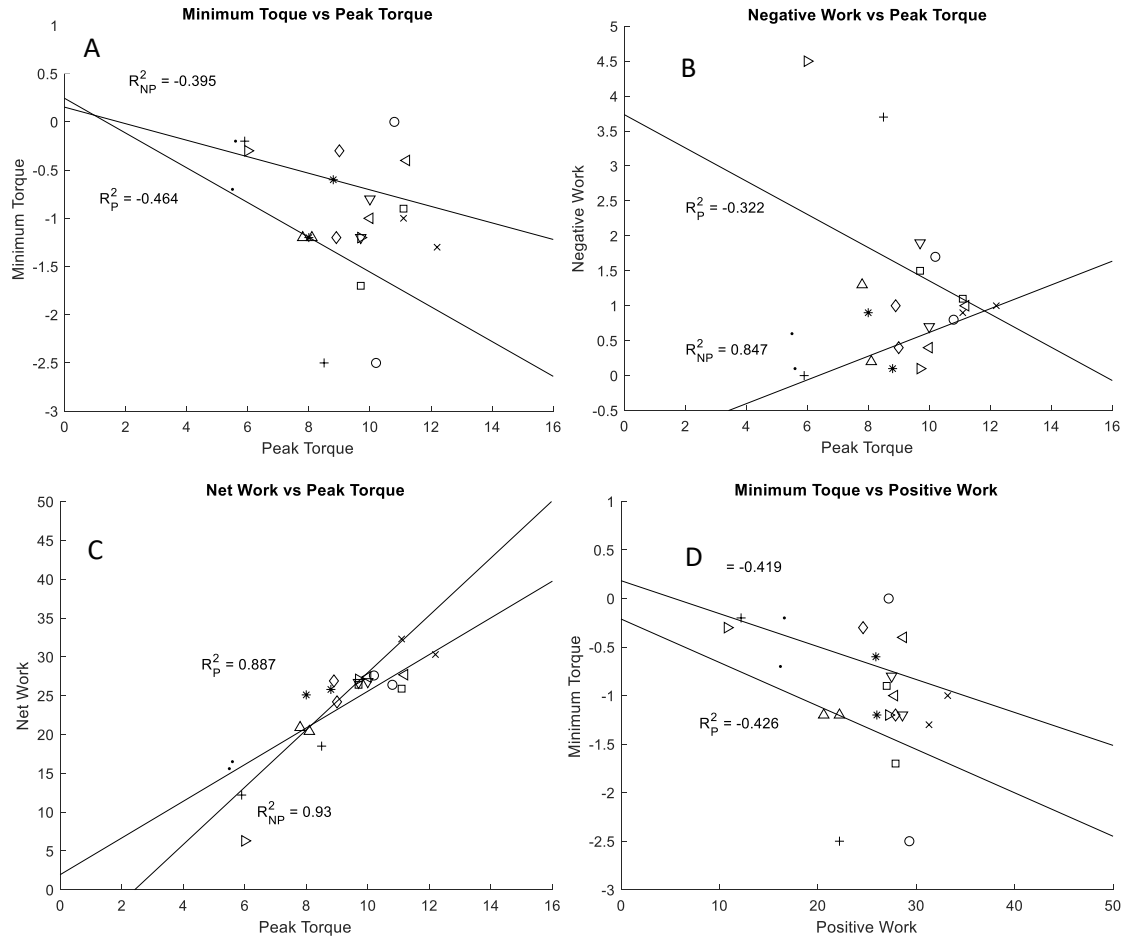


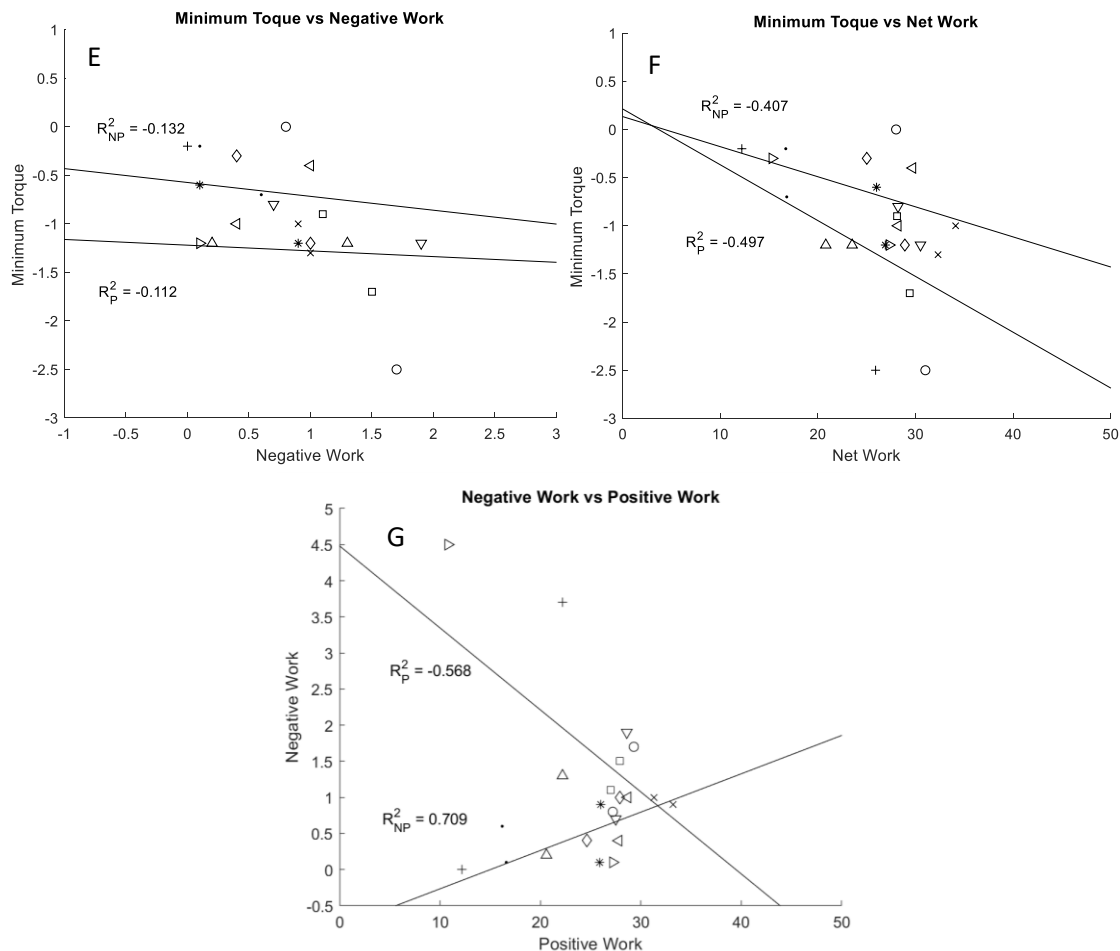


**Figure B.3: Comparison of torque and work measurements for control participants.** Torque and work measurements taken during familiarization session shown for comparing each measure to one another. A) Minimum torque vs peak torque, B) Negative work vs peak torque, C) Net work vs peak torque, D) Minimum torque vs positive work, E) Minimum torque vs negative work, F) Minimum torque vs net work, and G) negative work vs positive work.

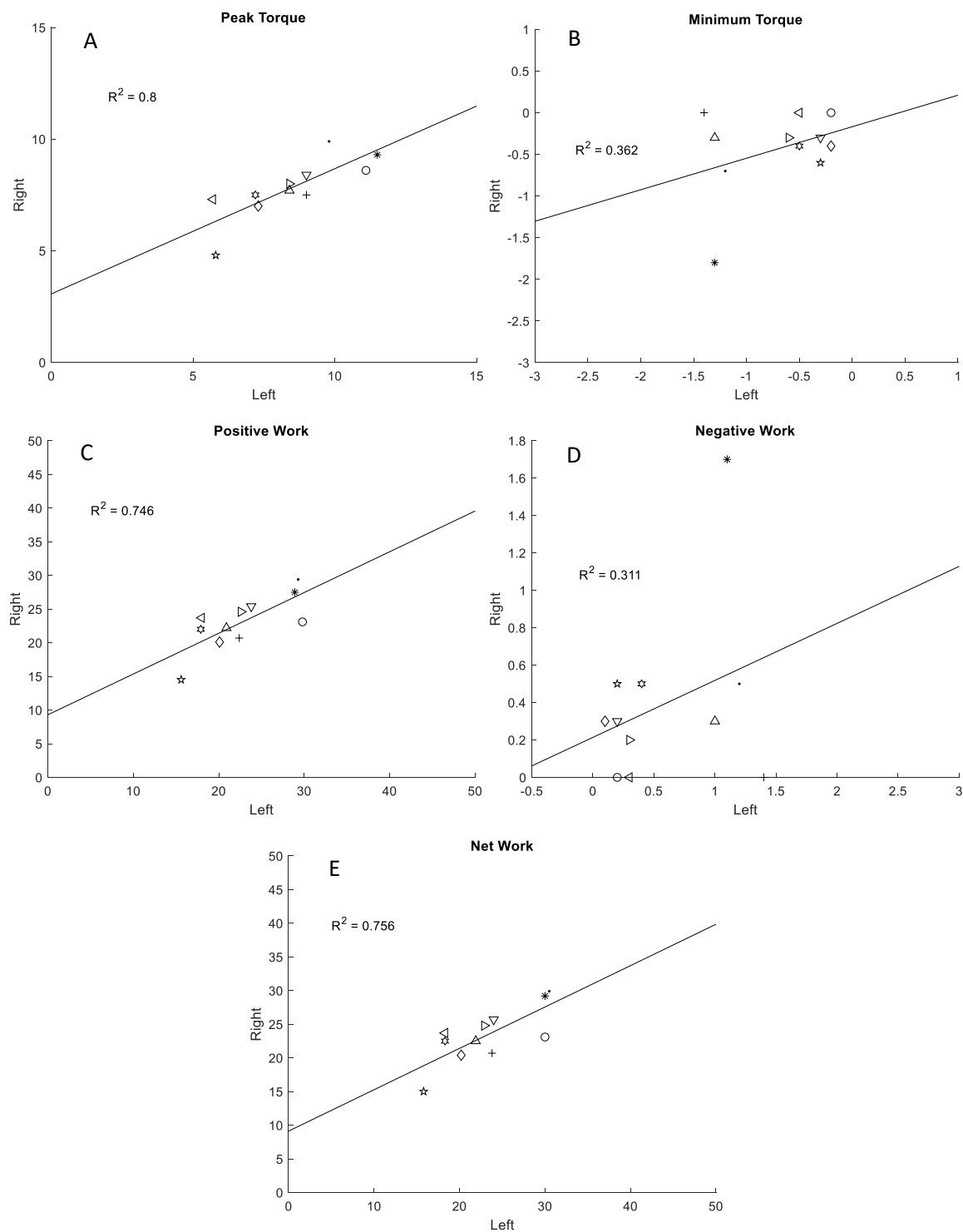


**Figure B.4: Correlations of each measure of torque and work for non-paretic versus paretic.** A) Peak torque measurement, B) Positive work completed, C) negative work completed, and D) net work completed.

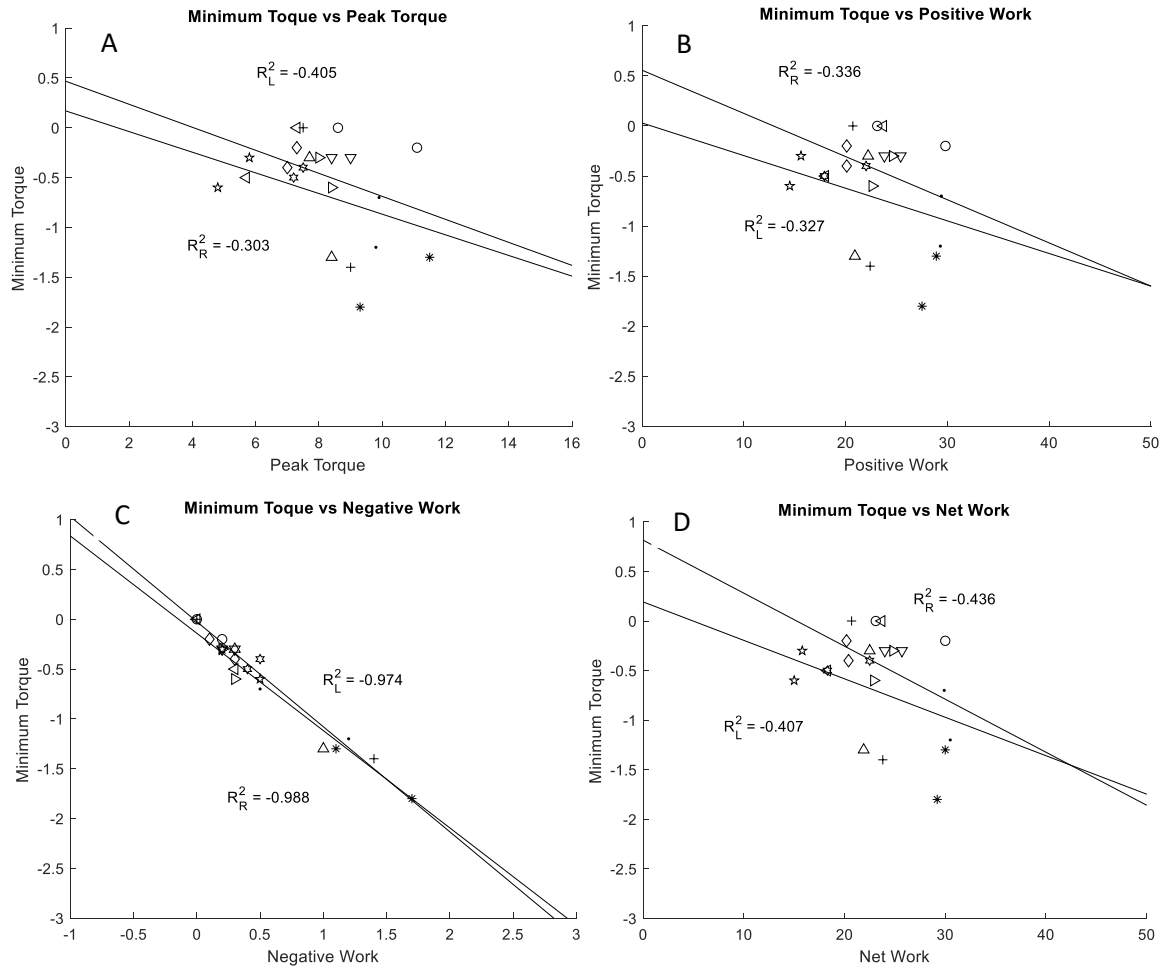


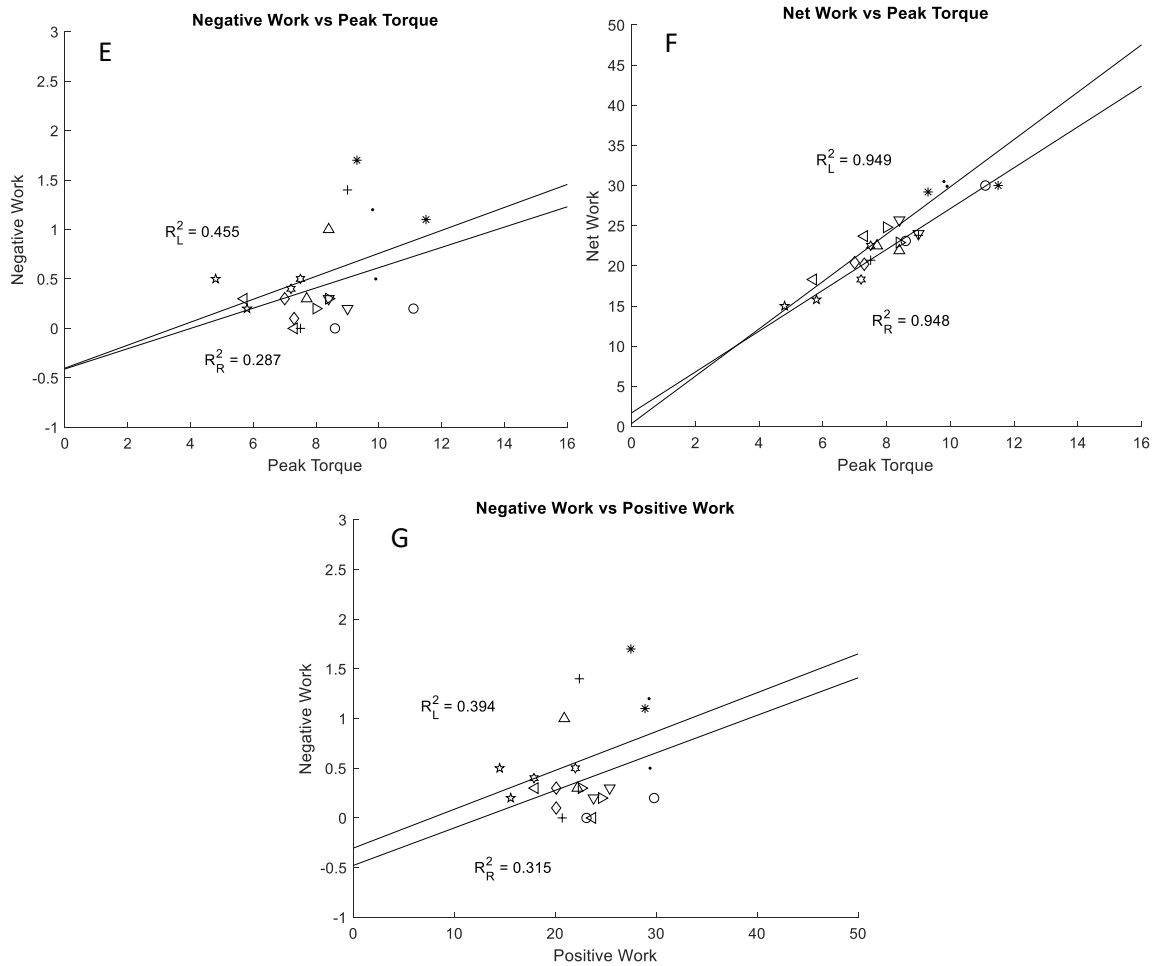


**Figure B.5: Comparison of torque and work measurements for stroke participants.** Torque and work measurements taken during familiarization session shown for comparing each measure to one another. A) Minimum torque vs peak torque, B) Negative work vs peak torque, C) Net work vs peak torque, D) Minimum torque vs positive work, E) Minimum torque vs negative work, F) Minimum torque vs net work, and G) negative work vs positive work.

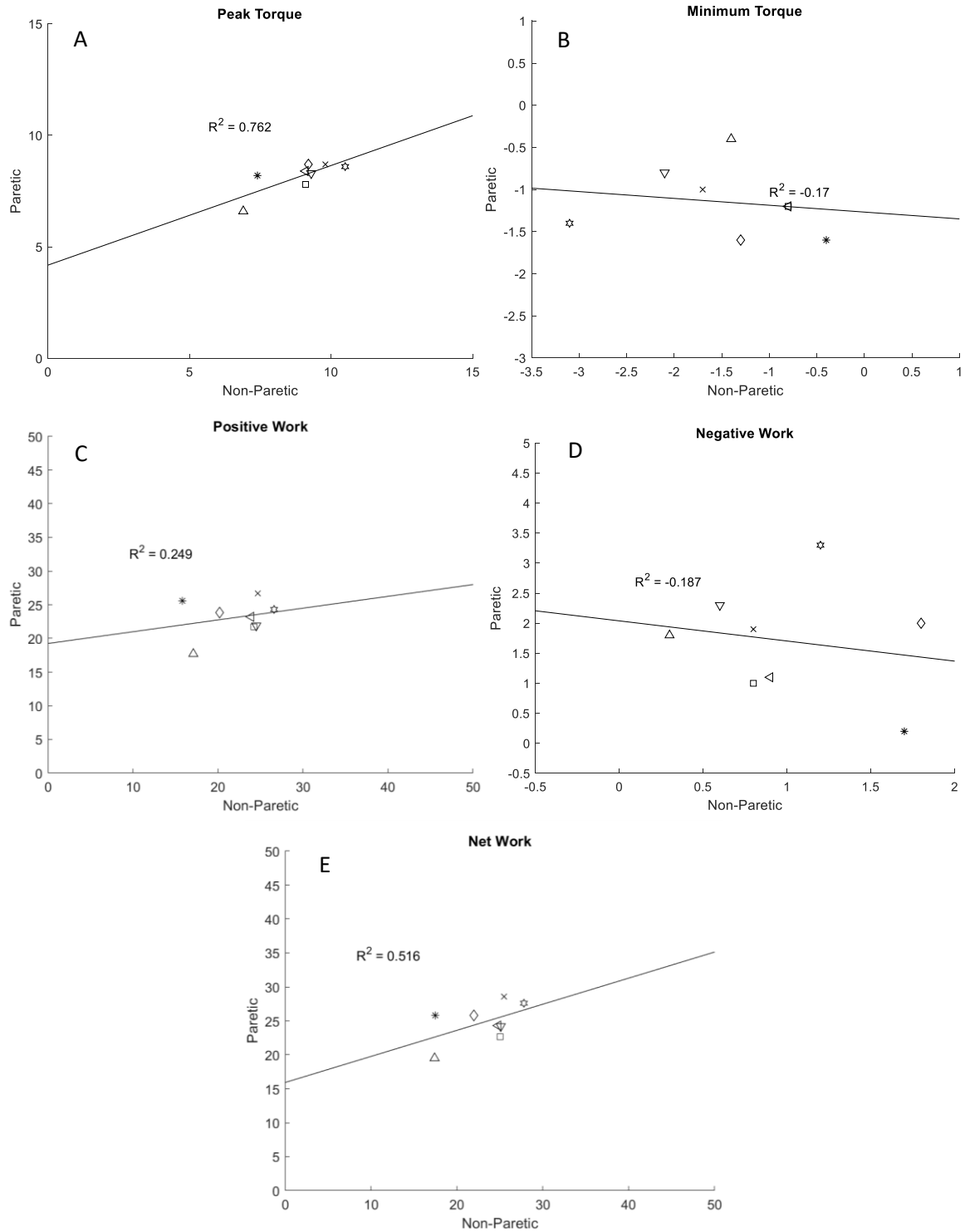


**Figure B.6: Correlations of each measure of torque and work for right versus left during fMRI pedaling.** A) Peak torque measurement, B) Positive work completed, C) negative work completed, and D) net work completed.

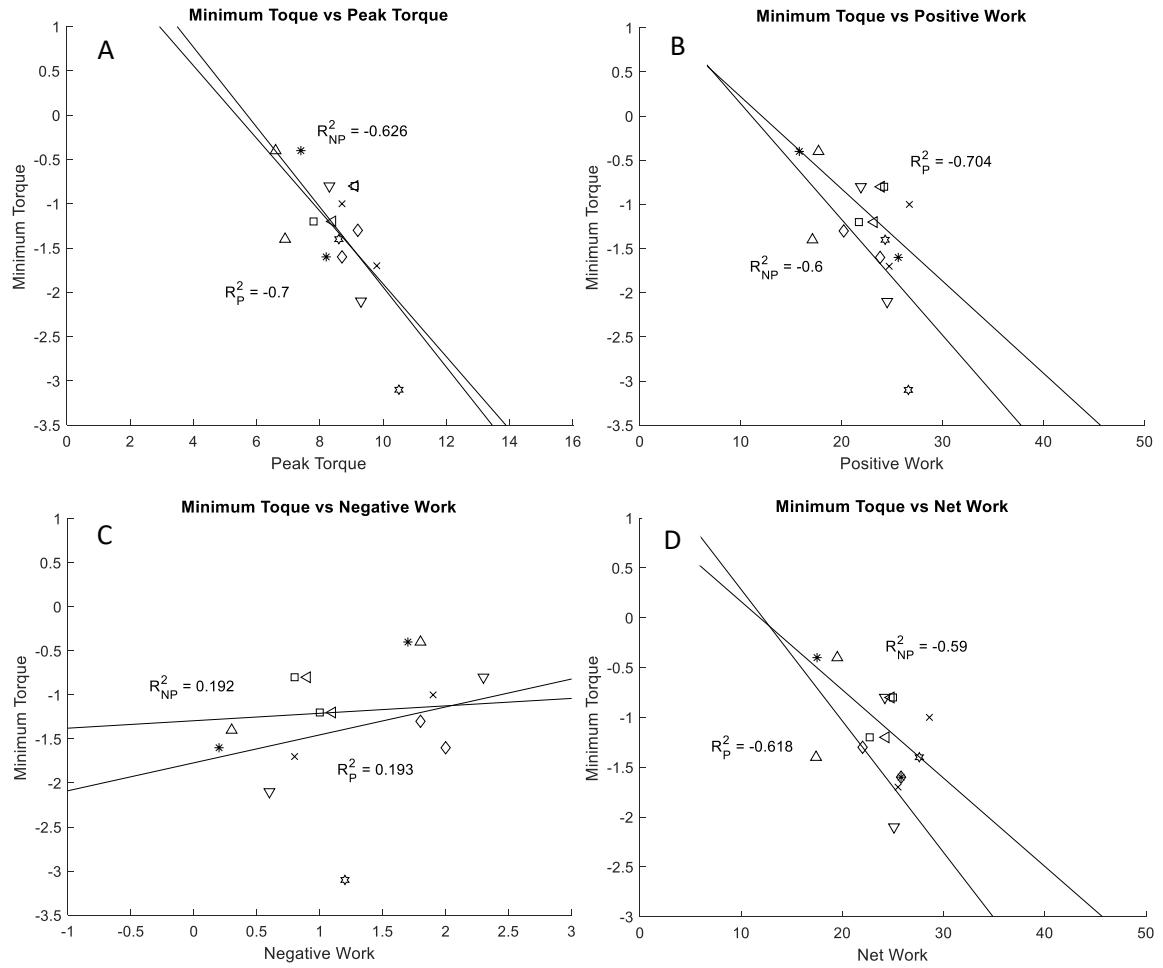




**Figure B.7: Comparison of torque and work measurements for control participants during fMRI pedaling.** Torque and work measurements taken during familiarization session shown for comparing each measure to one another. A) Minimum torque vs peak torque, B) Negative work vs peak torque, C) Net work vs peak torque, D) Minimum torque vs positive work, E) Minimum torque vs negative work, F) Minimum torque vs net work, and G) negative work vs positive work.



**Figure B.8: Correlations of each measure of torque and work for non-paretic versus paretic during fMRI pedaling.** A) Peak torque measurement, B) Positive work completed, C) negative work completed, and D) net work completed.



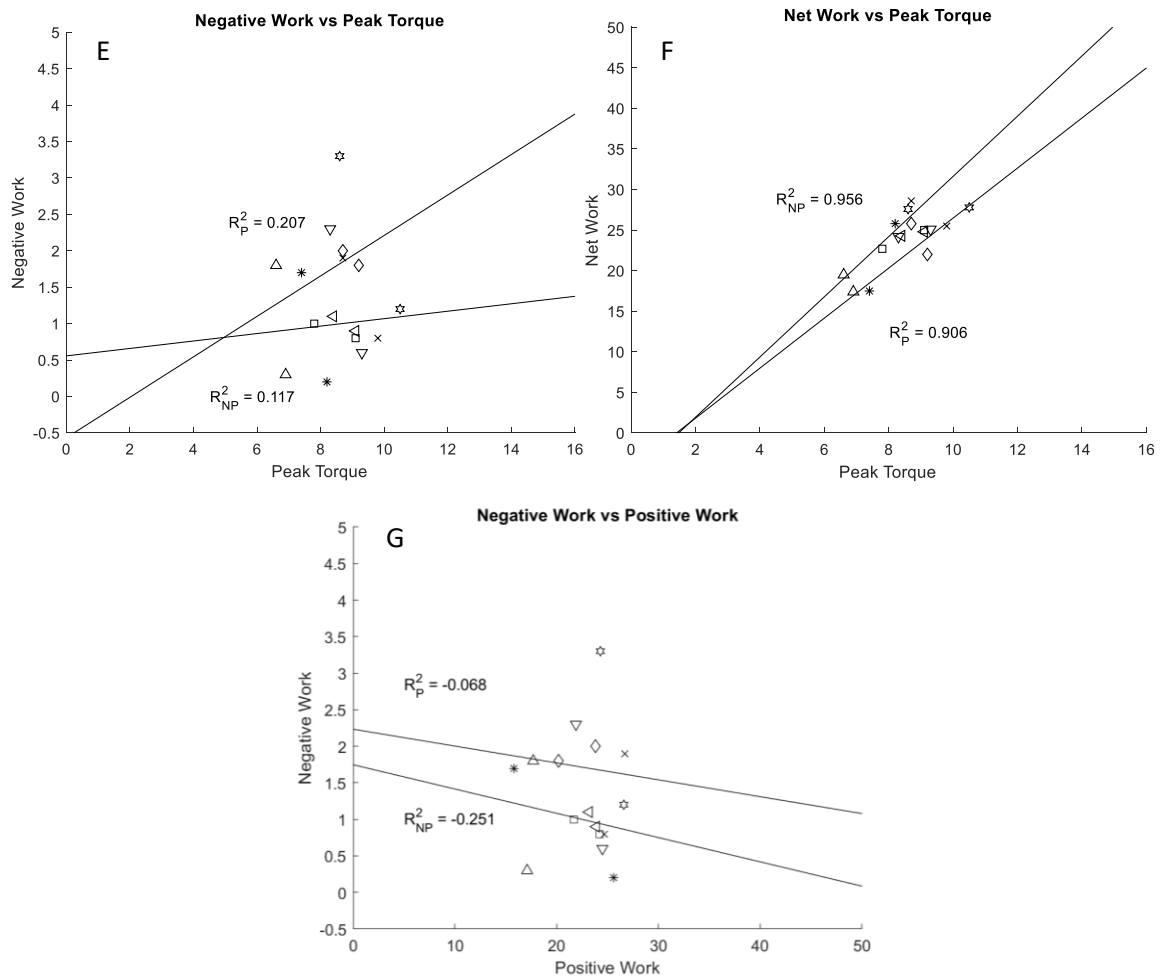
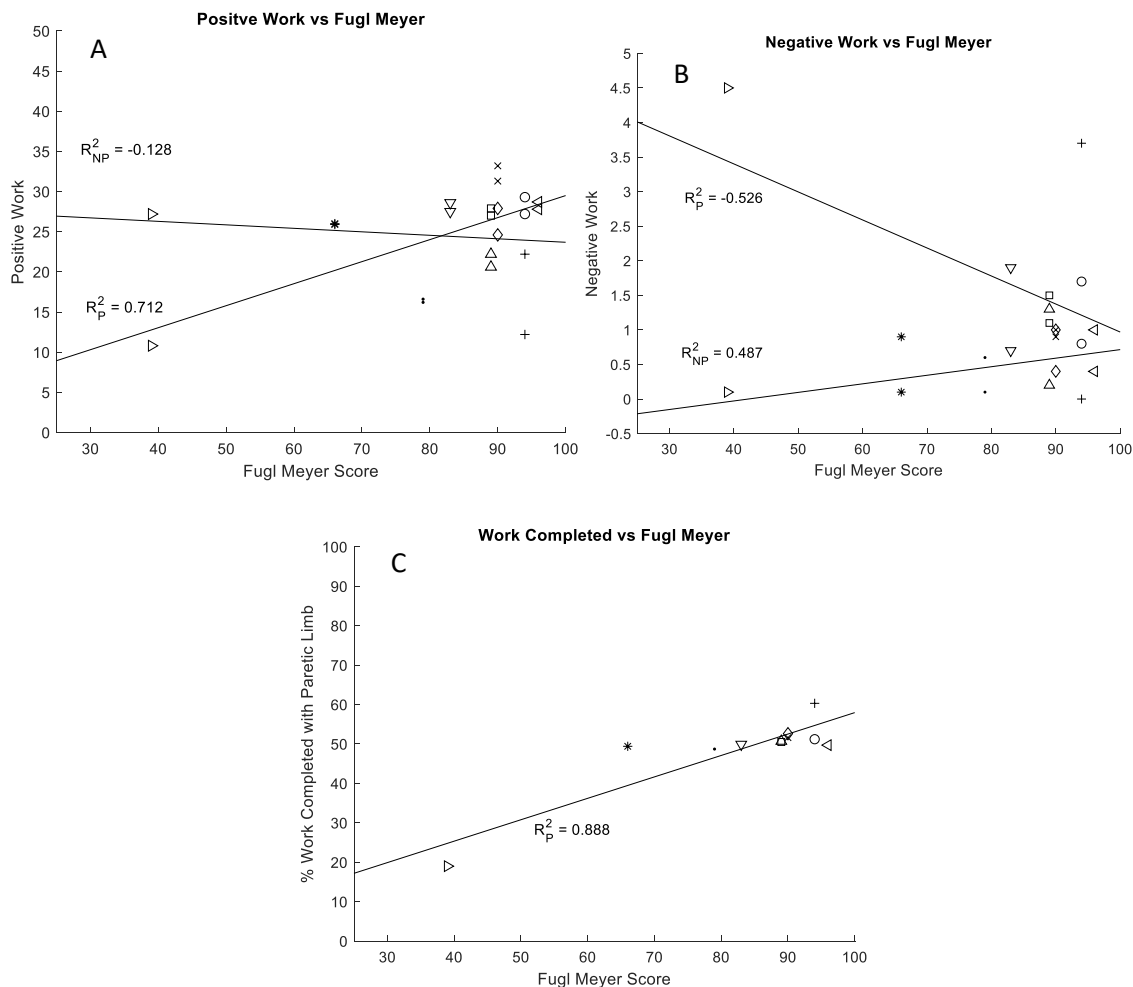


**Figure B.9: Comparison of torque and work measurements for stroke participants during fMRI pedaling.** Torque and work measurements taken during familiarization session shown for comparing each measure to one another. A) Minimum torque vs peak torque, B) Negative work vs peak torque, C) Net work vs peak torque, D) Minimum torque vs positive work, E) Minimum torque vs negative work, F) Minimum torque vs net work, and G) negative work vs positive work.



**B.10: Fugl Meyer compared to positive work, negative work and work completed.** The Fugl Meyer is significantly correlated with the paretic limb during positive work ( $p=0.01$ ) and completed work ( $p=0.0$ ). Fugl Meyer is not correlated with any other measure evaluated.

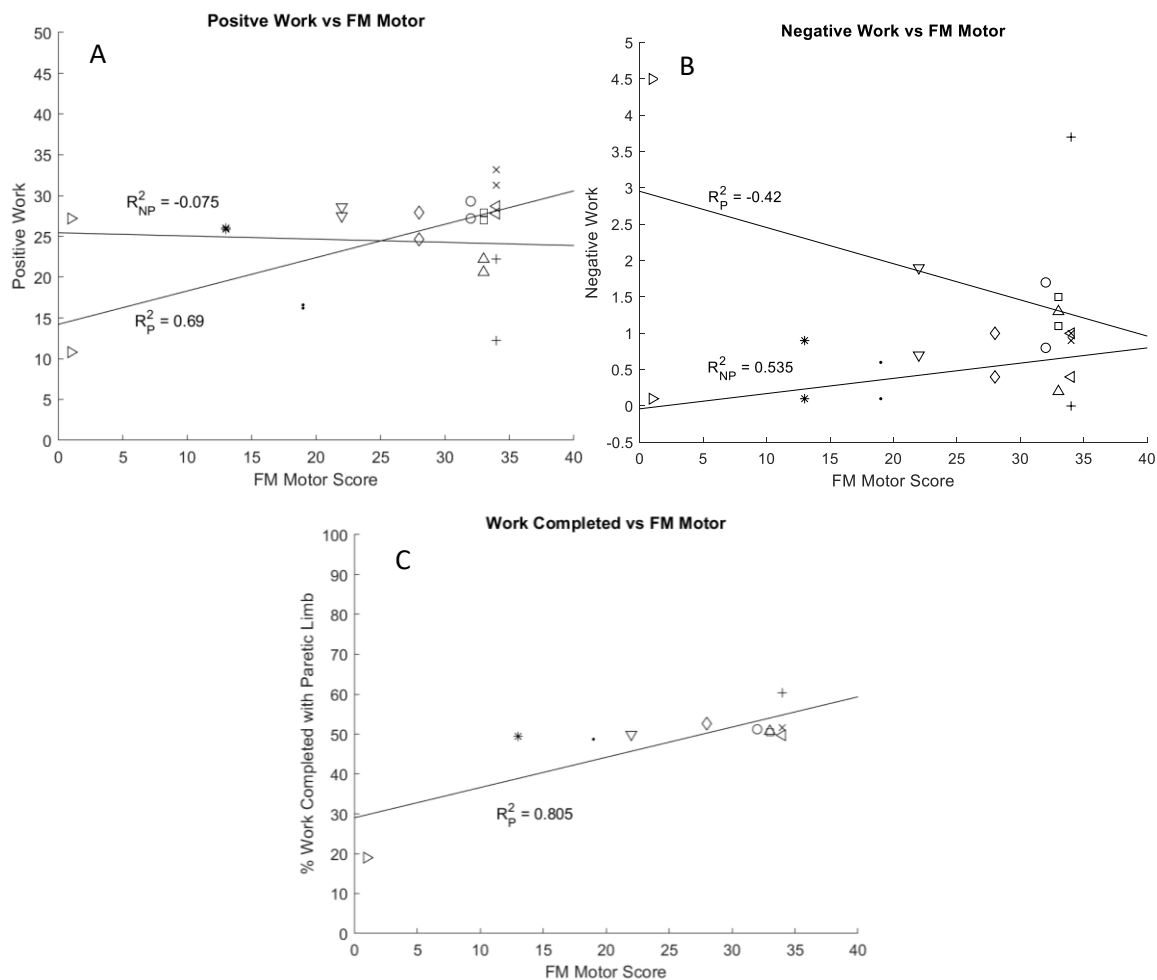


**Figure B.11: Motor component of the Fugl Meyer compared with positive work, negative work, and completed work with the paretic limb.** Fugl Meyer is significantly correlated with the paretic limb of positive work ( $p = 0.02$ ) and work completed ( $p = 0.003$ ). Fugl Meyer was not significantly correlated with any other measure evaluated.

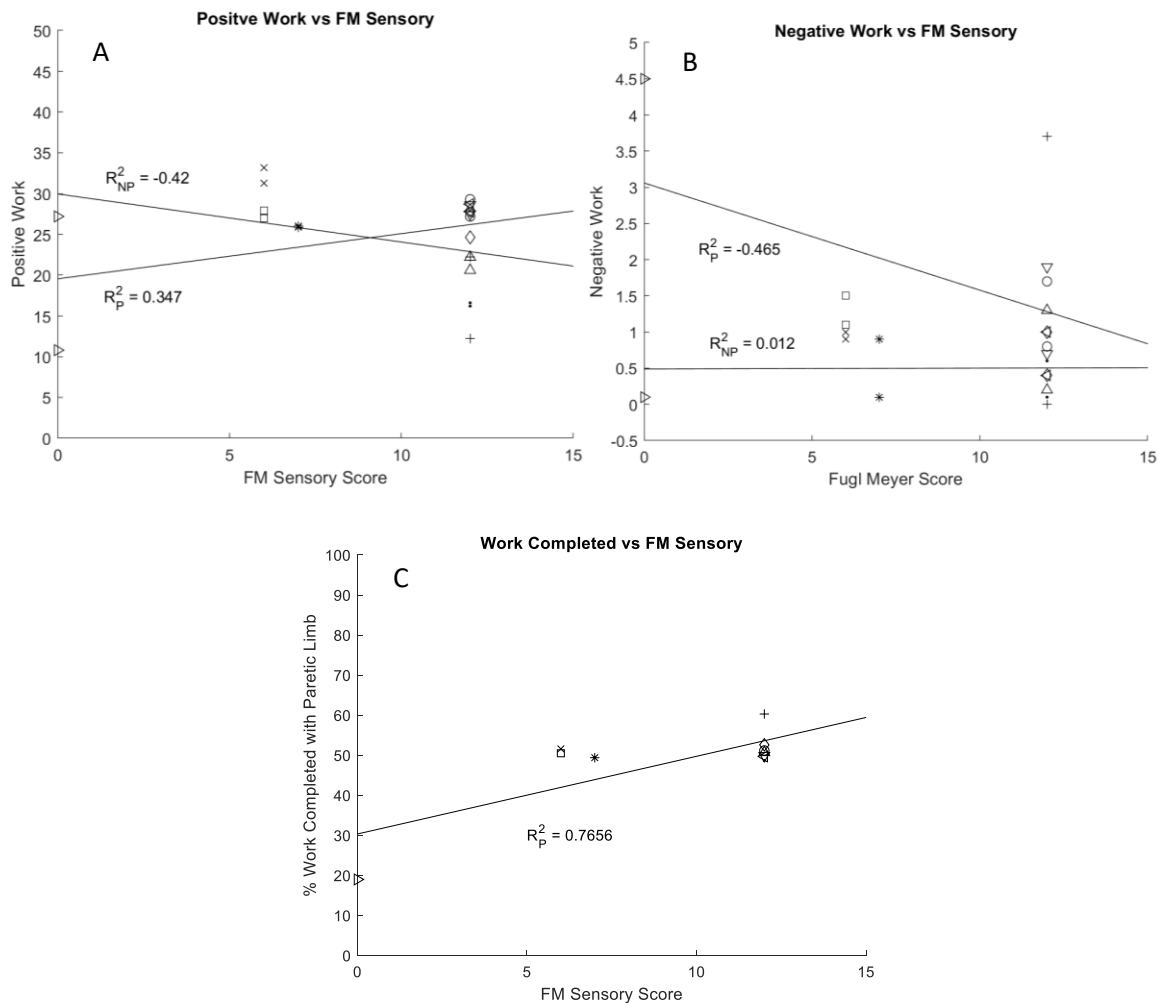


**Figure B.12: Sensory component of the Fugl Meyer compared with positive work, negative work, and completed work with the paretic limb.** Fugl Meyer is significantly correlated with the work completed of the paretic limb ( $p = 0.006$ ). Fugl Meyer was not significantly correlated with any other measure evaluated.

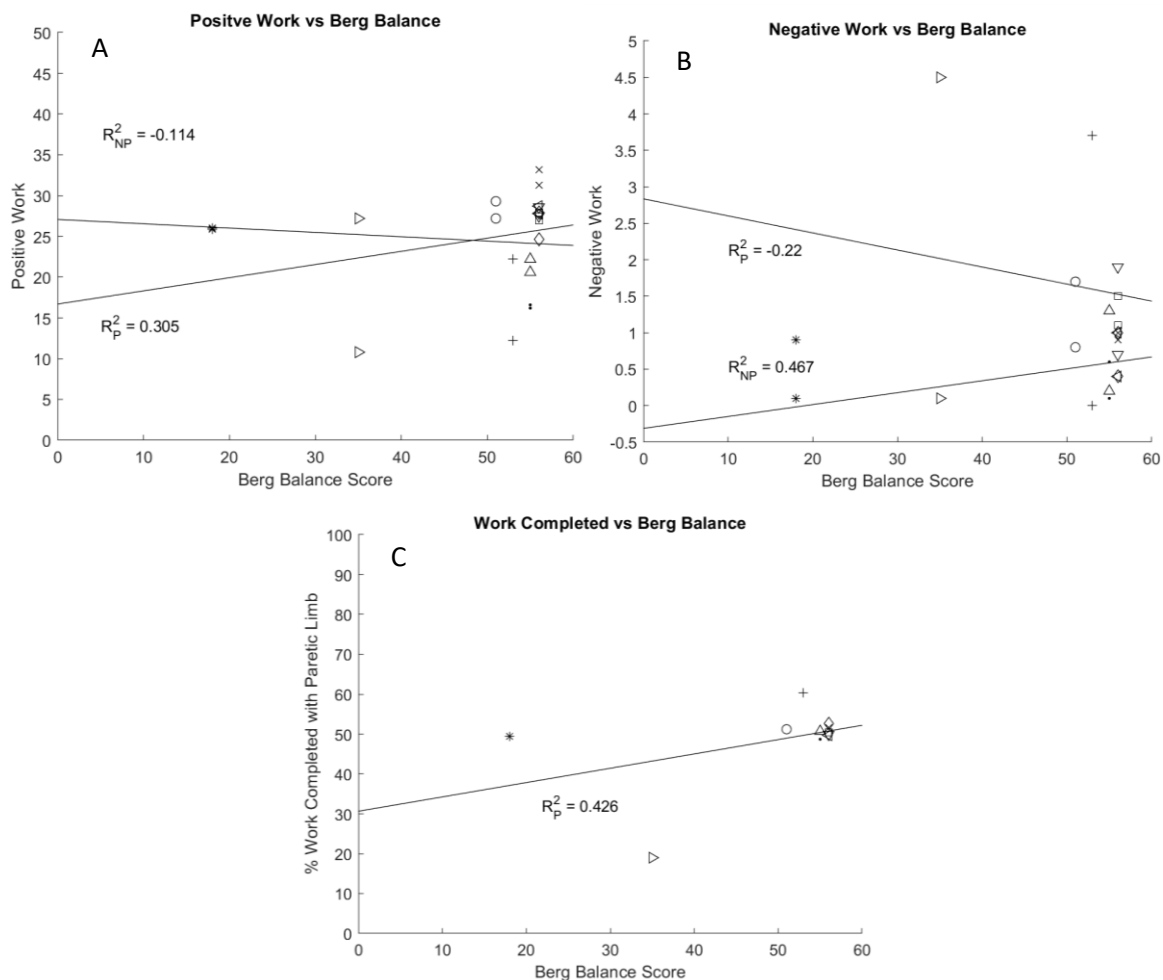


**Figure B.13: Berg Balance Assessment compared with positive work, negative work, and completed work with the paretic limb.** Berg Balance Assessment was not significantly correlated with any measure evaluated.

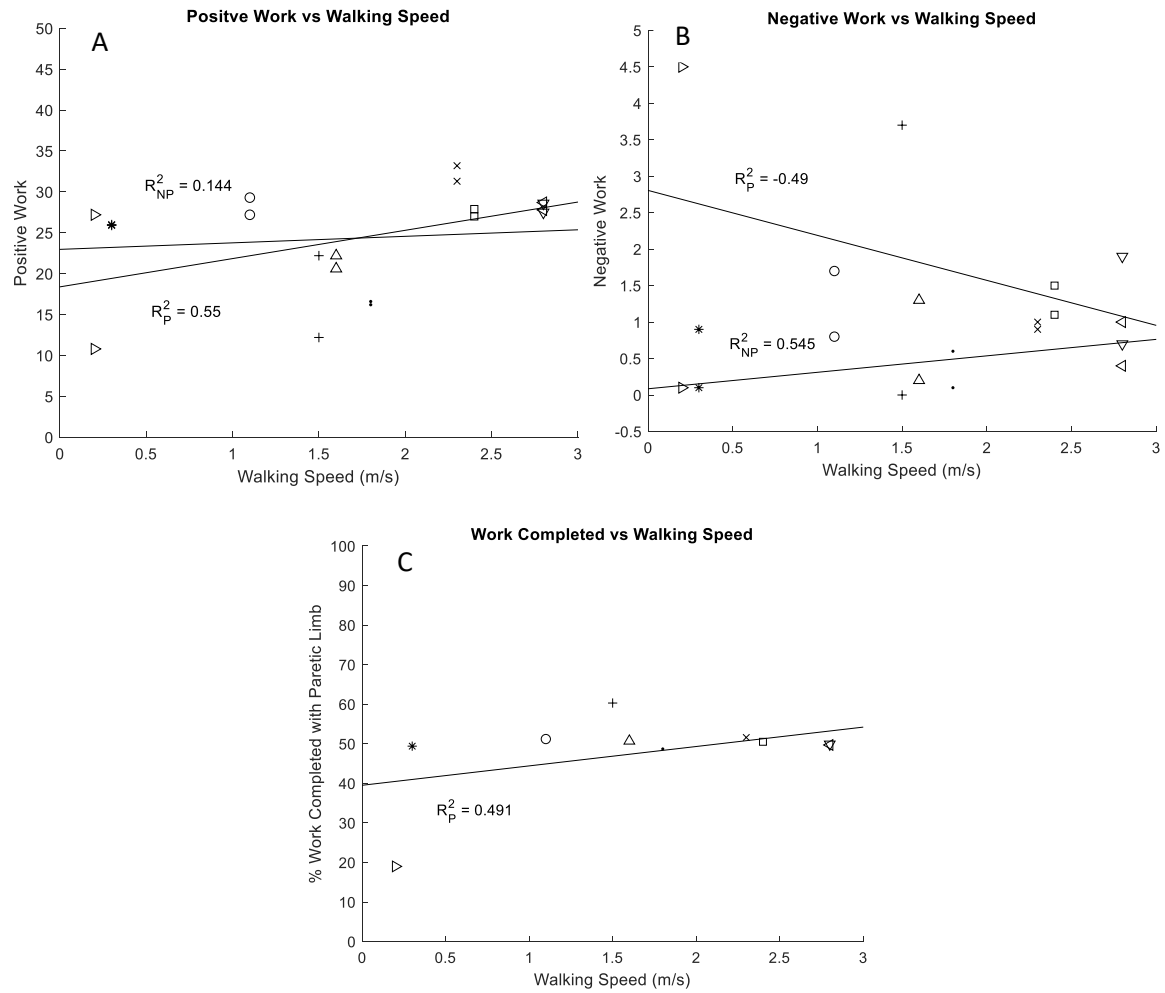


**Figure B.14: Walking speed compared with positive work, negative work, and completed work with the paretic limb. Walking speed was not significantly correlated with any measure evaluated.**

**Equation B.1: Conversion equation from voltage to torque for the left crank. A)**

positive voltages and B) negative voltages. Offsets were removed after calculation to all positive and negative values.

$$A) \text{ torque} = 8.18 * \text{voltage} - 0.03$$

$$B) \text{ torque} = 9.02 * \text{voltage} + 0.31$$

**Equation B.2: Conversion equation from voltage to torque for the right crank. A)**

positive voltages and B) negative voltages. Offsets were removed after calculation to all positive and negative values.

$$A) \text{ torque} = 3.91 * \text{voltage} + 0.35$$

$$B) \text{ torque} = 2.73 * \text{voltage} - 0.06$$